

UCGE Reports

Number 20273

**Department of Geomatics Engineering**

**Enhanced Detection of GNSS Signals Based on Spatial  
Combining**

(URL: <http://www.geomatics.ucalgary.ca/research/publications>)

**by**

**Mohammad Upal Mahfuz**

**September 2008**



UNIVERSITY OF CALGARY

Enhanced Detection of GNSS Signals Based on Spatial Combining

by

Mohammad Upal Mahfuz

A THESIS

SUBMITTED TO THE FACULTY OF GRADUATE STUDIES  
IN PARTIAL FULFILMENT OF THE REQUIREMENTS FOR THE  
DEGREE OF MASTER OF SCIENCE

DEPARTMENT OF GEOMATICS ENGINEERING

CALGARY, ALBERTA

SEPTEMBER 2008

© Mohammad Upal Mahfuz 2008

## Abstract

Weak and non-line of sight (NLOS) signals severely degrades the detection performance of Global Navigation Satellite Systems (GNSS) signals. High attenuation and severe multipath introduces a challenge in the detectability of GNSS signal indoors. The use of antenna arrays in GNSS allows for the provision that multiple spatially separated antennas receive uncorrelated signal fading independent of each other. Being quite common in point-to-point wireless communications, the concept of antenna array in GNSS is considered as a new application. The independent fading statistics are used to reduce noise and to increase signal to noise ratio (SNR) at the receiver, which ultimately increases the detectability of the signals in any environment. This research discusses the enhanced detection of GNSS signals based on spatial combining of multiple antenna outputs. From spatially apart multiple antenna receivers, there is a possible diversity gain when the individual antenna outputs are combined in an appropriate fashion. For two antennas, the diversity gain is in the range of 4 to 5 dB relative to a single antenna. The theory of multiple signals combining along with the experimental setup to demonstrate the approach with real GPS data is presented. The data presented supports the fact there is significant gain in signal to noise ratio (SNR) which improves the detection of GNSS signals in degraded signal environments, e.g. indoors. A deeper investigation on the spatial correlation of GPS L1 multiple receiver channels shows that the data collaborates the theory and, above all the spatial diversity method enhances detection in a statistically significant manner.

## **Acknowledgements**

I owe everything that I have been able to achieve to my parents Mohammad Mahfuzul Huq and Selina Khatun who have supported me all through my life. Without their love and affection I would not have come this far.

Thanks to my supervisors, Professors Gérard Lachapelle and John Nielsen. I am thankful to them for their guidance. I am grateful to Dr. Surendran K. Shanmugam for all the direction and guidance that he has kindly provided me regarding my research.

Thanks also to my colleagues in the Department of Geomatics Engineering who have been my friends during the past two years.

I am thankful to my brothers Rachaen Mahfuz Huq and Raihan Mahfuz Huq for all their inspirations and encouragements. Finally, my deepest thanks to my wife Suraiya Akter for all her love, patience and moral support that have helped me progress in my work.

## Table of Contents

Approval Page	ii
Abstract	iii
Acknowledgements	iv
Table of Contents	v
List of Tables	vii
List of Figures and Illustrations	viii
List of Symbols, Abbreviations and Nomenclature	xi
CHAPTER ONE: INTRODUCTION	1
1.1 The Indoor Detection and Positioning Problem	1
1.2 Indoor GNSS Challenges	2
1.2.1 Multipath Propagation Errors	2
1.2.2 Signal Attenuation and Fading	4
1.2.3 Approaching the Challenges	6
1.3 Research Overview	9
1.3.1 Motivation and Limitations of Previous Research	9
1.3.2 Objectives and Novel Contributions	10
1.3.3 Thesis Outline	15
CHAPTER TWO: SPATIAL DIVERSITY FOR GNSS SIGNALS	16
2.1 Background and Importance of GNSS Multi-antenna Signal Reception	16
2.2 GPS Signal Reception by Uniform Linear Array (ULA) Antenna	18
2.3 Diversity Technology for GNSS	21
2.4 Spatial Diversity Techniques	22
2.5 Combining Methods	32
2.5.1 Selection Combining	32
2.5.2 Switched combining	33
2.5.3 Equal gain combining	34
2.5.4 Maximum ratio combining	35
2.6 Diversity Gain	36
2.7 Spatial Diversity Performance Criterion	39
2.7.1 Antenna Correlation	39
2.7.2 Post-Correlation Signal to Noise Ratio (PSNR)	41
2.8 Conclusions	43
CHAPTER THREE: SPATIAL DIVERSITY COMBINING OF WEAK GNSS SIGNALS	45
3.1 System Description	45
3.1.1 Spatial Covariance Estimation	46
3.2 Spatial Combining of GNSS Signals	49
3.2.1 Single antenna processing	49
3.2.2 Diversity Combining Schemes	51

3.2.3 Maximum-Ratio Combining	53
3.2.4 Equal-Gain Combining	56
3.3 Estimator-Correlator (EC) Based Spatial Combining	58
3.4 Performance Evaluation	70
3.5 Conclusions	80
<b>CHAPTER FOUR: TEST METHODOLOGY AND GNSS SIGNAL PROCESSING</b>	<b>81</b>
4.1 GPS Signal Structure	81
4.2 GNSS Receiver Signal Processing	82
4.2.1 Signal conditioning: Antenna Element	83
4.2.2 RF Down-conversion and Sampling	83
4.2.3 Baseband Signal Processing	84
4.3 GPS Signal Acquisition	86
4.3.1 Correlation	86
4.3.2 Non-Coherent Combining Detector	88
4.4 Software Implementation of Dual-Antenna Array GPS Receiver	89
4.4.1 Signal Acquisition Results	94
4.4.2 Signal Tracking Results	95
4.4.3 Phase Stability	99
4.4.4 Navigation Bit Synchronization	101
4.4.5 Continuous Wave Interference Issues and Frequency Excision	104
4.4.6 High-Sensitivity Performance with Extended Coherent Integration	108
4.5 Conclusions	112
<b>CHAPTER FIVE: EXPERIMENTAL ANALYSIS AND SEMINAL RESULTS</b>	<b>113</b>
5.1 Overview of the Recorded Data Sets and Data Processing	113
5.2 Experimental Results	117
5.2.1 Indoor Fading Characteristics	118
5.2.2 Envelope Correlation	121
5.2.3 Diversity Gain	123
5.2.4 Post-correlation Signal-to-Noise Ratio (PSNR)	127
5.2.5 Improvement in Detection Performance	131
5.3 Conclusions	135
<b>CHAPTER SIX: CONCLUSIONS AND RECOMMENDATIONS</b>	<b>137</b>
6.1 Synopsis	137
6.2 Research Contributions	139
6.3 Future Research	140
<b>REFERENCES</b>	<b>142</b>
<b>APPENDIX-A</b>	<b>151</b>
<b>APPENDIX-B</b>	<b>154</b>

## List of Tables

Table 5.1 System parameters

117

## List of Figures

Figure 1.1 Flowchart of GPS Antenna Array Receiver Signal Processing	14
Figure 2.1 GNSS signal reception using a uniform-linear-array (ULA) antenna	19
Figure 2.2 Illustration of two individually received signals and the concept of signal combining by diversity technique. The combined signal always has the highest signal level compared to the individual signals	21
Figure 2.3 Flow chart of spatial diversity technique	23
Figure 2.4 Plane wave incident from a satellite at a GNSS receiver	25
Figure 2.5 Theoretical antenna correlation as a function of antenna spacing	31
Figure 2.6 Selection combining method for $M$ antenna elements	32
Figure 2.7 Switched combining method for $M$ antenna elements	33
Figure 2.8 Equal gain combining method for $M$ antenna elements	35
Figure 2.9 Maximum ratio combining method for $M$ antenna elements	36
Figure 2.10 CDFs of Rayleigh fading signals for different numbers of diversity branches	38
Figure 2.11 Peak correlation value and post-correlation noise floor	42
Figure 3.1 Antenna array setup for spatial combining (a) Synthetic array formation using linear motion of single antenna (b) Dual antenna configuration	48
Figure 3.2 System model for single antenna based GNSS signal detection	51
Figure 3.3 Generalized spatial signal combining algorithm for GNSS	53
Figure 3.4 Spatial and temporal samples of GNSS signal reception	59
Figure 3.5 Estimator-correlator (EC) based spatial combining	62
Figure 4.1 Generic GPS digital receiver block diagram	84
Figure 4.2 Doppler removal and code correlation	88
Figure 4.3 Non-coherent combining detector for GPS signal acquisition	89
Figure 4.4 Schematic diagram of the test setup	91
Figure 4.5 Schematic diagram of the dual antenna system with linear motion table	92
Figure 4.6 Plan view of the test locations in CCIT building, University of Calgary	92
Figure 4.7 Software signal processing of GNSS signal acquisition	93
Figure 4.8 Acquisition results of a strong GPS signal (a) Full search space (b) Doppler frequency space (c) Code offset space	94
Figure 4.9 Fine Doppler search for Rx1 and Rx2, PRN-16, $T_{coh}=10$ ms, $d=2\lambda$	96
Figure 4.10 Code-offset search for Rx1 and Rx2, $T_{coh}=1$ ms, $N=10$ , $T=10$ ms, $d=2\lambda$	96

Figure 4.11 Inphase and quadrature correlation outputs for Rx1 and Rx2 sampled at 1 kHz rate, PRN-16, $T_{\text{coh}}=1$ ms, $d=2\lambda$	97
Figure 4.12 Accumulated phase in radians for Rx1 and Rx2 sampled at 1 kHz rate, PRN-16, $T_{\text{coh}}=1$ ms, $d=2\lambda$	98
Figure 4.13 Signal tracking results (a) Doppler tracking (b) Code tracking (System parameters: Sampling frequency $F_S = 10$ MHz, $F_C = 3.42$ MHz, first order loop filter with BW = 5 Hz, selected indoor location)	99
Figure 4.14 Phase difference of PRN-26 over 5 mins, due to PLL ambiguity, between two antennas at open-sky-condition	101
Figure 4.15 Effect of bit synchronization on coherent integration output	102
Figure 4.16 Hard decision technique for navigation bit synchronization	103
Figure 4.17 Navigation data bit extraction from correlation output values, $T_{\text{coh}} = 1$ ms, $C/N_0 = \text{approx. } 40$ dB-Hz	104
Figure 4.18 Observed continuous wave interference (CWI)	106
Figure 4.19 Effects of CWI on antenna correlation outputs (a) before and (b) after frequency excision is applied	107
Figure 4.20 Code phase and Doppler tracking after frequency excision. The outliers are removed after frequency excision	108
Figure 4.21 Extended integration detection output for $T_{\text{coh}}=100$ ms, $T=5$ s	109
Figure 4.22 Extended integration detection output for $T_{\text{coh}}=200$ ms, $T=5$ s	110
Figure 4.23 Extended integration detection output for $T_{\text{coh}}=400$ ms, $T=5$ s	110
Figure 4.24 Detection output without data bit information, $T_{\text{coh}}=500$ ms, $T=5$ s	111
Figure 4.25 PSNR sampled at 20 ms over an interval of $T=6$ s. Total points=300	111
Figure 5.1 Selected indoor data collection site (a) indoor (b) sky-view plot of reference antenna	115
Figure 5.2 Orientation and sky-view plot of the dual-antenna system	116
Figure 5.3 $C/N_0$ fading plots for two antennas at indoor location using a synthetic antenna configuration	118
Figure 5.4 Cumulative distribution function for two antennas in a synthetic array configuration (with best fit Ricean pdf of $K=-28$ dB and $\rho=0.07$ , indoor location inside, $d=2.5\lambda$ , PRN-4)	120
Figure 5.5 Fading histogram during weak GNSS signal acquisition. (a) Correlation output with extended coherent integration, $T_{\text{coh}} = 200$ ms, $T = 1$ s (b) Fading histogram, indoor	121
Figure 5.6 Squared envelope correlation $\rho$ as a function of antenna spacing, indoor location	123
Figure 5.7 Deflection coefficient characteristics (a) as a function of time (b) CDF of deflection coefficient, PRN-13, $d=0.5\lambda$ , $T_{\text{coh}}=100$ ms	126
Figure 5.8 Performance evaluation as a function of antenna spacing	127
Figure 5.9 Averaged PSNR for different combining schemes as a function of coherent integration times, indoor location	129
Figure 5.10 Averaged PSNR for different combining schemes as a function of antenna spacing, indoor location, $T_{\text{coh}}= 8$ ms, $T=1$ s	130

Figure 5.11 Cumulative distribution function of PSNR at different coherent integration times, location: inside office room	131
Figure 5.12 CDF of detection output using synthetic array case, $T_{\text{coh}}=100$ ms and $T=5$ s, indoor location	133
Figure 5.13 Receiver operating curves (ROC) for single antenna and spatial diversity combining schemes (PRN 13, $d = 0.5\lambda$ , $T_{\text{coh}} = 100$ ms, $T = 300$ s)	134
Figure 5.14 Detection probability improvement over single antenna ( $P_D=0.66$ ) performance. Results are averaged over 6 available PRNs for indoor location with $P_{FA}=0.05$	135
Figure B.1 Diversity gain from dual antenna combining schemes with $P_{FA} = 0.1$ and $P_D = 0.9$ (Nielsen et al 2008)	155

## List of Abbreviations

Symbol	Definition
ASIC	Application Specific Integrated Circuit
BER	Bit Error Rate
CDF	Cumulative Distribution Function
DOF	Degrees of Freedom
ECC	Estimator Correlator Combining
EGC	Equal Gain Combining
FFT	Fast Fourier Transform
GNSS	Global Navigation Satellite System
GPS	Global Positioning System
HSGPS	High Sensitivity Global Positioning System
IF	Intermediate Frequency
LOS	Line of Sight
NLOS	Non Line of Sight
NI	National Instruments
RF	Radio Frequency
SNR	Signal to Noise Ratio
$T_{coh}$	Coherent integration time
UofC	University of Calgary

## List of Symbols

Symbol	Definition
$a_i$	Weight for antenna, $i$
$c$	Speed of light
$\mathbf{C}, \mathbf{C}_h, \mathbf{C}_x, \mathbf{C}_w, \mathbf{C}_y$	Covariance matrices
$d$	Antenna spacing
$d^2$	Deflection coefficient
$f_c$	Carrier frequency
$f_{IF}$	Intermediate frequency
$f_{Doppler}$	Doppler frequency
$h$	Channel impulse response
$H_0$	Hypothesis: Signal is not present
$H_1$	Hypothesis: Signal is present
$\mathbf{I}$	Identity matrix
$J_0(\cdot)$	Bessel's function of the first kind and order zero
$k$	Coherent integration epoch
$K_{Sat}$	No. of satellites
$M$	No. of antennas
$N_{noise}$	Average noise power per branch
$n$	Received signal sample epoch
$P_D$	Probability of detection
$P_{FA}$	Probability of false alarm
$\mathbf{s}$	Signal vector
$t$	Continuous time vector
$T$	Test statistic
$\mathbf{V}$	Eigen vector matrix
$\mathbf{v}_i$	$i$ -th eigenvector
$x$	Coherent output
$y$	Received signal
$z$	Correlation output
$\beta$	Angle of arrival
$\sigma^2$	Noise variance
$\sigma_h^2$	Channel variance
$\tau$	Time delay, code-delay
$\kappa$	Phase constant
$\theta_i$	Phase for antenna, $i$
$\xi$	Mean SNR
$\gamma$	Instantaneous SNR
$\gamma'$	SNR threshold

$\gamma_s / \xi$	SNR threshold
$\rho_c$	Complex correlation
$\rho$	Correlation coefficient
$\lambda', \lambda''$	Threshold
$\lambda_i$	$i$ -th eigenvalue
$\widehat{(\bullet)}$	Estimate of $(\bullet)$
$(\bullet)^H$	Hemitian (conjugate transpose) of $(\bullet)$
$\Lambda$	Eigen value matrix
$\Omega$	SNR per antenna
$\chi_\nu^2$	Chi-square distribution of $\nu$ degrees of freedom

## **CHAPTER 1: Introduction**

### **1.1 The Indoor Detection and Positioning Problem**

The existence of NLOS signals in Global Navigation Satellite System (GNSS) severely degrades position-domain and time-domain performances of GNSS signals. This issue is directly related to degradation of positioning accuracy that results from inaccuracy in the estimation of the time-of-arrival (TOA) of signals coming from the satellite. The scenarios of urban canyons, where there are few line-of-sight (LOS) signals and indoors where there is almost no LOS signals present are quite different. This results in a performance variation in positioning accuracy as well as in time-domain or in correlation-domain accuracies. The other aspect of the problem is the detection of GNSS signals in mixed LOS/non-LOS and completely non-LOS environments. Signal detection and positioning performances are closely interlinked with each other because in order to have a position solution, satellites with a reasonably good signal-to-noise ratio (SNR) have to be acquired first and tracked. Also, in the case of cold-start the problem is first to use a binary hypothesis to check whether there are any GNSS signals present or not. The problem soon moves to a multiple-hypothesis problem of satellite selection over the Doppler and code-phase dimensions. In addition to this, the GNSS channels are unknown and they are quite different from ordinary point to point wireless communications. This is because the signals received from satellites suffer from Doppler both when the receiver is in static and dynamic modes. This is why in order to have an improved indoor positioning solution, research into the detection performance and characterization of GNSS channels in degraded and indoor environments is necessary.

## **1.2 Indoor GNSS Challenges**

GNSS suffers from the following fundamental limitations when used indoors:

Accurate detection of GNSS signals is very difficult because GNSS signals indoors suffer from attenuation and fading. This ultimately leads to the need for improved SNR of signals when indoor situations are considered (Watson 2005).

In the GNSS research and development community, there has always been a challenge to overcome these limitations and to develop receivers that provide better performance indoors, especially in terms of better TOA estimation accuracy and SNR improvement so that the signal detection and positioning problems indoors become gradually resolved.

That is why for such situations in the indoors, when an SNR is predefined as the working SNR, the performance is generally bounded by the Cramer-Rao lower bound (CRLB) of TOA estimation. The initial step in this procedure is to understand the reasons for the receiver performance degradation. The two basic limitations are briefly reviewed in the remainder of this section. Interested readers who are not familiar with GNSS technology can consult the review of GPS fundamentals in any textbook dealing with GNSS technology. For instance, a comprehensive resource for GPS information includes Parkinson & Spilker (1996), Kaplan (1996), and Misra & Enge (2006).

### **1.2.1 Multipath Propagation Errors**

Multipath errors in GPS systems are one fundamental issue that has to be mitigated with special care. The GPS relies on LOS propagation between satellites and users in order to ensure accurate ranging and therefore positions. The signal propagates at the speed of light. This makes the GPS fundamentally a timing system. The concept of GPS is

different from that of conventional digital communication systems in that for the purpose of digital communications, the measure of success is the bit error rate (BER) encountered at the receiver, which overlooks the effects of propagation paths as long as a desired BER is achieved in the receiver (Watson 2005). However, with GPS, an error in TOA estimation is added due to the effects of NLOS signal propagations. Such a phenomenon adds a timing error and therefore compromises positioning accuracy (Watson 2005).

The GPS LOS signal propagation channel consists of free space and Earth's atmosphere. GPS timing error effects, which are not insignificant for metre-level positioning even on the LOS channel, have already been modelled by many researchers and can be largely mitigated using existing receiver technologies and techniques (Watson 2005). For details, interested readers are referred to Ray (2000) and Parkinson & Spilker (1996). For instance, the use of dual-frequency receivers mitigates ionospheric effects; single- and double-differencing methods largely mitigate tropospheric, orbital, and clock errors (Watson 2005, Lachapelle 2006). What is left are the remaining significant errors due to NLOS propagation and receiver noise (Watson 2005). The effect of NLOS propagation is collectively referred to as *multipath propagation errors*. When the outdoor is considered, NLOS signal propagation effects can be insignificant to severe depending on the circumstances. Minor low-power reflections may be considered as insignificant when strong LOS signals are simultaneously present (Watson 2005). On the other hand, in the worst cases where only a reflected signal is available, positioning is severely affected. These are two extreme circumstances that can be found outdoors. Most outdoor scenarios are somewhere in between these two extreme circumstances. Thus outdoors, a varying

degree of position degradation is found because of the various combinations of LOS and NLOS signals available (Watson 2005). Apart from this scenario, there is a high likelihood of NLOS propagation effects in indoor environments. Often, there is no LOS signal available at all indoors due to obstruction by various building materials, such as thick concrete, metal, or other obstructive media. In addition to this, the large number of surrounding objects available indoors cause reflections and scattering. The complex nature as well as wide variation of different indoor environments have made the characterization of NLOS propagation effects indoors difficult to achieve (Watson 2005).

### **1.2.2 Signal Attenuation and Fading**

Assuming a GPS receiver antenna with hemispherical gain pattern, the minimum received signal level of the GPS signal under open-sky conditions is defined as -160 dBW for the L1 coarse/acquisition (C/A) code (ICD200C 2000, Watson 2005). The power is then spread over an equivalent bandwidth of approximately 1 MHz by a spread spectrum (SS) or direct sequence code division multiple access (DS-SS) technique. This DS-SS spreading of power leads to a peak power spectral density (PSD) near -220 dBW/Hz. This is significantly lower than the average radio frequency (RF) noise levels of about -204 to -208 dBW/Hz (Parkinson & Spilker 1996, Pritchard 1997, Ray 2007). This requires a significant processing gain in order to extract GPS signals from the noise even under ideal conditions (Watson 2005). Indoor signal levels are weaker than those received outdoors principally because of the fact that propagation through building materials induces an attenuation in the range from 0 dB to 30 dB or even more on LOS signals, depending on specific indoor scenarios. In addition, in indoor situations the interference received between multiple NLOS signals causes fading. Indoors, as the

signal travels through roofs, walls, windows or other obstacles en route to the receiver, a portion of the signal energy is lost due to reflection, refraction, and diffraction by indoor scatterers and energy absorption by building construction materials (Hu 2006). Stavrou & Saunders (2003) reported that factors like signal frequency, position and nature of buildings and their internal construction as well as construction materials can influence the radio wave propagation from outdoor to indoor. However, the findings in Stavrou & Saunders (2003) were obtained through simulations, and include the non-linear variation of loss with material thickness or frequency and the average predicted penetration loss versus frequency, for a windowed wall. A detailed explanation of why these effects take place was given and some contradicting issues were discussed (Stavrou & Saunders 2003). Referring to Aguirre et al (1994), Hu (2006) mentioned that the median penetration losses for propagations at 912 MHz, 1920 MHz, and 5990 MHz were 7.7 dB, 11.6 dB, and 16.1 dB, respectively. Schwengler & Gilbert (2000) reported the field test results at 5.8 GHz in a residential area in that the mean penetration loss in a residential building was found as 3.3 dB, 13.2 dB, and 16.2 dB for locations at a closed window, front and rear of the house, respectively (Hu 2006). Klukas et al (2004) reported several results of experiments conducted to study the signal penetration effects of building materials at GPS L1 frequency and found attenuations of 0.5 dB, 2.4 dB and 23 dB for gyprock, plywood and cinder blocks, respectively. In general, fading is particularly detrimental to GPS signal reception because characteristics of the propagation environment make the signal level highly variable. When strong multipath signals are received, deep and long lasting fades can take place because of the geometry of the

propagation environment. As a result, environmental geometry also has an impact on indoor GNSS signal fading (Watson 2005).

### **1.2.3 Approaching the challenges**

Given that GNSS signals suffer from severe conditions in the indoors, it is very important that an understanding be developed about the NLOS indoor characteristics of the GNSS receivers in order to improve their performance indoors. Receiver performance and channel characteristics are both important to consider before testing and implementing any new algorithms. New algorithms must be developed and tested to improve detectability of GNSS signals indoors. Since GNSS channels indoors incorporate signal attenuation and fading effects, research should aim at improving the SNR of received GNSS signals. Results of some early experiments to increase the integration time with high-sensitivity GPS (HSGPS) receiver in order to obtain a higher SNR was first reported by Peterson et al (1997). The performance of HSGPS receivers under various degraded GPS environments were also studied by MacGougan et al (2002), MacGougan (2003), Cannon et al (2003), and Lachapelle et al (2003). Hu (2006) reported on the replication of GPS signals in indoor environments using a hardware simulator, the results being backed by several field tests with real GPS data. The research in Hu (2006) mainly studied the characteristics of measured degraded GPS signals from selected environments, followed by a validation in terms of the correlation coefficient between the simulated and field results.

In this thesis, a two-antenna GPS receiver system has been considered and a new scheme using spatial diversity with two GPS receivers for improving signal detectability indoors is introduced.

## **Modern Technologies**

A certain number of technologies have been developed to overcome the limitations of indoor GNSS and to improve its overall performance in the signal acquisition and tracking domain. Improvement in post-correlation SNR (PSNR) is the primary target of such research (Shanmugam 2008). High-sensitivity GPS (HSGPS) and assisted GPS (AGPS), pre-detection-differential and post-detection-differential combining are among the modern technologies that have been developed so far. Using spatial channel information, more commonly known as ‘space diversity’, to combine GNSS signals spatially is the technique that is the subject of the research presented in this thesis.

## **Spatial Diversity**

The concept of spatial resource i.e. ‘spatial diversity’ is new in GPS for it to achieve better post-correlation SNR. The concept of spatial diversity has been successfully used in standard wireless communications for a long time. Spatial diversity in transmitter and receiver sides in standard wireless communication is commonly known as multiple-input-multiple-output (MIMO) communication systems. For example, spatial diversity has been broadly covered in Haykin (2001). Diversity techniques in  $N \times M$  dimensional receivers are discussed in Van Trees (Part-1, 2001). Space-time wireless systems have also been extensively discussed in Bolcskei et al (2006). However, the application of spatial diversity to GNSS appears to be new. The use of multiple antennas, better known as multiple-receiver processing, exploits receiver antenna space diversity to improve receiver performance at the GNSS signal detection level. When GPS signals are received with multiple receiver channels, the receiver antennas experience mostly independent fading which, after some signal processing techniques, provides significant gain in terms

of SNR as shown in the results section. Multiple spatially separated antennas receive uncorrelated faded signals. The plane wave arriving from the satellites at the receiver antenna is subject to independent fading behavior in the receivers that are spatially apart by a certain distance from each other. The independent fading statistics are used to mitigate noise and so to increase SNR at the receiver, which ultimately increases the ‘detectability’ of GNSS signals in any environment. For instance, multiple GNSS antenna signal processing can be performed using equal-gain (EG) and estimator-correlator (EC) combining algorithms and this yields a higher detection output and correspondingly higher PSNR. Propagation channels can be analyzed in terms of fading distribution with the help of cumulative distribution functions and diversity combining gain can be achieved from multiple antennas. This fact brings about many potential benefits that can be achieved from using a multiple-antenna GPS receiver system. Potential benefits may include improved signal detection capability as equally important as position-domain performance. The following sections outline the optimum multi-antenna detection of GPS signals, as they apply to the research conducted herein. For a LOS satellite signal, the latter is correlated among multiple antennas and it is less likely that all receiver antennas will experience deep fades at the same time. As a result, signal combining with spatially apart antennas will provide much SNR gain by reducing the noise floor and increasing the signal value. For a PRN that is unavailable at that location at that instant of time, the signal combining from multiple receivers provides reasonable SNR improvement by reducing the noise floor. In fading environments, for instance indoors, the uncorrelated signal reception is achieved by spacing the antenna elements at least one half wavelength apart; in fact, the required antenna separation depends on the spatial coherence of the

indoor channel, which may be greater than half a wavelength (O'Driscoll & Lachapelle 2007, Pratt 2000). Often multipath signal is also correlated over longer distances.

### **1.3 Research Overview**

#### **1.3.1 Motivation and Limitations of Previous Research**

The degradation of SNR indoors for GNSS signals is the overarching motivation for this research. To exploit the spatial information of GNSS signals using multiple antenna arrays for SNR improvement is the principal objective of the thesis. The characterization and information theoretical analysis of antenna array reception for the GPS L1 channel is another motivation for this thesis.

In satellite-based navigation and positioning systems, received signal power on the earth is very low even under open sky condition (Tsui 2005). When the GPS receiver is taken indoors, due to the unavailability of LOS signals and also reflections from the several reflectors, the received GPS signal is attenuated. So, it becomes very hard to detect GPS signals in weak and degraded signal conditions, which ultimately causes poor detectability. Though several authors have illustrated pre-correlation and post-correlation combining of GPS L1 signals (e.g. Shanmugam et al 2005), all of the combining algorithms used a single antenna. In this research, the use of spatial diversity is proposed for a GPS receiver with the realization of a 2-element GPS receiver array antenna system in order to provide SNR gain at the post-correlation level. It will be shown that gain improves by four to five dB typically when two antennas are used. This SNR improvement is obtained after averaging the SNR improvements over a variety of locations. This will ultimately be useful for weak signal tracking indoors and in degraded

signal conditions such as in urban canyons. The overall objective is to improve the detectability by combining the complex correlation signals. In this research several post-correlation combining methods are explored in relation to improving the SNR at the post-correlation level. At the same time multiple GPS receivers can provide means to combat multipath. While measurements for single GPS antennas are well documented in the literature, there are a very few sources (e.g. Backén 2007) that discuss channel impulse response (CIR) measurements based on multiple antennas for GPS L1 band signal reception. Backén (2007) mainly proposes an ASIC based live GPS data collection and processing scheme using GPS antenna array. Since the satellites are moving in a particular orbit, the estimation accuracy in estimation of the Doppler shift is an issue to consider. Though there is a large body of literature regarding CIR measurements for MIMO wireless systems at different frequencies, generally these are point-to-point measurements and not applicable to the indoor GPS single-input-multiple-output (SIMO) GPS case. In addition, considering the correlation between the two antenna elements the estimator-correlator (EC) based GNSS signal processing should also be useful in this case because it provides an idea of how much the SNR can improve for correlated GPS signals due, for example, to close antenna spacing (e.g. in  $d < 0.5 \lambda$  cases).

### **1.3.2 Objectives and Novel Contributions**

The primary objective of the present research is to develop an optimum spatial post-correlation signal processing and detection algorithm using a signal combining technique for multiple-antenna array GPS receivers in different types of LOS and NLOS environments. This is achieved through the use of multi-antenna array GPS receiver,

which has been implemented in hardware, at different antenna spacing to exploit spatial information of the channels. In addition, to investigate different new spatial signal combining algorithms at the post-correlation level for GPS L1 band signals in different types of environments are considered and this constitutes the secondary objective of this thesis.

The major objectives are summarized as follows:

1. To propose a practical post-correlation signal combining detection algorithm under multipath environments using spatial diversity of GNSS receivers
2. To apply spatial diversity combining using multiple antennas and to compare the performances of GPS antenna array receivers for equal-gain and estimator-correlator (EC) based diversity combining algorithms in multipath environments. This will also include the development of spatial covariance matrix for GPS L1 band receiver channels using the single antenna and multiple antennas and an eigen-analysis of the receiver channel covariance matrices.
3. To assemble an actual hardware platform for realizing the GPS antenna array system using two front-ends and a data-collection scheme
4. To study spatial combining performances for different GPS antenna spacing. As part of this objective, a software program is developed to implement the proposed algorithm and verify it with actual measured field data. For this research, selected NLOS indoor locations have been considered for the data collection. Assistance has been provided by using a reference antenna located at rooftop with unobstructed view of the sky. Collected field data have been further processed with the software algorithm thus developed.

To implement the above objectives, the following issues are addressed.

- The two GNSS receiver front-ends must be time-synchronized. This is ensured by driving the individual front-ends with on-board clocks, as developed in *National Instruments (NI)* based data collection system setup. The different channels of the *NI* system are time-synchronous.
- The antenna gain patterns do not matter for this research work. This is because the tests deal with uncorrelated multipath signal that appears all over the Poincaré polarization sphere. The Poincaré sphere, conceived around 1892 (Wikipedia 2008), provides a convenient way of representing polarized electromagnetic (EM) waves. To have an easy understanding of polarization, polarization states are often specified in terms of the polarization ellipse, specifically its orientation and elongation. A common parameterization uses the azimuth angle and the ellipticity (the ratio of the two semi-axes). An ellipticity of zero corresponds to linear polarization and an ellipticity of 1 corresponds to circular polarization. Thus the two poles – upper pole and lower pole – of Poincaré sphere represent left and right-circularly polarized EM wave respectively. Points on the equator indicate linear polarization. Other points on the sphere represent elliptical polarization. The description of Poincaré sphere is well known in the area of electromagnetic wave propagation. In addition to that, it can also be said that if the antennas are different in terms of polarization, for instance, for two orthogonally polarized GNSS antennas that are collocated, it is possible to have the benefits equivalent to spatial diversity.

- Although the phase of radio frequency (RF) wave is related to the cable length through which the wave propagates, the phase differences between the two receiver antennas do not matter here. This is because phase differences become part of correlation matrices and are taken care of by the correlation matrices for further signal processing.
- To test the spatial combining algorithm in indoor locations, at first the synthetic array configuration has been used for the received signal. The performance is later verified by two indoor antennas separated by a given antenna spacing.

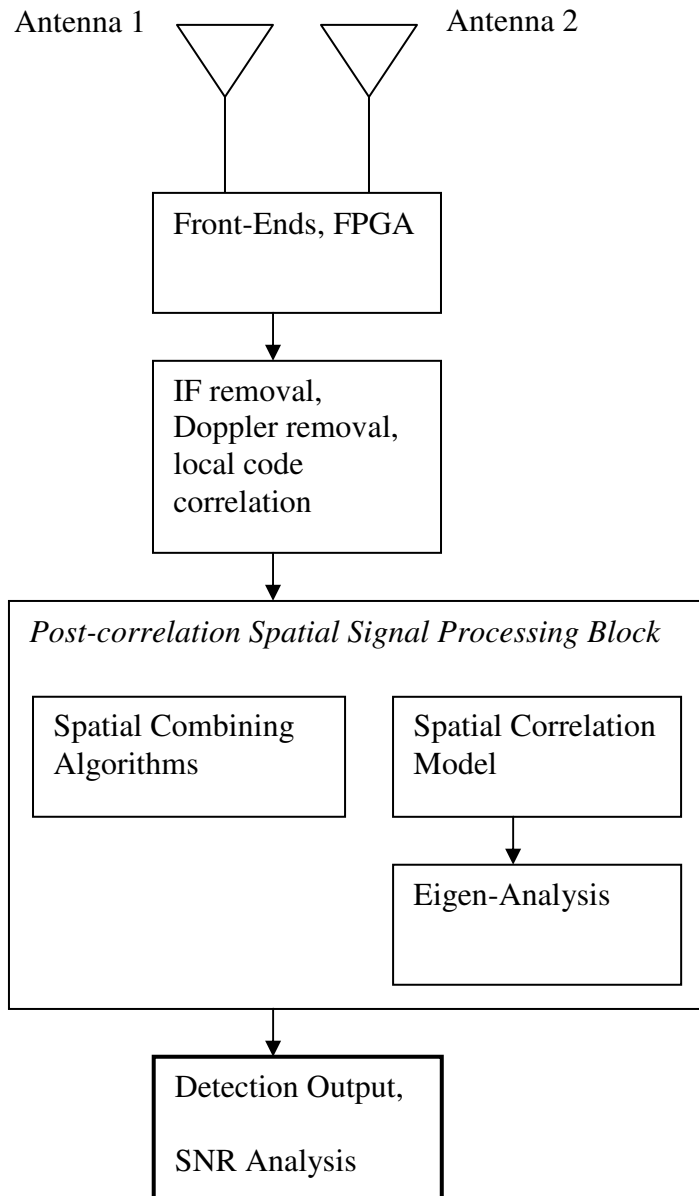


**Figure 1.1: Flowchart of GPS Antenna Array Receiver Signal Processing**

The proposed spatial combining of GNSS signals consists of the following steps.

Firstly, real-time GPS raw in-phase and quadrature-phase samples are collected using two receiver front-ends spatially apart by some distance. Secondly, the effects of intermediate frequency (IF) and Doppler are removed from the data and then the correlation matrix for

the two receivers using locally generated code are obtained. The correlation matrix is the basic asset for this research. The above correlation matrix procedure is carried out in NLOS locations and the correlation matrix is thus averaged over several spatial locations. As a third step, the post-correlation signal processing block mainly does the major work of spatial signal combining and spatial channel analysis. Two main tasks are done in this section. Post-correlation signal combining techniques are tested with real data. In the final stage, detection outputs are considered as a criterion of algorithm testing and thus SNR analyses are made to compare the performance of multiple-antenna spatial combining of GPS L1 signals as compared to the single receiver case. The probability of detection for a given probability of false alarm is evaluated in this case.

### **1.3.3 Thesis Outline**

The thesis is organized as follows: Chapter 2 provides with a brief description of spatial diversity for GNSS signals. The discussion is followed by Chapter 3 describing spatial diversity combining of weak GNSS signals. Chapter 4 provides the description of test methodology and GNSS signal processing as well as some intermediate results.

Correlation properties of dual-antenna GPS receiver system, its detection performance and SNR gain using spatial combining have been described in Chapter 5. Finally, Chapter 6 presents conclusions and recommended future works. Two appendices provide some fundamental and necessary background information necessary for a full understanding of the methodology used in the thesis.

## CHAPTER 2: Spatial Diversity for GNSS Signals

A GPS L1 band signal is an electromagnetic radio wave that is transmitted at L1 band carrier frequency of 1575.42 MHz. The GPS is one of the presently available GNSS. To understand spatial diversity for GNSS and the performance of spatial combining of GNSS signals, it is first important to understand electromagnetic signal reception by an array of GNSS antennas. This chapter begins with a brief description of electromagnetic wave reception with a multi-antenna GNSS receiver system. Subsequent spatial signal combining methods as well as the criteria for performance evaluation for multi-antenna GNSS receiver system are described next.

### 2.1 Background and Importance of GNSS Multi-Antenna Signal Reception

Most GPS receivers utilize the signals from a single antenna and this has been adequate for many non-integrated system solutions (Pratt 2000). On the other hand, according to Nyquist's spatial sampling theorem, when multiple antennas are used for signal reception, the GNSS faded signals received are independent from each other if the spacing between GNSS antennas is greater than half the wavelength of the carrier frequency (Intarapanich et al 2004, Park & Min 2005). Multi-antenna GNSS signal reception is very promising in order to have positioning solution in weak and multipath-rich signal environments e.g. indoors. The performance of multiple receivers for mitigation of carrier phase multipath errors has already been shown in Ray (2000). In order to extract the advantages from using multiple GPS antennas, improved multi-antenna signal processing has to be adopted (Pratt 2000). Though multiple antenna GPS systems are in use in land survey GPS receiver systems, attitude determination systems,

controlled reception pattern antenna (CRPA), the use of spatial diversity with multiple GPS receivers for improving signal detectability in weak and degraded signal environments is a new area in GNSS research. On the other hand, successful acquisition and tracking of weak GNSS signals requires longer integration times and correct multipath detection and rejection capability (Dedes & Dempster 2005). With weak signals, the SNR is too low to support the extraction of the 50 bits/s navigation message from the signal (Bryant et al 2001). While the technical issues confronting indoor GPS have been discussed in Van Digglen & Abraham (2001), some aspects on measurements of GPS signals indoors have been well discussed from a correlation domain perspective in Peterson et al (2001). From an interference point of view, however, due to extremely weak received signal power, the GNSS receiver design must take into account the effect of RF interference from either intentional or unintentional sources. It is well known that these interferers can severely impair synchronization performance of the receiver (Kim & Iltis 2004). Space-time adaptive processing (STAP) has been well documented in Kim & Iltis (2004) and Melvin (2004).

After signal processing at each receiver antenna, the post-correlation signal combining provides for SNR improvement and better signal detection. Spatial correlation between two antenna elements in a multi-antenna system is a well-known concept for point-to-point wireless communication. The spatial correlation is a function of the antenna element distance, array geometry, radiation pattern and signal distribution (Park & Min 2000). The use of spatial diversity in traditional wireless communications has been addressed in several available texts, e.g. in Stuber (2000) and Rappaport (2002).

However, the hardware complexity of the GNSS receivers did not interest researchers in

using multiple GNSS receivers for signal detection problem. But in recent years the size of GNSS antennas has been reduced to an extent that is interesting to study the performance of GNSS antenna array for multiple GPS receiver systems. This research investigates into the spatial diversity signal combining of multiple GPS antennas for weak and mixed signal conditions.

## **2.2 GPS Signal Reception by Uniform Linear Array (ULA) Antenna**

Figure 2.1 below shows the conceptual diagram of GPS signal reception with a uniform linear array (ULA) antenna. The satellite is the transmitting source and, considering the long paths of the transmitted signals as compared to the antenna array dimensions, the signals coming from the satellite are considered as plane waves. It is assumed that the antenna array consists of  $M$  identical elements and receives signals from  $K_{Sat}$  satellites. Each satellite is moving in a particular orbit and every transmitted signal comes from a particular direction. While deriving the mathematical formulations, only one transmitting satellite is considered, i.e.  $K_{Sat}=1$  is assumed. Later the algorithm is tested for all available PRNs to have an average performance evaluation. So, accordingly the antenna array consists of  $M$  identical elements and each of the elements receives signals from a single satellite in a direction  $\beta_1$ .

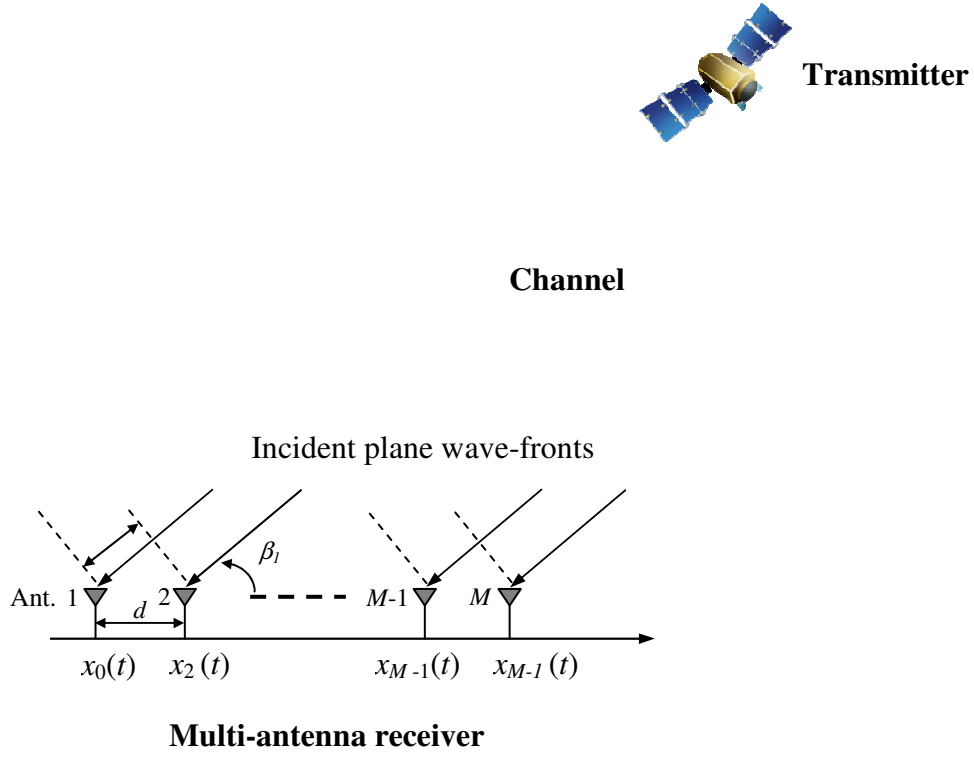


**Figure 2.1 GNSS signal reception using a uniform-linear-array (ULA) antenna**

If the first element is taken as a reference point and the signal from the satellite is base-band, the output data of the array is an  $M \times 1$  complex vector. For the signal source, the array output vector can be expressed as

$$x(t) = \begin{bmatrix} x_1(t) \\ x_2(t) \\ \dots \\ x_M(t) \end{bmatrix} = \begin{bmatrix} s_1(t) \\ s_1(t - \tau) \\ \dots \\ s_1(t - (M - 1)\tau) \end{bmatrix} + \begin{bmatrix} w_1(t) \\ w_2(t) \\ \dots \\ w_M(t) \end{bmatrix} = \begin{bmatrix} 1 \\ e^{-j2\pi f_c \tau} \\ \dots \\ e^{-j2\pi f_c (M-1)\tau} \end{bmatrix} s_1(t) + \begin{bmatrix} w_1(t) \\ w_2(t) \\ \dots \\ w_M(t) \end{bmatrix} \quad (2.1)$$

$$= \mathbf{a}(\beta_1) s_1(t) + \mathbf{w}(t)$$

where  $\mathbf{a}(\beta_1) = \left[ 1, e^{-j2\pi f_c \tau}, \dots, e^{-j2\pi f_c (M-1)\tau} \right]^T$  is an  $M \times 1$  vector called the *array*

*direction vector*, the symbol ( $^T$ ) denotes the transpose,  $f_c$  is the carrier frequency of the

incident signals,  $\tau = \frac{d \cos(\beta_1)}{c}$  is the delay between two elements, where  $d$  is the spacing between two antenna elements,  $\mathbf{w}(t)$  is the  $M \times 1$  complex noise vector. The noise at different antenna elements can be either *independent and identically distributed (i.i.d.)* zero-mean Gaussian stationary random process or correlated depending on its source of radiation. It is known that the spatial correlation between signals received at two antenna elements is related to the spatial structure of the antenna array, the direction of arrival of the satellite signal, mutual coupling between two antenna elements and individual antenna gain pattern. Each of these parameters plays a decisive role in the analysis. The spatial correlation, mutual coupling as well as some design considerations regarding antenna array have been discussed in Pozar (1990).

### 2.3 Diversity Technology for GNSS

Diversity in GNSS is a technique by which the multipath GNSS signals inherently present in a GNSS receiver are combined in order to mitigate fading and improve the overall quality of GNSS signal detection. Diversity is a common technique for standard wireless devices. However, the concept of spatial diversity is comparatively new in GNSS. The basic principle of diversity is that the receiver combines more than one version of the transmitted signal, where each version is received through a different path or branch (Gao 2007). Figure 2.2 illustrates two uncorrelated Rayleigh fading signals and the combined signal.

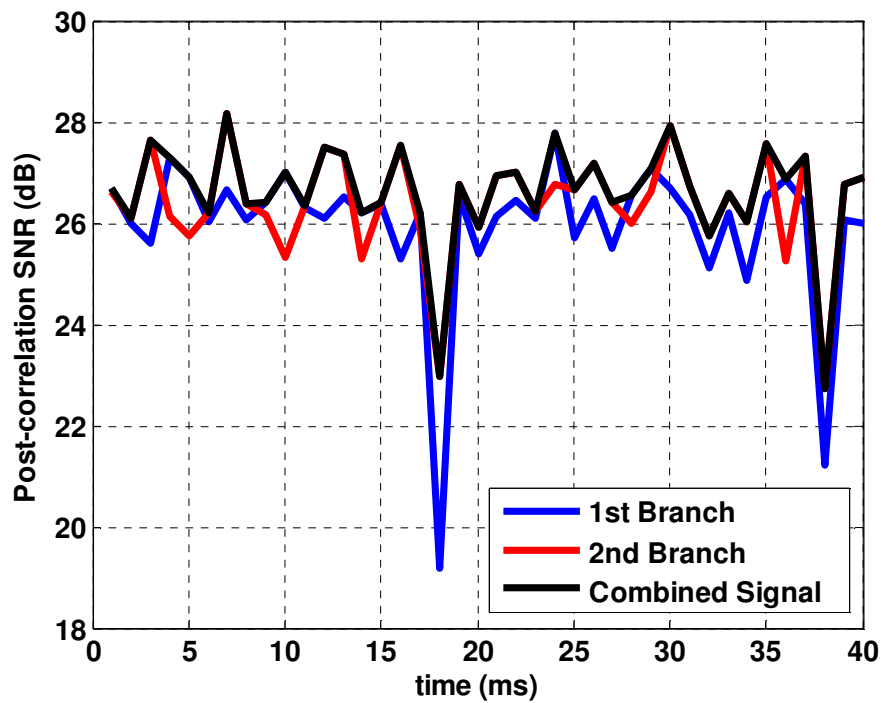


**Figure 2.2 Illustration of two individually received signals and the concept of signal combining by diversity technique. The combined signal always has higher SNR compared to the individual branch signals.**

For two uncorrelated faded signals, it is rare that both signals will be in a deep null due to deep fading at the same time. Figure 2.2 shows that the combined signal has a higher mean SNR at the correlator output when compared to a single branch. The effectiveness of a diversity system is measured by a quantity known as the diversity gain (Gao 2007), which is defined as the SNR improvement by using diversity signals as compared to a single version of the signal received with a single antenna for a given cumulative probability. There are several ways of achieving independent fading paths in a GNSS system, such as frequency diversity, time diversity, and antenna diversity. However, the focus of this thesis is on spatial or antenna diversity, which can be regarded as a measure of effectiveness for multiple receiver antennas spatially separated from one another. The principal focus is on the acquisition of GNSS signals.

#### **2.4 Spatial Diversity Techniques**

As mentioned earlier, spatial diversity techniques exploit the spatial resource using multiple antennas. Spatial diversity is also known as *diversity antennas* or *antenna diversity* as shown in Figure 2.3. The arrangement of multiple antennas to receive multiple signals with uncorrelated fading and the subsequent signal combining at the receiver are the most important issues in spatial diversity. These aspects of spatial diversity are briefly discussed herein.



Channel

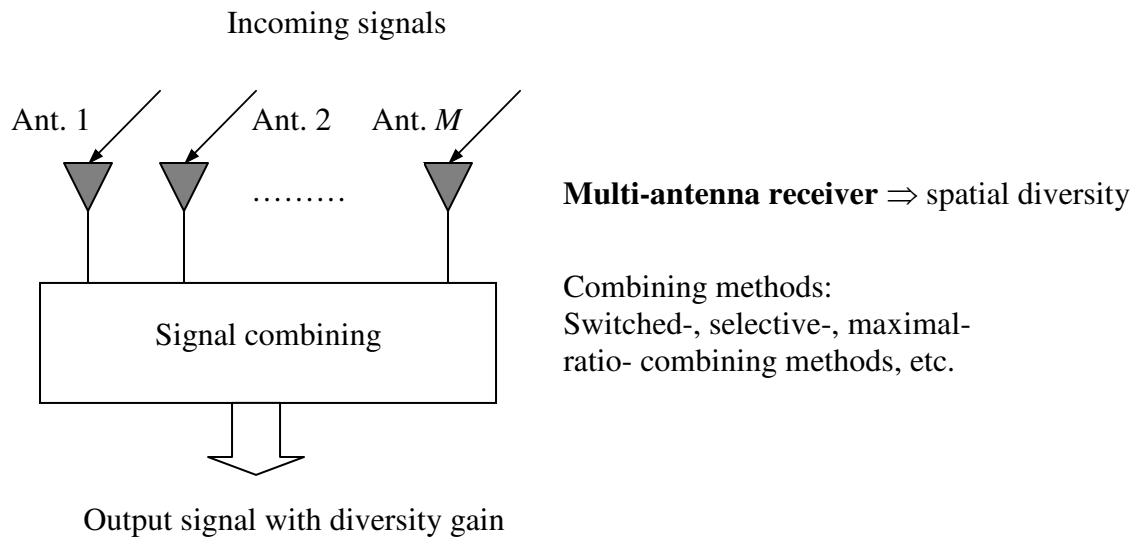


**Figure 2.3 Flow chart of spatial diversity technique**

Multiple antennas are separated from each other spatially to achieve independent fading paths. Due to the spatial separation, i.e. antenna spacing, between two antennas, the relative phase of the multipath signal is significantly different at both antennas. The distance between two antennas usually has a minimum spacing requirement depending on different fading environments such that sufficient decorrelation can be achieved (Jakes 1994, Gao 2007).

Research work on the spatial diversity on a GNSS receiver has been carried out in this thesis. In the following the traditional mathematical formulation for spatial correlation between two antennas is derived assuming GNSS multi-antenna signal reception. Let us first consider a GNSS antenna located at a position  $x$  on a plane. Also, let us consider another GNSS antenna at a distance  $\Delta x$  from the first antenna. The electromagnetic wave coming from the satellite is considered a *plane wave*. The received signal envelopes for the two antennas are  $\varphi_0 = |y_0|$  and  $\varphi_1 = |y_1|$  respectively, where  $y_0$  and  $y_1$  are the received complex signals on the first and second antenna, respectively. Suppose that the separation between the antennas in space is  $\Delta x$ . The correlation between the two GNSS antennas can now be expressed as

$$\rho(\Delta x) = E[\varphi_0(x)\varphi_1(x + \Delta x)]. \quad (2.2)$$

For a short proximity of the two antennas and assuming that the wireless channel does not vary much in a short duration of time, we can use the concept of synthetic antenna array to derive the expression of antenna correlation. Figure 2.4 shows the antenna position at  $x$  and  $\Delta x$  with respect to the incoming signal. With the synthetic array concept, it is understood that both  $\varphi_0(x)$  and  $\varphi_1(x + \Delta x)$  corresponding to the two receive antennas can be thought of being collected by a single antenna sequentially at two non-overlapping time intervals. It is reasonable to assume that in such a case the fading experienced by the same antenna at two locations would be uncorrelated, which is equivalent to capturing signals with two antennas at the same time instant. So, one can write equivalently

$$\begin{aligned} \rho(\Delta x) &= E[\varphi_0(x)\varphi_1(x+\Delta x)] \\ &\equiv E[\varphi_0(t)\varphi_0(t+\Delta t)] \end{aligned} \tag{2.3}$$

where the spatial separation between the antennas is  $\Delta x = v \cdot \Delta t$ , assuming that the antenna takes  $\Delta t$  time to move from the first position  $x$  to the second position  $(x + \Delta x)$  at a velocity  $v$ .

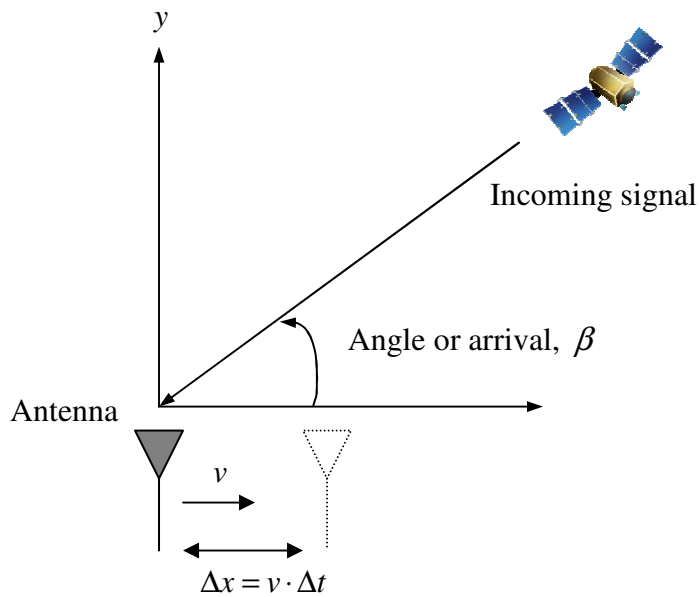


**Figure 2.4 Plane wave incident from a satellite at a GNSS receiver**

Since the synthetic array concept is assumed,  $\rho(\Delta x)$  eventually becomes the auto-correlation of the envelope  $\varphi_0$  received by the first antenna, which can be expressed as

$$\begin{aligned}\rho_{\varphi_0\varphi_0}(\Delta t) &\equiv E[\varphi_0(t)\varphi_0(t+\Delta t)] \\ &= \frac{\pi}{2} |\rho_{GG}(0)| F\left[-\frac{1}{2}, -\frac{1}{2}; 1, \frac{|\rho_{GG}(\Delta t)|^2}{|\rho_{GG}(0)|^2}\right]\end{aligned}\quad (2.4)$$

where  $F[\cdot, \cdot; \cdot, \cdot]$  is the hypergeometric function expressed as

$$F\left[-\frac{1}{2}, -\frac{1}{2}; 1, x\right] = 1 + \frac{1}{4}x + \frac{1}{64}x^2 + \dots\quad (2.5)$$

However, a useful approximation according to Stuber (2000) yields

$$\rho_{\varphi_0\varphi_0}(\Delta t) \approx \frac{\pi}{2} |\rho_{GG}(0)| \left[ 1 + \frac{1}{4} \frac{|\rho_{GG}(\Delta t)|^2}{|\rho_{GG}(0)|^2} \right].\quad (2.6)$$

where  $\rho_{GG}(\Delta t)$  is the autocorrelation of the received complex envelope

$G(t) = G_I(t) + jG_Q(t)$ . Equation (2.6) is the expression for the antenna correlation. In

order to compute (2.6) in the well-known form of Bessel functions, it is necessary to

compute  $|\rho_{GG}(\Delta t)|^2$  as

$$|\rho_{GG}(\Delta t)|^2 = \rho_{G_I G_I}^2(\Delta t) + \rho_{G_I G_Q}^2(\Delta t).\quad (2.7)$$

Here  $\rho_{G_I G_I}(\Delta t)$  and  $\rho_{G_I G_Q}(\Delta t)$  are the real and imaginary parts of  $\rho_{GG}(\Delta t)$  respectively.

The computation of  $|\rho_{GG}(\Delta t)|^2$  is first derived as follows, which after being inserted into

(2.6) gives the well-known expression of antenna correlation in the form of a zero-order

Bessel function of the first kind  $J_0(\bullet)$ .

The received signal  $y_0 = G(t)$  can be expressed as inphase and quadrature-phase

components as

$$y_0(t) = G_I(t) \cos 2\pi f_c t - G_Q(t) \sin 2\pi f_c t \quad (2.8)$$

$$G_I(t) = \sum_{n=1}^N C_n \cos \psi_n(t)$$

$$G_Q(t) = \sum_{n=1}^N C_n \sin \psi_n(t)$$

where  $f_c$  is the carrier frequency,  $C_n$  and  $\psi_n$  are the amplitude and the phase of the  $n$ -th component of the signal respectively. The autocorrelation function of  $y_0 = G(t)$  is

$\rho_{y_0 y_0}(\Delta t) = \rho_{GG}(\Delta t)$ . Assuming  $y_0$  to be a wide-sense-stationary process, its

autocorrelation becomes

$$\begin{aligned} \rho_{y_0 y_0}(\Delta t) &= \rho_{GG}(\Delta t) \quad (2.9) \\ &= E[y_0(t) y_0(t + \Delta t)] \\ &= E\left[\left\{G_I(t) \cos 2\pi f_c t - G_Q(t) \sin 2\pi f_c t\right\} \right. \\ &\quad \left. \left\{G_I(t + \Delta t) \cos 2\pi f_c(t + \Delta t) - G_Q(t + \Delta t) \sin 2\pi f_c(t + \Delta t)\right\}\right] \\ &= E[G_I(t) G_I(t + \Delta t)] \cos 2\pi f_c \Delta t - E[G_Q(t) G_Q(t + \Delta t)] \sin 2\pi f_c \Delta t \\ &= \rho_{G_I G_I}(\Delta t) \cos 2\pi f_c \Delta t - \rho_{G_Q G_Q}(\Delta t) \sin 2\pi f_c \Delta t \end{aligned}$$

where  $\rho_{G_I G_I}(\Delta t) = \rho_{G_Q G_Q}(\Delta t)$  and  $\rho_{G_I G_Q}(\Delta t) = \rho_{G_Q G_I}(-\Delta t)$ .

Now, due to the long distance from the receiver to the transmitting satellite in space, the radio propagation environment can be considered as two-dimensional. As the antenna moves at a velocity of  $v$  to a second position at a distance  $\Delta x$ , the Doppler introduced in the receiver is given by  $f_D = f_m \cos \beta$  Hz, where  $f_m = v / \lambda_c$  is the maximum Doppler frequency when  $\beta = 0$  and  $\lambda_c$  is the wavelength of the incoming plane wave. The phases  $\psi_n$  in  $G_I$  and  $G_Q$  are assumed to be uniformly distributed over  $[-\pi, \pi]$ . Using these properties, the autocorrelation of  $G_I$  is (Stuber 2000)

$$\begin{aligned}
\rho_{G_I G_I}(\Delta t) &= E[G_I(t)G_I(t + \Delta t)] \\
&= E\left[\left\{\sum_{n=1}^N C_n \cos \psi_n(t)\right\}\left\{\sum_{n=1}^N C_n \cos \psi_n(t + \Delta t)\right\}\right] \\
&= E_{\Delta t, \beta}[G_I(t)G_I(t + \Delta t)]
\end{aligned} \tag{2.10}$$

where

$$\begin{aligned}
\Delta \mathbf{t} &= (\Delta t_1, \Delta t_2, \dots, \Delta t_N) \\
\beta &= (\beta_1, \beta_2, \dots, \beta_N) \\
\bar{\mathfrak{U}} &= E[G_I^2(t)] + E[G_Q^2(t)] = \sum_{n=1}^N C_n^2
\end{aligned} \tag{2.11}$$

for  $n = \{1, 2, \dots, N\}$ . Here,  $\bar{\mathfrak{U}}$  is the total received envelope power. Finally, it becomes

$$\begin{aligned}
\rho_{G_I G_I}(\Delta t) &= \frac{\bar{\mathfrak{U}}}{2} E_{\beta}[\cos 2\pi f_D \Delta t] \\
&= \frac{\bar{\mathfrak{U}}}{2} E_{\beta}[\cos(2\pi f_m \cos \beta \Delta t)]
\end{aligned} \tag{2.12}$$

And, in a similar way, it is found that

$$\begin{aligned}
\rho_{G_I G_Q}(\Delta t) &= E[G_I(t)G_Q(t + \Delta t)] \\
&= E\left[\left\{\sum_{n=1}^N C_n \cos \psi_n(t)\right\}\left\{\sum_{n=1}^N C_n \sin \psi_n(t + \Delta t)\right\}\right] \\
&= \frac{\bar{\mathfrak{U}}}{2} E_{\beta}[\sin(2\pi f_m \cos \beta \Delta t)]
\end{aligned} \tag{2.13}$$

However, the expectations in (2.12) and (2.13) above require that both probability distribution of incident power  $p(\beta)$  and receiver antenna gain  $G_R(\beta)$  be expressed as a function of the angle or arrival  $\beta$ . According to the well-known Clarke's isotropic two-dimensional scattering model (Clarke 1968),  $p(\beta)$  can be assumed as uniformly

distributed over  $[-\pi, \pi]$ , which provides the pdf of  $p(\beta)$  as  $p(\beta) = \frac{1}{2\pi}$  for

$\beta \in [-\pi, \pi]$  and  $p(\beta) = 0$  elsewhere. According to the same model, the receive antenna gain is assumed as  $G_R(\beta) = 1$ . As a result, (2.12) and (2.13) finally become functions of  $J_0(\bullet)$ , as shown in the following expressions:

$$\begin{aligned}
\rho_{G_I G_I}(\Delta t) &= \frac{\bar{\mathcal{U}}}{2} E_\beta [\cos(2\pi f_m \cos \beta \Delta t)] & (2.14) \\
&= \frac{\bar{\mathcal{U}}}{2} \int_{-\pi}^{\pi} \cos(2\pi f_m \cos \beta \Delta t) p(\beta) G_R(\beta) d\beta \\
&= \frac{\bar{\mathcal{U}}}{2} \frac{1}{2\pi} \int_{-\pi}^{\pi} \cos(2\pi f_m \cos \beta \Delta t) d\beta \\
&= \frac{\bar{\mathcal{U}}}{2} \frac{1}{\pi} \int_0^{\pi} \cos(2\pi f_m \sin \beta \Delta t) d\beta \\
&= \frac{\bar{\mathcal{U}}}{2} J_0(2\pi f_m \Delta t) \\
&= \frac{\bar{\mathcal{U}}}{2} J_0\left(2\pi \frac{v}{\lambda_c} \Delta t\right) \\
&= \frac{\bar{\mathcal{U}}}{2} J_0\left(2\pi \frac{\Delta x}{\lambda_c}\right)
\end{aligned}$$

$$\begin{aligned}
\rho_{G_I G_Q}(\Delta t) &= \frac{\bar{\mathcal{U}}}{2} E_\beta [\cos(2\pi f_m \cos \beta \Delta t)] & (2.15) \\
&= \frac{\bar{\mathcal{U}}}{2} \frac{1}{2\pi} \int_{-\pi}^{\pi} \sin(2\pi f_m \cos \beta \Delta t) d\beta \\
&= 0
\end{aligned}$$

This gives

$$\begin{aligned}
|\rho_{GG}(\Delta t)|^2 &= \rho_{G_I G_I}^2(\Delta t) + \rho_{G_I G_Q}^2(\Delta t) & (2.16) \\
&= \rho_{G_I G_I}^2(\Delta t) + 0 \\
&= \rho_{G_I G_I}^2(\Delta t)
\end{aligned}$$

And taking (2.7) into consideration, it becomes

$$|\rho_{GG}(0)|^2 = \rho_{G_i G_i}^2(0). \quad (2.17)$$

Using two-dimensional isotropic scattering, (2.17) becomes

$$|\rho_{GG}(\Delta t)|^2 = \{\rho_{G_i G_i}(\Delta t)\}^2 = \frac{\bar{\mathfrak{U}}^2}{4} J_0^2\left(2\pi \frac{\Delta x}{\lambda_c}\right). \quad (2.18)$$

Using (2.18), the auto-covariance function can finally be expressed as (Stuber 2000)

$$\begin{aligned} \mu(\Delta x) &= E[\rho_0(t)\rho_0(t+\Delta t)] - E[\rho_0(t)]E[\rho_0(t+\Delta t)] \\ &= \frac{\pi}{2} |\rho_{GG}(0)| \left[ 1 + \frac{1}{4} \frac{|\rho_{GG}(\Delta t)|^2}{|\rho_{GG}(0)|^2} \right] - \frac{\pi}{2} |\rho_{GG}(0)| \\ &= \frac{\pi}{8} \frac{|\rho_{GG}(\Delta t)|^2}{|\rho_{GG}(0)|} \\ &= \frac{\pi}{8} \frac{1}{\bar{\mathfrak{U}}} \frac{\bar{\mathfrak{U}}^2}{4} J_0^2\left(2\pi \frac{\Delta x}{\lambda_c}\right) \\ &= \frac{\pi \bar{\mathfrak{U}}}{16} J_0^2\left(2\pi \frac{\Delta x}{\lambda_c}\right) \end{aligned} \quad (2.19)$$

After normalization, the antenna correlation becomes

$$\frac{\mu(\Delta x)}{\frac{\pi \bar{\mathfrak{U}}}{16}} = J_0^2\left(2\pi \frac{\Delta x}{\lambda_c}\right). \quad (2.20)$$

For an antenna spacing of  $d$ , the antenna correlation between the first and second antenna elements can be expressed as

$$\rho_{12} = J_0^2\left(2\pi \frac{d}{\lambda_c}\right) = J_0^2(\kappa d) \quad (2.21)$$

where  $\kappa$  is the phase constant and is defined as  $\kappa = 2\pi / \lambda_c$ .

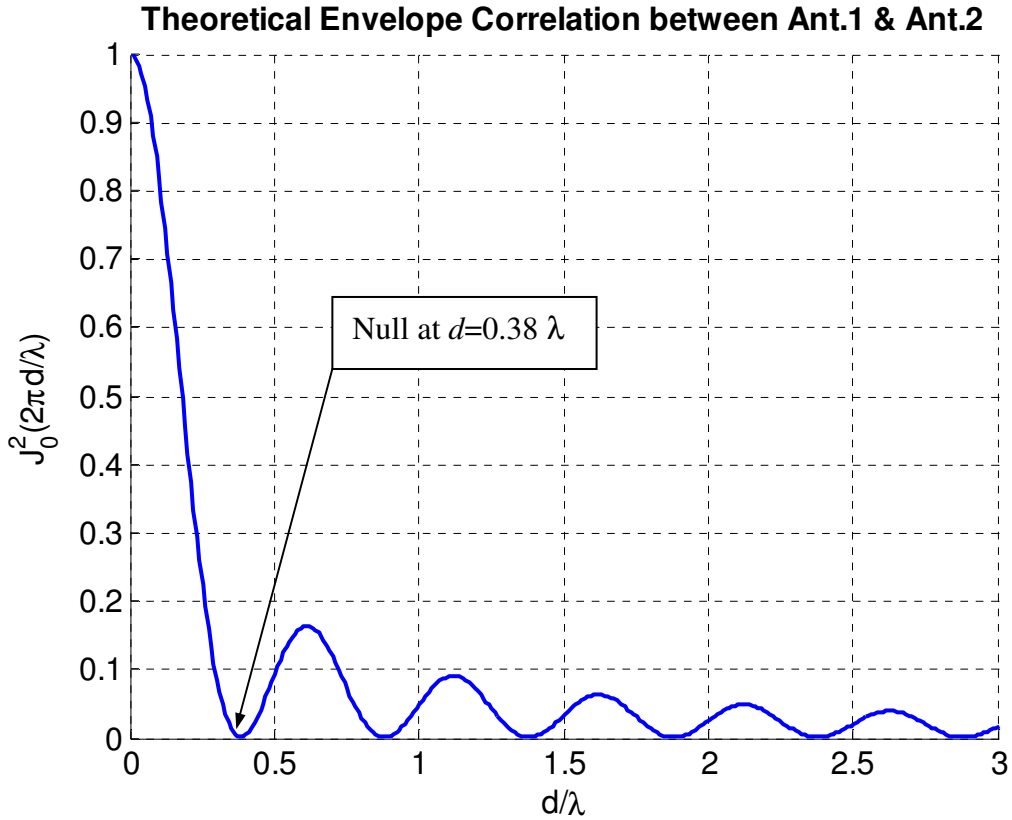


**Figure 2.5 Theoretical antenna correlation as a function of antenna spacing**

As shown in Figure 2.5, the first null occurs at  $d=0.38 \lambda$ ; however, according to several publications, the minimum distance for negligible correlation between two antennas in space is considered 0.5 wavelength (Park & Min 2005). The decorrelation distance of  $0.5 \lambda$  is due to the fact there is a multipath angular spread in the received signal, affecting the antenna correlation. However, as described above the main factors that contribute to antenna correlation in an antenna array system are antenna configuration, physical properties of the antenna elements, mutual coupling between antennas, radiation pattern, multipath angular spread, and scattering environment surrounding the antenna system.

## 2.5 Combining Methods

Having received the GNSS signals in multiple independent fading paths, the next important consideration in spatial diversity technology is to apply diversity combining. The received GNSS signals at each antenna can be combined in a number of different ways to mitigate the effects of fading. Switched combining, selection combining, equal gain combining and maximum ratio combining techniques are briefly described in this section.

### 2.5.1 Selection combining

In the selection combining technique the instantaneous SNR at the output of  $M$  branches is monitored by using  $M$  processing modules, i.e. there is one processing module for each of the diversity branches, as shown in Figure 2.6 and the branch with the highest output SNR at any time is selected as the active output signal (Gao 2007).

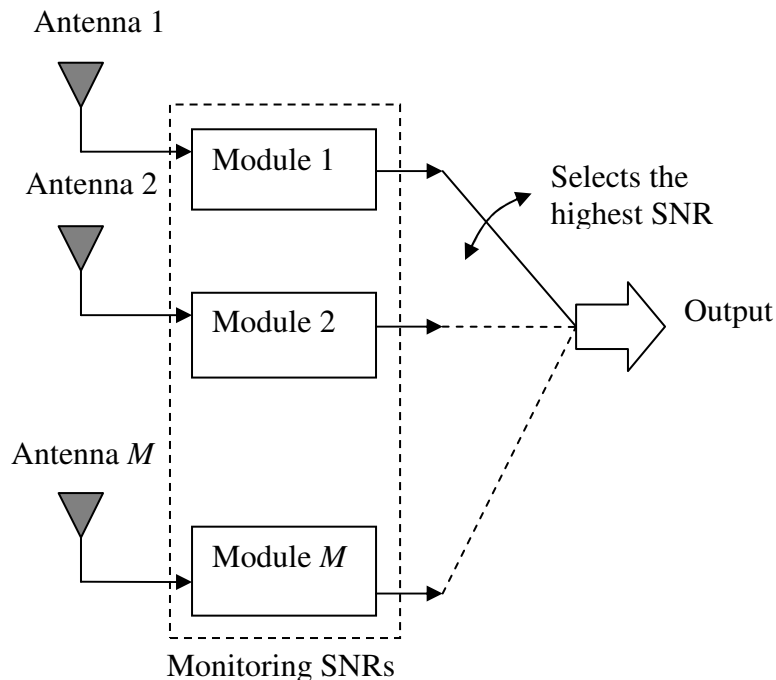


**Figure 2.6** Selection combining method for  $M$  antenna elements

### 2.5.2 Switched combining

The switched combining technique is similar to the selection combining technique to some extent. It only requires one processing module for all of the  $M$  branches as shown in Figure 2.7, whereas other combining techniques require  $M$  modules for  $M$  separate antennas. The receiver is switched to another branch only when the SNR on the current branch is lower than a predefined SNR threshold (Gao 2007). The performance of the switched combining technique is inferior to that of selection combining since unused branches may have SNRs higher than the current branch. However, a practical sense limits the switched combining method to be used with a snapshot of signals because of the practical implication that the antennas are tested for equivalent SNRs in a sequential manner.

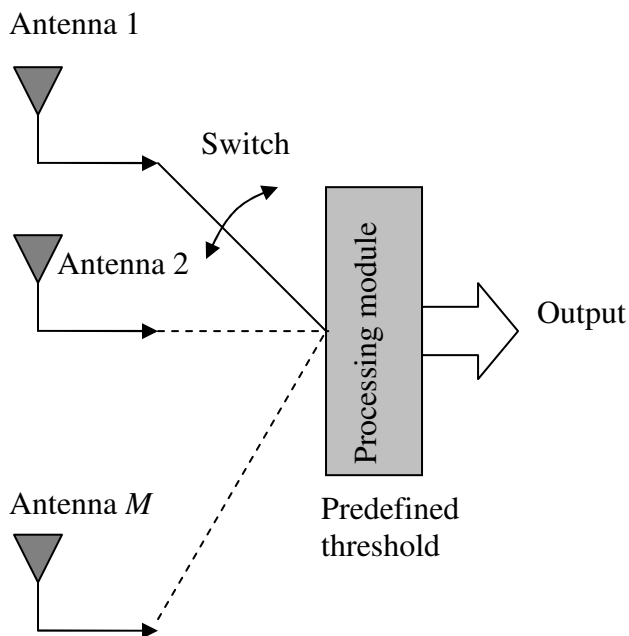


**Figure 2.7** Switched combining method for  $M$  antenna elements

### ***2.5.3 Equal gain combining***

As described above, both switched and selection combining techniques only use the signal from one of the branches as the output signal at any given time, so the signal energy in the other branches is not utilized. In order to improve the performance of diversity combining, the signals from all branches can be combined. If this is done directly using the complex signals, their random real and imaginary signal components would combine incoherently (Gao 2007). In order to obtain an effective diversity combining performance and a larger available output SNR, the signals must be co-phased so that they add in a coherent fashion. The signal in each branch must be multiplied by a complex phasor or weight having a phase  $\theta_i$  where  $\theta_i$  is the phase corresponding to branch  $i$  as shown in Figure 2.8 and then the outputs from each branch are added together. When this is achieved, all the signals are combined coherently. For each of the antenna elements, a co-phasing circuit would be necessary to estimate the phase  $\theta_i$ .

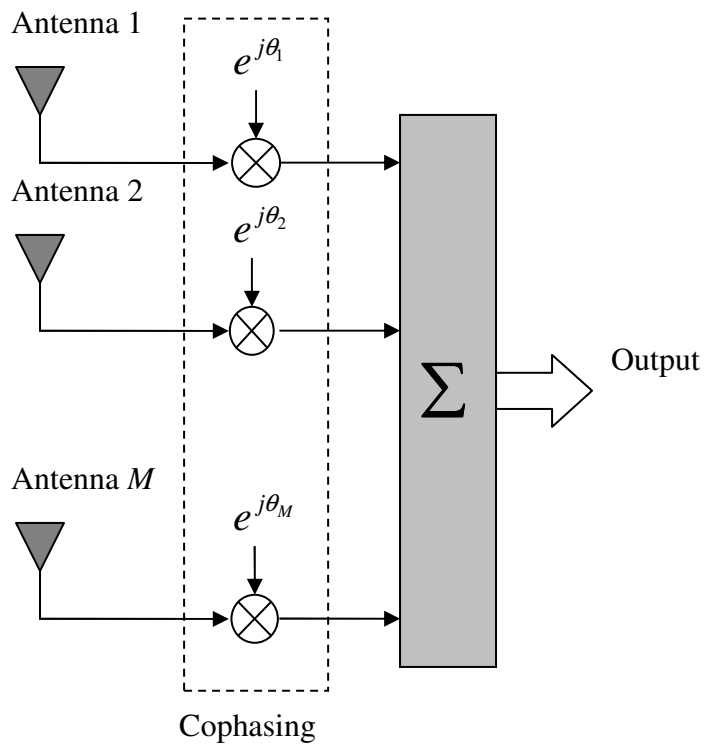


**Figure 2.8 Equal gain combining method for  $M$  antenna elements**

#### **2.5.4 Maximum Ratio Combining**

Equal-gain (EG) combining is a special case of the maximum-ratio (MR) diversity combining technique. In the maximum ratio combining method, the diversity branches are weighted according to their individual SNRs. In the equal gain combining technique, sometimes it may happen that the branches may not have the same SNR, for instance, sometimes one of the branches may have a much lower SNR than the other branches. Due to equal weighting in the sum, the overall output SNR may occasionally be reduced to a lower value (Gao 2007). To maximise the SNR at the output, a weight  $a_i$  is applied to the  $i$ -th branch before all the signals are combined coherently, as shown in Figure 2.9.

A diversity branch with a lower SNR is given a lower weighting and a diversity branch with a higher SNR is given a higher weighting. When the weights  $a_i = 1$ , where  $i = 1, 2, \dots, M$ , maximum-ratio (MR) combining becomes equal-gain (EG) combining scheme.

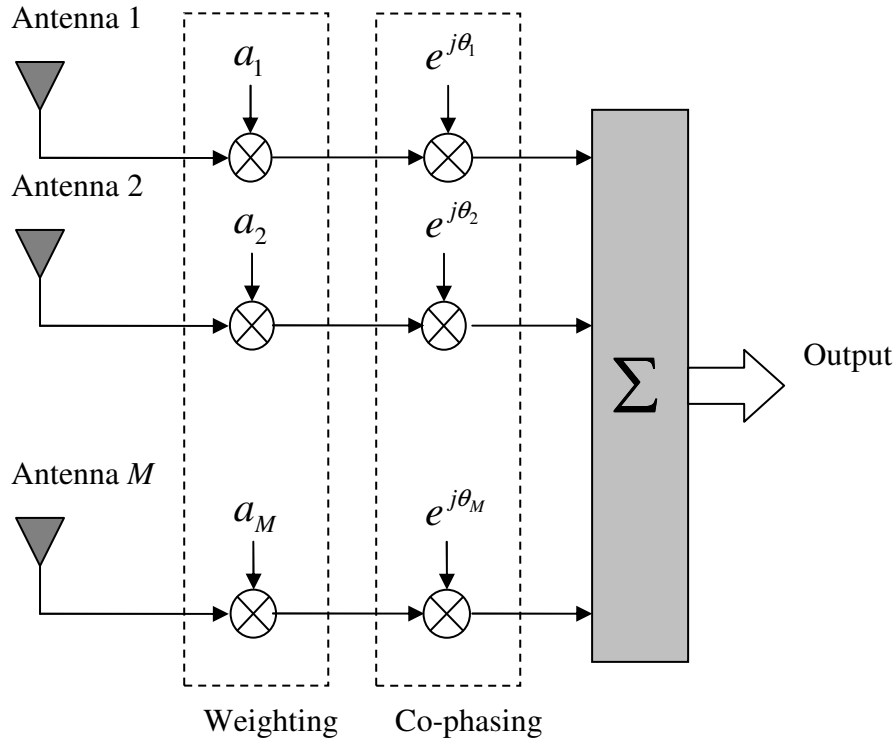


**Figure 2.9 Maximum ratio combining method for  $M$  antenna elements**

### 2.6 Diversity Gain

The diversity gain is a measure to evaluate the performance of a diversity system. The effectiveness of the diversity combining technology is usually assessed in terms of diversity gain, which is defined as the improvement in the SNR of the signals at the output of the diversity combiner or switch, with respect to the SNR from a single branch or antenna for a given reliability. In general, assuming a Rayleigh channel, which is a

multipath propagation environment, the cumulative distribution function (cdf) of a Rayleigh channel is given as (Gao 2007)

$$P(\gamma < \gamma_s / \xi) = 1 - e^{-\frac{\gamma_s}{\xi}} \quad (2.22)$$

where  $\xi$  is the mean SNR,  $\gamma$  is the instantaneous SNR, and  $P(\gamma < \gamma_s / \xi)$  is the probability that the SNR will fall below the given threshold  $\gamma_s / \xi$ . For a selection combiner with  $M$  independent antennas, assuming that the  $M$  antennas have received independent faded signals and equal mean SNRs, the probability of all antennas having a SNR below  $\gamma_s$  is equivalent to the probability for a single antenna raised to the power  $M$  and can be expressed as (Gao 2007)

$$P(\gamma < \gamma_s / \xi)_M = \left( 1 - e^{-\frac{\gamma_s}{\xi}} \right)^M \quad (2.23)$$

where  $M$  is the number of branches or antennas. Figure 2.10 shows the reduction of the probability of fading below a given threshold when increasing the number of antennas,  $M$ . Figure 2.10 also shows the diversity gain in terms of the increase in the normalized SNR of a combined output compared to a single antenna. According to Gao (2007), the normalized SNR or threshold is defined as  $\gamma_s / \xi$ . The diversity gain is marked off where  $P(\gamma < \gamma_s / \xi) = 1\%$  (i.e. 99% reliability) and  $P(\gamma < \gamma_s / \xi) = 10\%$  (i.e. 90% reliability). Figure 2.10 shows that for a 99% reliability level, there are diversity gains of 10 dB and 13 dB for the two-antenna and three-antenna selection combiners, respectively, whereas for a 90% reliability level, there are 5 dB and 7.5 dB diversity gains for the two-antenna and three-antenna selection combiners, respectively (Gao 2007).

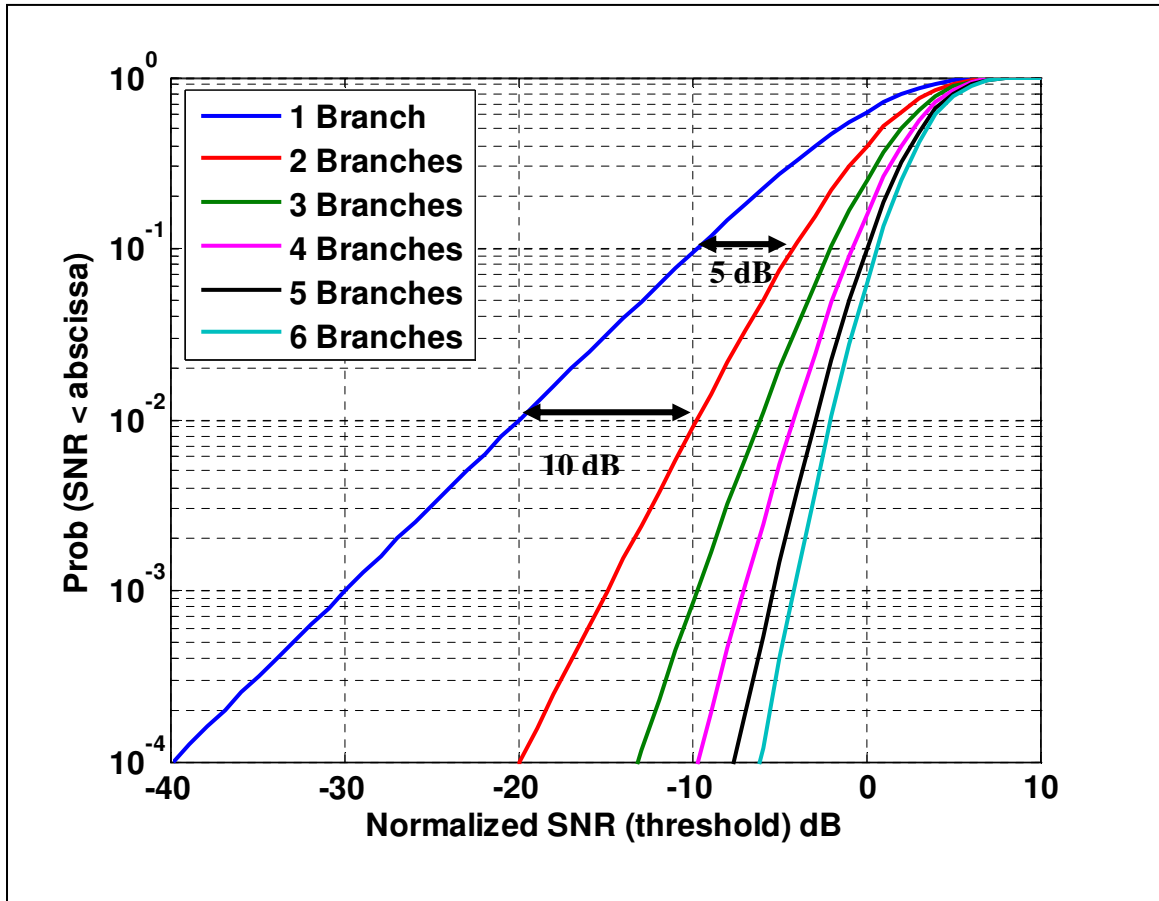


**Figure 2.10 CDFs of Rayleigh fading signals for different numbers of diversity branches**

For low instantaneous SNR, the following approximation can be made for the formula above:

$$P(\gamma < \gamma_s / \xi)_M \approx \left( \frac{\gamma_s}{\xi} \right)^M. \quad (2.24)$$

While diversity gain quantifies the improvement in SNR of a received signal obtained from different receiver antennas, it also permits a direct comparison in SNR improvement

offered by multiple antennas compared to a single antenna. The diversity gain for a given cumulative probability is expressed as

$$G_{div} = \gamma_{div} - \gamma_1$$

where  $\gamma_{div}$  is the SNR with diversity and  $\gamma_1$  is the SNR of a single antenna without diversity combining. And thus diversity gain is the increase in SNR due to diversity combining for a given level of cumulative probability or reliability. The theory of diversity gain involves the concept of mutual information and is widely popular in field of standard point-to-point wireless communication. For example, Gesbert et al (2003) is a good tutorial paper that discusses the diversity gain and its information theoretical perspectives in a detailed manner. It begins with fundamental results that compare single-input single-output (SISO), single-input multiple-output (SIMO), and multiple-input multiple-output (MIMO) capacities and then it moves to more general cases taking possible a-priori channel knowledge into account. Finally, the paper investigates useful limiting results in terms of the number of antennas or SNR.

## **2.7 Spatial Diversity Performance Criterion**

As mentioned in a previous section, spatial diversity gain is the measure of the effectiveness of a spatial diversity system. A significant spatial diversity gain can be achieved when the received signals from multiple antennas have low correlation among themselves, and the SNRs of the received signals with the two antennas are not too different from each other. In the following, some of the related terms of spatial diversity and their relationship are analyzed.

### 2.7.1 Antenna Correlation

One important condition to obtain a significant diversity gain is that a low correlation is to be ensured between the signal fading received in the branches of the diversity system. The antenna correlation can be described as complex and envelope correlations (Colburn 1998). The complex antenna correlation is denoted as  $\rho_c$ . The instantaneous magnitudes and relative phases of the received signals at different branches are used to compute the complex correlation  $\rho_c$ , as shown in Gao (2007). The envelope correlation coefficient  $\rho$  is related to the complex correlation  $\rho_c$  as shown below, assuming that the received signals have a Rayleigh distributed envelope and randomly distributed phase (Clarke 1996, Gao 2007):

$$\rho = |\rho_c|^2. \tag{2.25}$$

The envelope correlation  $\rho$  has been derived previously in Section 2.4 and followed in this thesis. In principle, the theoretical diversity gain assumes that independently faded signals are received at the diversity antennas, i.e. there is theoretically no correlation in the fading received (i.e.  $\rho = 0$ ). If the correlation coefficient  $\rho$  is greater than zero ( $\rho > 0$ ), then the diversity gain will be reduced (Gao 2007). Therefore, the correlation coefficient should be kept low enough such that the diversity is effective. The effects of envelope correlation on the diversity gain can be found in Schwartz & Bennett (1966). The analysis showed that for the correlation coefficient  $\rho \leq 0.7$ , the degradation of the diversity gain due to envelope correlation is given by the following *degradation factor* (DF), as shown in Gao (2007) and Schwartz & Bennett (1966):

$$DF = \sqrt{1 - \rho} \quad (2.26)$$

where  $\rho$  is the envelope correlation between the antennas.

### 2.7.2 Post-Correlation Signal to Noise Ratio (PSNR)

Another important condition for achieving a high diversity gain requires that the SNR of the signals delivered by the antennas in the diversity system should not vary significantly from each other. In GNSS receivers with post-processing of in-phase and quadrature-phase data samples, the PSNR is one way of illustrating this. The PSNR is thus observed for the two antennas and their difference in dBs is as follows:

$$PSNR \text{ Difference} = PSNR_{Antenna_1} - PSNR_{Antenna_2} \quad (2.27)$$

where  $PSNR_{Antenna_1}$  and  $PSNR_{Antenna_2}$  are the post-correlation SNR (PSNR) calculated from the first and the second antennas, respectively. Figure 2.11 shows the peak correlation and noise floor calculated at the post-correlation level.

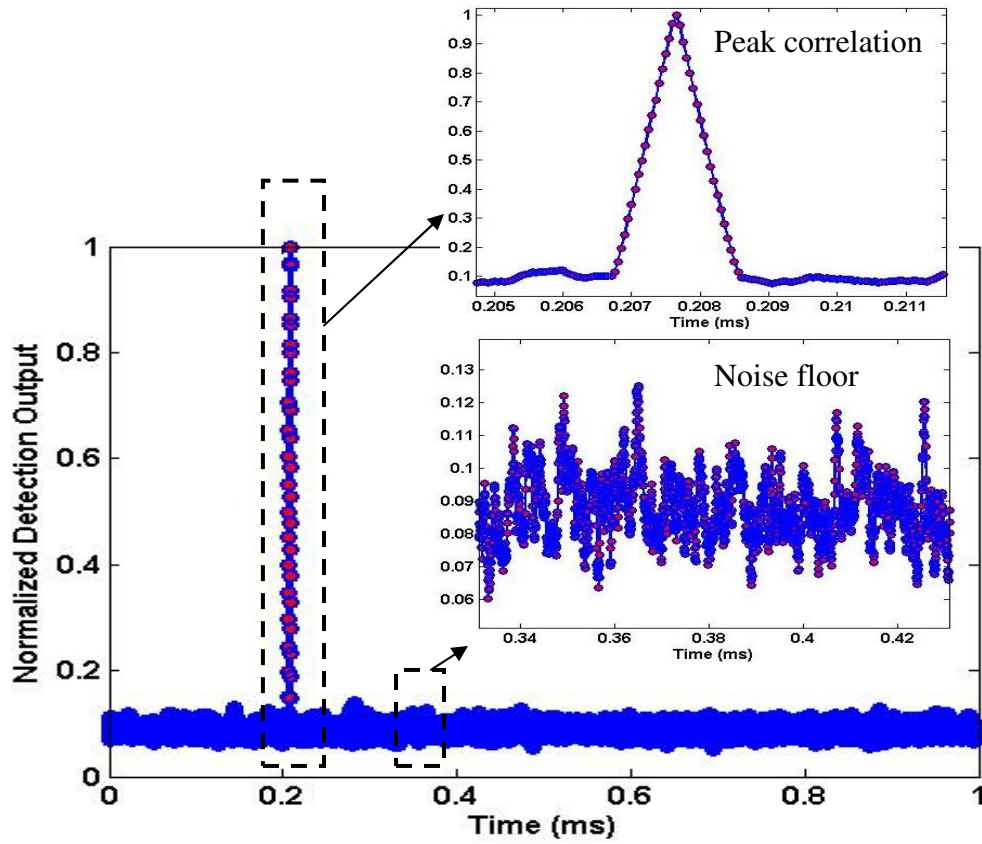


**Figure 2.11 Peak correlation value and post-correlation noise floor**

In statistical detection signal processing, the PSNR is expressed as the *Deflection Coefficient*. The performance of the schemes is evaluated in terms of the post-correlation deflection coefficient as (Kay 1998)

$$d^2 = \frac{[E(T|H_1) - E(T|H_0)]^2}{\text{var}\{T|H_0\}} \quad (2.28)$$

where  $T(x)$  is a test statistic with the hypotheses  $H_0$  representing no peak detection and  $H_1$  representing peak detection. The above equation of deflection coefficient is applicable for Gaussian signals where the test statistic  $T(x)$  is also Gaussian. However,

for non-Gaussian signals the deflection coefficient is a little bit different in form as shown in eq. 5.3 of Chapter 5. For example, in the case of spatial signal combining with a dual-antenna system, the test statistic is a sum of two Chi-square random variables and so the deflection coefficient of eq. (5.3) is valid. The probability of detection  $P_D$  and the probability of false alarm  $P_{FA}$  can then be computed by using the probability distribution of the test statistic  $T(x)$  under the  $H_1$  and  $H_0$  conditions, respectively, for given value of the threshold. The definition of PSNR is different from that of conventional SNR. In defining the PSNR, the noise bias at  $H_0$  is subtracted from both the signal and noise components. The reason for using PSNR as a criterion to investigate the spatial diversity and spatial combining gain as well as GNSS signal detection is that with real GNSS signal samples, a bias remains in both signal ( $H_1$ ) and noise ( $H_0$ ) and this noise floor distribution is not predictable. So, the conventional SNR computation is not recommended. However, analysis with simulated GNSS signals may use the conventional SNR computation because in simulated environments, the noise floor distribution is predictable and so the conventional SNR computation method can be reasonably applied. As PSNRs computed from both antennas are observed, the PSNR difference gives an indication of the correlation between the two antennas as well as the presence of any mutual coupling between them.

## **2.8 Conclusions**

In this chapter, the concept of spatial diversity was explained first by illustrating GNSS signal reception with an  $M$ -element uniform linear array. Different types of combining methods were described. The concept of spatial diversity is new in the context of GNSS.

The performance criterion of spatial diversity for GNSS was explained in terms of spatial diversity gain, correlation and PSNR. In Chapter-3, further details are discussed and necessary mathematical formulations are developed.

## CHAPTER 3: Spatial Diversity Combining of Weak GNSS Signals

This chapter describes the system in detail and introduces the basic theory of spatial diversity combining for weak GNSS signal detection. The chapter begins with a description of spatial covariance estimation. This is followed by a detailed analysis of spatial combining of GNSS signals, which starts with the signal processing technique applicable for single GNSS antenna; this is then followed by an analysis of diversity schemes applied to GNSS signals. As part of the analysis of GNSS diversity schemes, the fundamental mathematical formulations for equal-gain (EG) and maximum-ratio combining techniques are shown. Consequently, necessary mathematical formulations for estimator-correlator (EC) based combining technique are developed for both uncorrelated and correlated GNSS antennas. Performance evaluation of GNSS diversity schemes are made in conjunction with single antenna performance. While this chapter acts as the theoretical foundation of this research, for the test methodology and experimental setup as well as spatial combining processing, readers are referred to the next chapter.

### 3.1 System Description

The proposed multiple antenna system consists of  $M$  antennas whose continuous time complex outputs are denoted by  $x_m(t)$  where “ $m$ ” is the antenna index in the range from 0 to  $M-1$ . It is assumed that  $x_m(t)$  are despread and coherently integrated over a period of  $T_{coh}$ , where  $T_{coh}$  is determined by the minimum Doppler search bin size. Let us denote the correlator outputs as  $z_{m,n}$ , where  $m$  denotes the antenna index and  $n$  denotes the coherent integration epochs. The residual Doppler and the code phase of the signal of interest are known a priori. The fading is assumed to be Rayleigh and hence  $z_{m,n}$  is modeled as a

circularly Gaussian random variable. The correlation between the antennas has been determined spatially using a synthetic array and later verified by dual indoor antenna configuration. For practical reasons, the number of antenna elements is limited to two here, which can be readily justified for the case of handheld GNSS applications.

### **3.1.1 Spatial Covariance Estimation**

The spatial correlation as a function of antenna separation has been obtained using a synthetic array technique and later verified with results obtained from a dual indoor antenna configuration. Spatial correlation for various antenna separations ranging from  $0.1 \lambda$  to  $3.75 \lambda$ , where  $\lambda$  is the wavelength of GPS L1 carrier frequency and is equal to 19.04 cm, has been considered. Figure 3.1 shows how the antenna was mounted on a linear motion table. The arrow in the middle shows the central position of the linear motion table. The table was programmed such that it first moved from the central position to one extreme and then data were collected while the antenna was moved at a constant velocity. The data thus collected were processed using a synthetic array technique to yield spatial covariance measurements between two synthetic antenna locations. Later, two indoor antennas with a particular antenna spacing  $d$  were mounted in the same way on the linear motion table to verify the results obtained with a synthetic array technique. In this way sufficient amount of raw GPS IF data were collected. The linear motion table allowed for data sets to be collected at a number of locations (e.g.  $L$  locations). Figures 3.1(a) and (b) below show the schematic diagram for computing the estimated spatial covariance matrix, in such a case with synthetic array formation and with two individual antennas respectively. However, in Figure 3.1(b) the different

antenna positions with two indoor patch antennas were obtained by mounting the two indoor patch antennas on the linear motion table. The data received for spatial covariance measurements are represented by  $x_0$  and  $x_1$  for the first and second receivers respectively. During post-mission processing, the GPS IF data was initially conditioned through IF down conversion and two-dimensional acquisition. The two-dimensional search for a particular signal of interest (i.e. PRN) was carried out in code phase and Doppler frequency whereby correct code phase and Doppler values were estimated. Subsequently, the Doppler removal and code correlation were performed and the correlation outputs were coherently accumulated over  $T_{coh}$  seconds. The code phase corresponding to the maximum correlation value was then utilized for the spatial covariance estimation from the multiple antennas. For instance, in Figure 3.1(b), at position-1, after IF down-conversion and Doppler removal, the correlation peaks for coherent integration of  $T_{coh}$  seconds for the two antennas are shown as  $z_{0,k}$  and  $z_{1,k}$  respectively, where  $k$  is the coherent epoch index. The correct code phases for the two antennas are also indicated. Furthermore, the spatial covariance matrix obtained in this fashion was further averaged among different PRN's and finally over  $L$  locations.

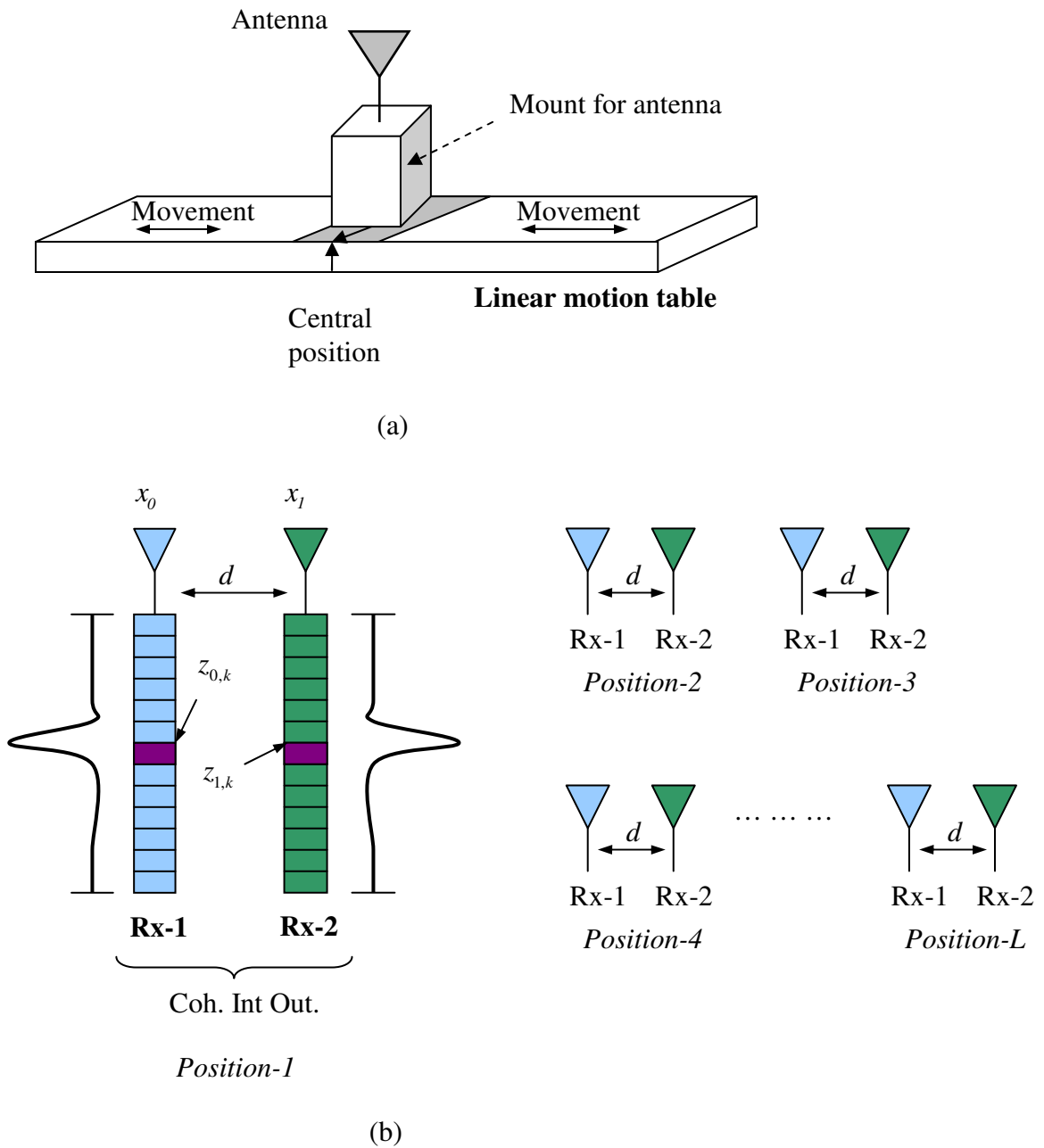


**Figure 3.1** Antenna array setup for spatial combining (a) Synthetic array formation using linear motion of single antenna, and (b) Dual antenna configuration

### 3.2 Spatial combining of GNSS signals

#### 3.2.1 Single antenna processing

For the analysis of spatial combining techniques, the detection performance of the single antenna was utilized as a benchmark. As described earlier, the single antenna processing involves the Doppler removal and code correlation. The corresponding correlation output was coherently integrated over  $T_{coh}$  seconds to yield the final detection statistic. The down-converted discrete-time sampled received signal is given by

$$y(n) = \sum_{j=0}^{J-1} h_j(n) A_j g_j(n) + w(n) \quad (3.1)$$

where  $g_j(n)$  and  $A_j$  are the transmitted GNSS signal and the corresponding amplitude respectively, pertaining to satellite “ $j$ ” and  $h_j(n)$  is the complex channel gain, which is modeled as circular complex Gaussian. For convenience, the individual PRN index (i.e.  $j$ ) is dropped resulting in a single satellite assumption. Here  $w(n)$  is the thermal noise that is modeled as a complex additive Gaussian noise (AWGN). The signal  $g(n)$  can be further expressed as

$$\begin{aligned} g(n) &= d(n) c(n) \exp(j\phi(n)) \\ \phi(n) &= 2\pi\Delta F n + \phi_0 \end{aligned} \quad (3.2)$$

where  $\phi(n)$  is the residual carrier phase with the frequency and phase offset being  $\Delta F$  and  $\phi_0$  respectively. The symbol  $d(n)$  is the navigation data modulation and  $c(n)$  is the underlying PRN code of length 1023 in chips. The correlation output can then be expressed as

$$\begin{aligned} x_1 &= \frac{1}{N} \sum_{n=0}^{N-1} y(n) g^*(n) \\ &= R(\Delta\tau) \frac{\sin(\pi N \Delta F)}{\pi N \Delta F} \exp(j\phi_{err}) \left( \frac{1}{N} \sum_{n=0}^{N-1} h(n) \right) + \frac{1}{N} \sum_{n=0}^{N-1} w(n) g^*(n) \end{aligned} \quad (3.3)$$

where  $R(\Delta\tau)$  is the correlation function and  $\phi_{err}$  is the relative phase difference between the reference and receiver signal,  $N$  is the total number of samples pertaining to the coherent integration period  $T_{coh}$  and is related to the sampling duration  $T_s$  as  $N = T_{coh} T_s^{-1}$ . The detection variable is essentially the squared magnitude output of the complex coherent integration output and is given by

$$z_0 = |x_0|^2 \quad (3.4)$$

Often the detection variable includes the noncoherent accumulation to further enhance the SNR prior to detection. In this case, the final detection variable is given by

$$z_0 = \frac{1}{K} \sum_{k=0}^{K-1} |x_0[k]|^2 \quad (3.5)$$

where  $k$  is the index denoting the  $k^{th}$  coherent integration output. Figure 3.2 shows the system model for the single antenna-based GNSS signal detection scheme. In the correlation process, the locally generated signal is shown as  $g^*(n)$ , the correlation operation is followed by coherent integration and non-coherent summations and thus the detection output is formed.

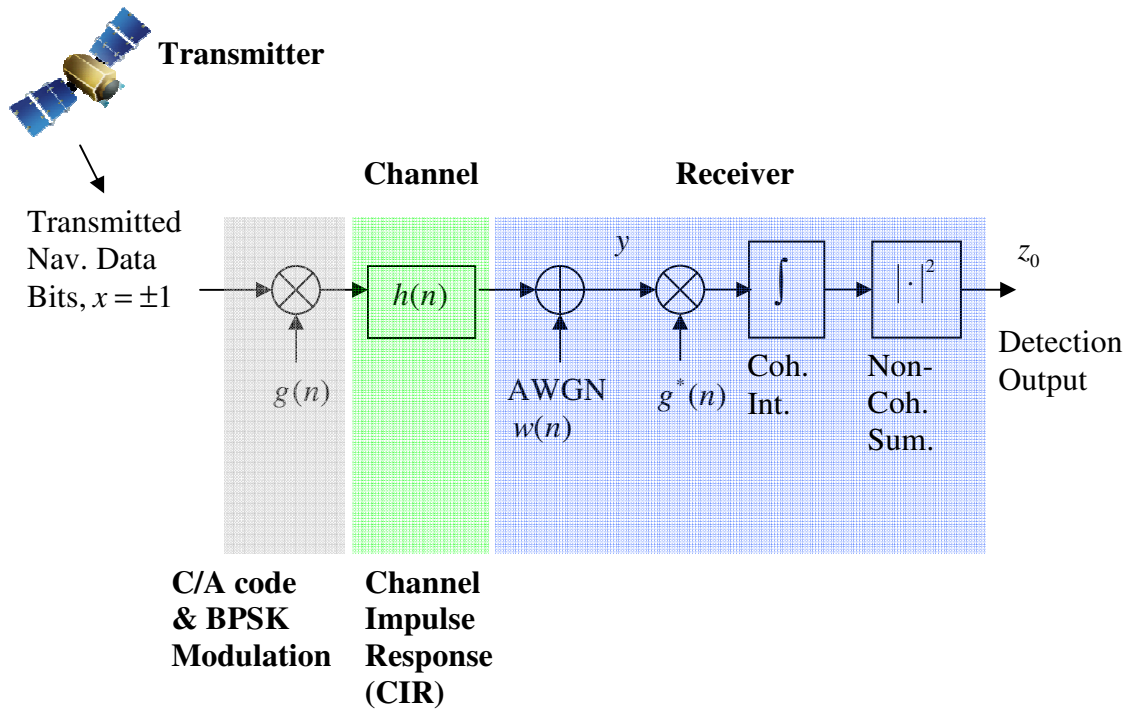


**Figure 3.2 System model for single antenna-based GNSS signal detection**

### 3.2.2 Diversity Combining Schemes

For spatial diversity combining, we consider  $M$  antennas spatially separated by a distance  $d$  between the antenna elements. Figure 3.3 shows the generic structure of spatial diversity combining when there are  $M$  diversity antennas in the receiving end. There exists a number of diversity schemes, such as selection combining, switched combining, equal-gain combining, maximum-ratio combining, and beamforming. Spatial diversity techniques are discussed in detail in Chapter 2. However, as a quick review, in selection diversity the instantaneous SNR is measured for the antenna elements and the antenna corresponding to the maximum SNR is selected. In equal-gain (EG) diversity the detection outputs of the individual antennas are equally weighed to obtain the final

detection variable. Referring to Figure 2.8, it is noted that EG combining does not require the co-phasing operation when combining with magnitude outputs is considered. Finally, the maximal ratio (MR) combining weighs the detection outputs of the individual antenna elements according to their instantaneous SNR prior to combining. The performance of equal-gain (EG) combining is expected to be superior to selection diversity combining but inferior to maximum-ratio combining. It should also be noted that the co-phasing among antenna elements is utilized in maximal-ratio combining such that the signals are actually added constructively. On the other hand, EG combining does not involve the estimation of individual SNRs and the phase of each antenna, when combining with magnitudes is considered. Alternatively, the individual antenna elements can be weighed and combined in a way to maximize the SNR at the output of the combining, which is accomplished by beamforming. However, beamforming assumes knowledge of the signal covariance matrix that is often difficult to obtain in practice. On the other hand, the signal covariance matrix can be estimated from the received signal, which readily allows for blind beamforming. The blind beamforming method typically assumes an estimator-correlator (EC) structure in its implementation. Figure 3.3 shows the generalized spatial signal combining algorithm for GNSS. In the following the mathematical formulation for equal-gain (EG) and maximum-ratio combining is shown, followed by the same for estimator-correlator (EC) based spatial signal combining for GNSS.

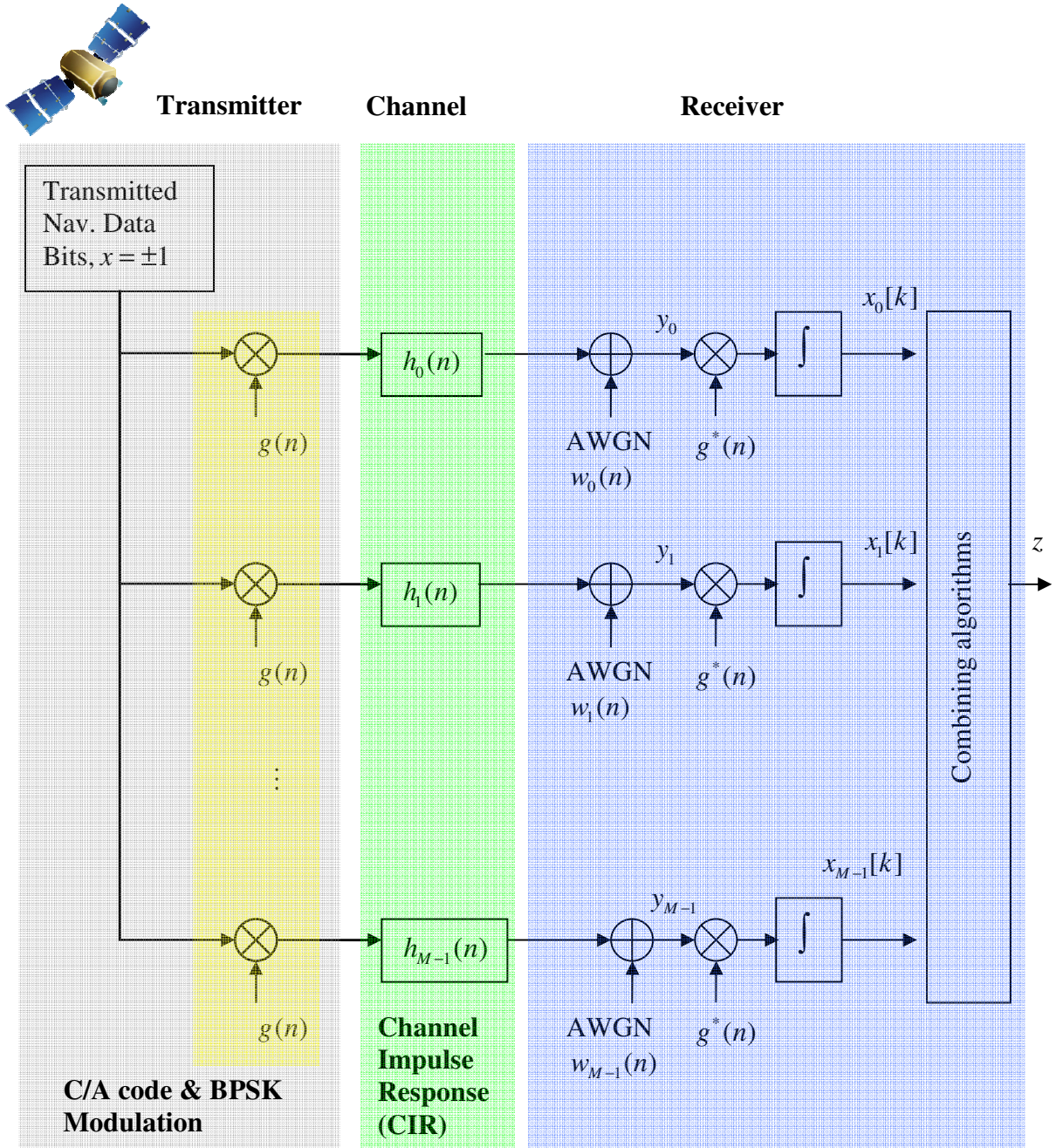


Figure 3.3 Generalized spatial signal combining algorithm for GNSS

### 3.2.3 Maximum-Ratio Combining (MRC)

As mentioned earlier, in maximum-ratio combining, the signals at each branch are weighed based on their instantaneous SNR estimates, having ensured a constructive

combining of the individual outputs through co-phasing. This allows for the envelope that is applied to the detector to be given by

$$z_M = \sum_{m=1}^M a_m z_m \quad (3.6)$$

where  $a_m$  is the weight of the  $m$ -th branch,  $z_m$  is the received signal at the  $m$ -th antenna and  $M$  is the total number of antenna elements in diversity reception. Assuming the noise in each of the branches to be independent with noise power  $\sigma^2$ , the total noise power that is applied to the detector is expressed as the weighted sum of the noise powers of all branches in the diversity reception and is denoted as

$$\sigma_T^2 = N_{noise} \cdot \sum_{m=1}^M a_m^2 \quad (3.7)$$

where  $N_{noise}$  is the average noise power at each channel. As a result, the total SNR applied to the detector after the diversity reception of  $M$  channels is expressed as

$$\begin{aligned} \gamma_M &= \frac{\text{Signal power}}{\text{Noise power}} \quad (3.8) \\ &= \frac{\left(z_M / \sqrt{2}\right)^2}{\sigma_T^2} \\ &= \frac{z_M^2}{2\sigma_T^2} \end{aligned}$$

Rappaport (2002) demonstrated that for maximum-ratio combining, if the branch weights

are chosen such that  $a_m = \frac{z_m}{N_{noise}}$ , then the total SNR applied to the detector will be

maximum. The maximum value of the detector is given as

$$\begin{aligned}
\gamma_M &= \frac{1}{2N_{noise}} \cdot \frac{\left( \sum_{m=1}^M \frac{z_m^2}{N_{noise}} \right)^2}{\sum_{m=1}^M \frac{z_m^2}{(N_{noise})^2}} \\
&= \sum_{m=1}^M \frac{z_m^2}{2N_{noise}} \\
&= \sum_{m=1}^M \gamma_m
\end{aligned} \tag{3.9}$$

where  $\gamma_m$  is the SNR at each antenna. So, referring to (3.9) it can be said that the output SNR applied to the detector using  $M$  branches is equal to the sum (in linear unit) of SNRs of various antenna signals. Also, this is the best that can be achieved by any spatial signal combiner. Here the  $m$ -th antenna SNR can be expressed as

$$\gamma_m = \frac{z_m^2}{2N_{noise}} \tag{3.10}$$

where  $z_m$  is the received signal envelope for the  $m$ -th branch. It is known that for a wireless channel the received signal envelope can be modeled as a sum of squares of two independent zero-mean Gaussian random variables as below

$$\gamma_m = \frac{z_m^2}{2N_{noise}} = \frac{1}{2N_{noise}} \left( |z_m|^2 \right) \tag{3.11}$$

which inevitably shows that  $\gamma_m$  is a Chi-square random variable with two degrees of freedom. As a result, it is found that the total SNR  $\gamma_M$  is a Chi-square random variable with  $2M$  degrees of freedom. This is a standard equation that can be found in any available literature on wireless communications, e.g. in Rappaport (2002); however, the fundamentals of Chi-square random variables can be found in Kay (1998). For each of the  $2M$  degrees of freedom in  $\gamma_M$ , the corresponding random variable has a variance of

$\Gamma/2$ , where  $\Gamma = \frac{\sigma^2}{N_{noise}}$  is the average SNR of each of the  $M$  channels, assuming  $N_{noise}$  is

the same average noise power in each channel. As a result, the average SNR applied to the detector due to diversity reception of  $M$  channels is

$$\bar{\gamma}_M = \sum_{m=1}^M \Gamma = M\Gamma \quad (3.12)$$

and thus it can be said that  $\bar{\gamma}_M$  varies linearly with the number of antenna elements  $M$ .

As a result, the pdf of the output SNR  $\gamma_M$  can be written as a Chi-square random variable

with  $2M$  degrees of freedom with average SNR (variance) equal to  $\sigma^2 / (2N_{noise}) = \Gamma/2$ ,

expressed as (Rappaport 2002)

$$\begin{aligned} p(\gamma_M) &= \frac{\gamma_M^{M-1} e^{-\frac{\gamma_M}{\Gamma}}}{\Gamma^M (M-1)!}; \quad \text{for } \gamma_M \geq 0 \\ &= 0 \quad \text{for } \gamma_M < 0 \end{aligned} \quad (3.13)$$

The cumulative distribution function (cdf) can be written as

$$\begin{aligned} P(\gamma_M) &= p(\gamma_M \leq \gamma') \\ &= \int_0^{\gamma'} p(\gamma_M) d\gamma_M \\ &= 1 - e^{-\gamma'/\Gamma} \sum_{k=1}^M \frac{(\gamma'/\Gamma)^{k-1}}{(k-1)!} \end{aligned} \quad (3.14)$$

### 3.2.4 Equal-Gain Combining

Equal-gain combining is a special case of the maximum ratio combining. The antenna

weights are  $a_k = 1$  and so there is no attempt to adjust the weight of the individual signals

before adding them, which means that all the antenna signals are weighed equally

regardless of their SNRs. Applying  $a_k = 1$  to the above discussion similar to maximum-ratio combining, the envelope that is applied to the detector is

$$z_M = \sum_{m=1}^M z_m . \quad (3.15)$$

The total noise power that is applied to the detector is expressed as

$$\sigma_T^2 = N_{noise} \cdot \sum_{m=1}^M 1 = N_{noise} M . \quad (3.16)$$

As a consequence the output SNR becomes

$$\begin{aligned} \gamma_M &= \frac{\text{Signal power}}{\text{Noise power}} & (3.17) \\ &= \frac{(z_M / \sqrt{2})^2}{\sigma_T^2} \\ &= \frac{z_M^2}{2\sigma_T^2} \\ &= \frac{z_M^2}{2N_{noise} M} \end{aligned}$$

The average SNR for equal-gain combining is thus written as

$$\begin{aligned} \bar{\gamma}_M &= \frac{1}{2N_{noise} M} \overline{\left( \sum_{m=1}^M z_m \right)^2} & (3.18) \\ &= \frac{1}{2N_{noise} M} \sum_{j,m=1}^M \overline{(z_j z_m)} \end{aligned}$$

Assuming Rayleigh fading channels, when  $j = m$ ,

$$\overline{z_j z_m} = \overline{z_m^2} = \text{var}(z_m) + \overline{(z_m^2)} = \left(2 - \frac{\pi}{2}\right) \sigma^2 + \left(\sqrt{\frac{\pi \sigma^2}{2}}\right)^2 = 2\sigma^2 \quad (3.19)$$

and when  $j \neq m$ , and given the assumption that each of the diversity branches receive uncorrelated fading due to the wireless channels, one gets

$$\overline{z_j z_m} = \overline{z_j} \cdot \overline{z_m} = \sqrt{\frac{\pi\sigma^2}{2}} \cdot \sqrt{\frac{\pi\sigma^2}{2}} = \frac{\pi\sigma^2}{2}. \quad (3.20)$$

As a result, the average output SNR becomes (Rappaport 2002)

$$\begin{aligned} \bar{\gamma}_M &= \frac{1}{2N_{noise}M} \sum_{j,m=1}^M (\overline{z_j z_m}) \\ &= \frac{1}{2N_{noise}M} \left[ 2M\sigma^2 + (M^2 - M) \frac{\pi\sigma^2}{2} \right] \\ &= \frac{1}{2N_{noise}M} \left[ 2M\sigma^2 + M(M-1) \frac{\pi\sigma^2}{2} \right] \\ &= \Gamma \left[ 1 + (M-1) \frac{\pi}{4} \right] \end{aligned} \quad (3.21)$$

where  $\Gamma = \frac{\sigma^2}{N_{noise}}$  represents the average SNR per diversity branch.

### 3.3 Estimator-Correlator (EC) Based Spatial Combining

While the generalized signal combining methods of maximum-ratio combining and equal-gain combining have been illustrated earlier, the concept of estimator-correlator (EC) based spatial signal combining approach for multi-antenna GNSS signal reception is introduced here. As shown in Figure 3.4, an antenna array system of  $M$  antenna elements receives data samples in the spatial domain from  $M$  antennas over  $N$  temporal samples.

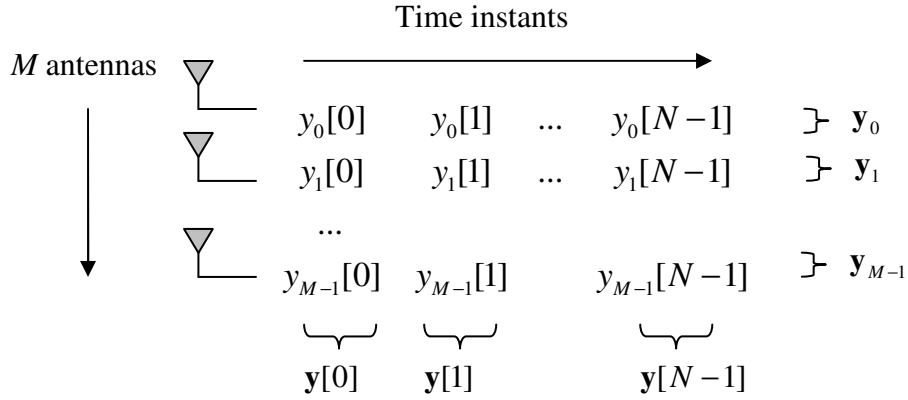


**Figure 3.4 Spatial and temporal samples of GNSS signal reception**

$y_m[n]$  denotes the discrete-time received down-converted signal from  $m$ -th antenna at  $n$ -th sample in time. The received signal  $y_m[n]$  is related to the GNSS signal as shown in (3.1) and (3.2). Correspondingly, the coherent integration output over a coherent integration time of  $T_{coh}$  seconds received with an array consisting of  $M$  antenna elements is given by

$$\mathbf{x}[k] = \begin{bmatrix} x_0[k] \\ x_1[k] \\ \dots \\ x_{M-1}[k] \end{bmatrix} \quad (3.22)$$

where  $k$  is the sample index representing the coherent integration epochs. Note that here for  $m = \{0, 1, \dots, M-1\}$ , the coherent integration outputs  $x_m[k]$  are complex quantities.

Accordingly, the covariance matrix of  $\mathbf{x}[k]$  can be expressed as

$$\begin{aligned}
\mathbf{C} &= E\left(\mathbf{x}[k]\mathbf{x}[k]^H\right) \tag{3.23} \\
&= E\begin{bmatrix} x_0[k]x_0^*[k] & x_0[k]x_1^*[k] & \dots & x_0[k]x_{M-1}^*[k] \\ x_1[k]x_0^*[k] & x_1[k]x_1^*[k] & & \cdot \\ \dots & & \dots & \cdot \\ x_{M-1}[k]x_0^*[k] & \dots & & x_{M-1}[k]x_{M-1}^*[k] \end{bmatrix} \\
&\approx \begin{bmatrix} C_{00} & C_{01} & \dots & C_{0(M-1)} \\ C_{10} & C_{11} & & \cdot \\ \dots & & \dots & \cdot \\ C_{(M-1)0} & \dots & & C_{(M-1)(M-1)} \end{bmatrix}
\end{aligned}$$

where  $(\bullet)^H$  and  $(\bullet)^*$  indicate the Hermitian transpose and conjugate operations respectively.  $C_{ij}$  are the inner products of the correlation outputs of the  $i^{\text{th}}$  and  $j^{\text{th}}$  antenna elements. The cross-diagonal terms  $C_{ij} = E\left(x_i[k]x_j[k]^H\right)$  for  $i \neq j$  indicate the spatial correlation between the antennas. Finally,  $\mathbf{C}$  is a matrix with dimension  $M \times M$ . The pdf of  $\mathbf{x}$  in this case can be computed for  $N=1$  as (Kay 1998)

$$\begin{aligned}
p(\mathbf{x}) &= \frac{1}{\pi^{MN} \det(\mathbf{C})} \exp\left[-(\mathbf{x} - \tilde{\boldsymbol{\mu}})^H \mathbf{C}^{-1} (\mathbf{x} - \tilde{\boldsymbol{\mu}})\right] \tag{3.24} \\
&= \frac{1}{\pi^M \prod_{m=0}^{M-1} \det(C_{mm})} \exp\left[-\sum_{m=0}^{M-1} (x_m - \mu_m)^H C_{mm}^{-1} (x_m - \mu_m)\right].
\end{aligned}$$

Having studied the ordering of the received data samples from multiple antennas, it is now time to illustrate the processing of the received data according to the estimator-correlator (EC) signal processing approach for GNSS signals. Correspondingly, we can express the final detection variable for the binary hypothesis (i.e. correct and wrong code phase) as

$$\begin{aligned}
H_0: \mathbf{x} = \mathbf{x}[k] &= \begin{bmatrix} w_0[k] \\ w_1[k] \\ \dots \\ w_{M-1}[k] \end{bmatrix} = \mathbf{w}[k] \\
H_1: \mathbf{x} = \mathbf{x}[k] &= \begin{bmatrix} s_0[k] \\ s_1[k] \\ \dots \\ s_{M-1}[k] \end{bmatrix} + \begin{bmatrix} w_0[k] \\ w_1[k] \\ \dots \\ w_{M-1}[k] \end{bmatrix} = \mathbf{s}[k] + \mathbf{w}[k]
\end{aligned} \tag{3.25}$$

The samples  $w_m[k]$  and  $s_m[k]$  represent noise and signal samples respectively, where  $m = 0, 1, \dots, M-1$  is the number of antenna elements and  $k$  is the coherent integration epoch. The symbol  $s_m[k]$  represents the signal component of the received signal and the corresponding signal covariance matrix is given by

$$\mathbf{C}_s = E(\mathbf{s}[k]\mathbf{s}^H[k]) = E \left( \begin{bmatrix} s_0[k] \\ s_1[k] \\ \dots \\ s_{M-1}[k] \end{bmatrix} \begin{bmatrix} s_0[k] \\ s_1[k] \\ \dots \\ s_{M-1}[k] \end{bmatrix}^H \right) \tag{3.26}$$

where  $\mathbf{C}_s$  is a  $M \times M$  spatial covariance matrix that is averaged over a large number of data collection points.  $\mathbf{w}[k]$  is a complex white Gaussian noise (CWGN) process with spatial covariance matrix  $\mathbf{C}_w = \sigma^2 \mathbf{I}_M$  where  $\mathbf{I}_M$  is an  $M \times M$  identity matrix. It is assumed that  $w_m[k]$  and  $s_m[k]$  are independent of each other for all values of  $m$ . As a result, one can apply the estimator-correlator (EC) processing in the spatial sense, and the test statistic i.e. the detection output can be expressed as

$$T(\mathbf{x}) = \mathbf{x}^H \hat{\mathbf{s}} > \gamma' \tag{3.27}$$

where  $\hat{\mathbf{s}} = \mathbf{C}_s (\mathbf{C}_s + \sigma^2 \mathbf{I}_M)^{-1} \mathbf{x}$  is the minimum-mean-square-error (MMSE) estimate of the quantity  $\mathbf{x}$  and  $\mathbf{C}_s$  and  $\mathbf{I}_M$  are as described above. Such a system with  $M$  antenna outputs is shown in Figure 3.5. The hypothesis  $H_1$  or  $H_0$  is depending on the value of the test statistic  $T(\mathbf{x})$  being greater or smaller than the threshold  $\gamma'$  respectively.

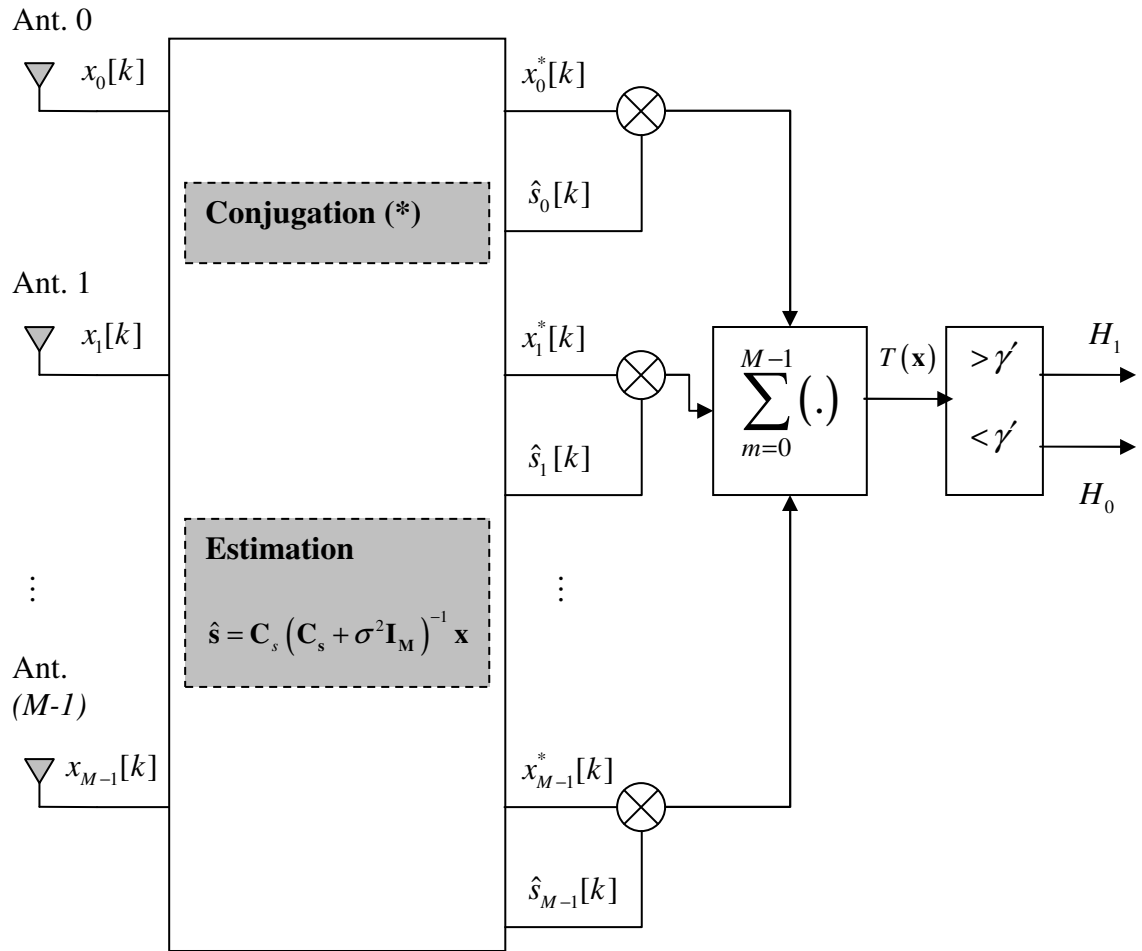


**Figure 3.5 Estimator-correlator (EC) based spatial combining**

The EC based spatial combining approach is discussed herein for the two-channel scenario. Firstly, an EC combining formulation for uncorrelated channel condition is developed. For this case,  $M$  uncorrelated channels are assumed and the corresponding test statistic is formed. In the second scenario, the correlated channel condition is investigated. For this case, only two correlated channels are investigated because consideration of more than two correlated channels certainly makes the mathematical analyses difficult to develop.

#### (A) Uncorrelated channels

Consider the condition where the complex channel gains are spatially uncorrelated. Accordingly, the received data, channel impulse response (CIR) and noise vectors are represented as

$$\mathbf{x} = \begin{bmatrix} x_0[k] \\ x_1[k] \\ \dots \\ x_{M-1}[k] \end{bmatrix}, \mathbf{h} = \begin{bmatrix} h_0[k] \\ h_1[k] \\ \dots \\ h_{M-1}[k] \end{bmatrix}, \mathbf{w} = \begin{bmatrix} w_0[k] \\ w_1[k] \\ \dots \\ w_{M-1}[k] \end{bmatrix}. \quad (3.28)$$

Assuming a Rayleigh channel condition, the channel and the noise can be expressed as

$$\mathbf{h} \sim CN \left( \begin{bmatrix} 0 \\ 0 \\ \dots \\ 0 \end{bmatrix}_{M \times 1}, \mathbf{C}_h \right) \quad (3.29)$$

where

$$\mathbf{C}_h = \sigma_h^2 \begin{bmatrix} 1 & 0 & \dots & 0 \\ 0 & 1 & & \cdot \\ \dots & & \dots & \cdot \\ 0 & \dots & & 1 \end{bmatrix}_{M \times M} = \sigma_h^2 \mathbf{I}_M. \quad (3.30)$$

Assuming a signal amplitude of  $A$ , with the uncorrelated channel condition and using (3.30) the covariance matrix of the signal component of the received signal is expressed as

$$\mathbf{C}_s = A^2 \mathbf{C}_h = A^2 \sigma_h^2 \mathbf{I}_M = \sigma_s^2 \mathbf{I}_M \quad (3.31)$$

where  $\sigma_s^2 = \sigma_h^2 \mathbf{I}_M$  and as a result one has

$$\begin{aligned} \hat{\mathbf{s}} &= \sigma_s^2 \mathbf{I}_M (\sigma_s^2 \mathbf{I}_M + \sigma^2 \mathbf{I}_M)^{-1} \mathbf{x} \\ &= \frac{\sigma_s^2}{\sigma_s^2 + \sigma^2} \mathbf{x} \end{aligned} \quad (3.32)$$

Using (3.32) and (3.27) provides the following test statistic  $T(\mathbf{x})$ :

$$\begin{aligned} T(\mathbf{x}) &= \mathbf{x}^H \hat{\mathbf{s}} \\ &= \mathbf{x}^H \cdot \left( \frac{\sigma_s^2}{\sigma_s^2 + \sigma^2} \mathbf{x} \right) \\ &= \frac{\sigma_s^2}{\sigma_s^2 + \sigma^2} (\mathbf{x}^H \mathbf{x}) \\ &= \frac{\sigma_s^2}{\sigma_s^2 + \sigma^2} \left( \begin{bmatrix} x_0[k] \\ x_1[k] \\ \dots \\ x_{M-1}[k] \end{bmatrix}^H \begin{bmatrix} x_0[k] \\ x_1[k] \\ \dots \\ x_{M-1}[k] \end{bmatrix} \right) \\ &= \frac{\sigma_s^2}{\sigma_s^2 + \sigma^2} (|x_0[k]|^2 + |x_1[k]|^2 + \dots + |x_{M-1}[k]|^2) \\ &= \frac{\sigma_s^2}{\sigma_s^2 + \sigma^2} \sum_{m=0}^{M-1} |x_m[k]|^2 \\ &= \frac{\sigma_s^2}{\sigma_s^2 + \sigma^2} \sum_{m=0}^{M-1} T_m(x_m) \end{aligned} \quad (3.33)$$

where  $T_m(x_m) = |x_m[k]|^2$  is the output energy of the  $m$ -th antenna. The pdf of the test

statistic is used to compute the probability of false alarm  $P_{FA}$  and probability of detection

$P_D$ . These are discussed in a later section that deals with the performance evaluation of the combining schemes.

### (B) Correlated channels

For the next scenario, let us consider the case where the complex channel gains are correlated among the  $M$  antennas. The spacing between any two antennas is  $d$ . Assuming a Rayleigh distribution, the complex channel gains can be expressed as (3.29); however, the covariance matrix for the channel gains in this case is

$$\mathbf{C}_h = \sigma_h^2 \begin{bmatrix} 1 & \rho_{12} & \cdots & \rho_{1M} \\ \rho_{21} & 1 & \rho_{23} & \cdot \\ \cdots & \rho_{32} & \cdots & \rho_{(M-1)M} \\ \rho_{M1} & \cdots & \rho_{M(M-1)} & 1 \end{bmatrix}_{M \times M} \quad (3.34)$$

where the symbol  $\rho_{ij}$  represents the correlation between the  $i$ -th and  $j$ -th antennas and

$\rho_{ij} = \rho_{ji}$ . For convenience, only two antenna elements are considered and they are

separated by a distance  $d$ , where  $d$  is varied as a fractional multiple of  $\lambda$ . The

consideration of two GPS antennas is justified in view of handheld GNSS devices.

Assuming  $\rho_{12} = \rho_{21} = \rho$ , the received spatial data samples, channel gains and the noise

samples for the dual-antenna system can thus be described as

$$\mathbf{x} = \begin{bmatrix} x_0[k] \\ x_1[k] \end{bmatrix}, \mathbf{h} = \begin{bmatrix} h_0[k] \\ h_1[k] \end{bmatrix}, \mathbf{w} = \begin{bmatrix} w_0[k] \\ w_1[k] \end{bmatrix}, \mathbf{h} \sim CN \left( \begin{bmatrix} 0 \\ 0 \end{bmatrix}, \mathbf{C}_h \right), \text{ where } \mathbf{C}_h = \sigma_h^2 \begin{bmatrix} 1 & \rho \\ \rho & 1 \end{bmatrix}. \quad (3.35)$$

Here, the quantity  $\rho$  is the correlation coefficient between the first and second antennas.

For the signal amplitude of  $A$ , with the correlated channel condition, the covariance

matrix of the signal component becomes

$$\mathbf{C}_s = A^2 \mathbf{C}_h = A^2 \sigma_h^2 \begin{bmatrix} 1 & \rho \\ \rho & 1 \end{bmatrix}. \quad (3.36)$$

Therefore, it yields

$$\begin{aligned} \hat{\mathbf{s}} &= A^2 \sigma_h^2 \begin{bmatrix} 1 & \rho \\ \rho & 1 \end{bmatrix} \left( A^2 \sigma_h^2 \begin{bmatrix} 1 & \rho \\ \rho & 1 \end{bmatrix} + \sigma^2 \mathbf{I}_M \right)^{-1} \mathbf{x} \\ &= A^2 \sigma_h^2 \begin{bmatrix} 1 & \rho \\ \rho & 1 \end{bmatrix} \cdot \frac{1}{\left[ (A^2 \sigma_h^2 + \sigma^2)^2 - (A^2 \sigma_h^2 \rho)^2 \right]} \cdot \begin{bmatrix} A^2 \sigma_h^2 + \sigma^2 & -A^2 \sigma_h^2 \rho \\ -A^2 \sigma_h^2 \rho & A^2 \sigma_h^2 + \sigma^2 \end{bmatrix} \mathbf{x}. \end{aligned} \quad (3.37)$$

This in turn provides us with the following test statistic  $T(\mathbf{x})$  (Nielsen 2008a):

$$\begin{aligned} T(\mathbf{x}) &= \mathbf{x}^H \hat{\mathbf{s}} \\ &= \mathbf{x}^H \left\{ A^2 \sigma_h^2 \begin{bmatrix} 1 & \rho \\ \rho & 1 \end{bmatrix} \cdot \frac{1}{\left[ (A^2 \sigma_h^2 + \sigma^2)^2 - (A^2 \sigma_h^2 \rho)^2 \right]} \cdot \begin{bmatrix} A^2 \sigma_h^2 + \sigma^2 & -A^2 \sigma_h^2 \rho \\ -A^2 \sigma_h^2 \rho & A^2 \sigma_h^2 + \sigma^2 \end{bmatrix} \right\} \mathbf{x} \end{aligned} \quad (3.38)$$

As a result, it is found that the correlation coefficient  $\rho$  in the off-diagonal term of  $\mathbf{C}_h$  makes the test statistic expression of (3.38) complicated. This is why it is advantageous to spatially decorrelate  $\mathbf{x}$  by using  $\mathbf{y} = \mathbf{V}^T \mathbf{x}$  where the decorrelation matrix  $\mathbf{V}$  is the modal matrix of  $\mathbf{C}_s$ . The matrix  $\mathbf{V}$  is an orthogonal matrix expressed as (Kay 1998)

$$\mathbf{V} = \begin{bmatrix} \frac{1}{\sqrt{2}} & \frac{1}{\sqrt{2}} \\ \frac{1}{\sqrt{2}} & -\frac{1}{\sqrt{2}} \end{bmatrix}, \quad (3.39)$$

where  $\mathbf{V}^H = \mathbf{V}^{-1}$  and so  $\mathbf{V}\mathbf{V}^H = \mathbf{I}$ . Here both  $\mathbf{V}$  and  $\mathbf{I}$  are  $2 \times 2$  matrices. So, let us now check the covariance matrix of the received data before and after this decorrelation is applied. Before applying  $\mathbf{y} = \mathbf{V}^H \mathbf{x}$  decorrelation processing to the received data, the covariance matrix of  $\mathbf{x}$  is given as

$$\begin{aligned}
\mathbf{C}_x &= \mathbf{C}_s + \sigma^2 \mathbf{I}_2 & (3.40) \\
&= A^2 \mathbf{C}_h + \sigma^2 \mathbf{I}_2 \\
&= A^2 \sigma_h^2 \begin{bmatrix} 1 & \rho \\ \rho & 1 \end{bmatrix} + \sigma^2 \begin{bmatrix} 1 & 0 \\ 0 & 1 \end{bmatrix} \\
&= \begin{bmatrix} A^2 \sigma_h^2 & A^2 \sigma_h^2 \rho \\ A^2 \sigma_h^2 \rho & A^2 \sigma_h^2 \end{bmatrix} + \begin{bmatrix} \sigma^2 & 0 \\ 0 & \sigma^2 \end{bmatrix} \\
&= \begin{bmatrix} A^2 \sigma_h^2 + \sigma^2 & A^2 \sigma_h^2 \rho \\ A^2 \sigma_h^2 \rho & A^2 \sigma_h^2 + \sigma^2 \end{bmatrix}
\end{aligned}$$

which says that  $\mathbf{x}$  is not spatially white, whereas after applying  $\mathbf{y} = \mathbf{V}^H \mathbf{x}$  to the received data, the covariance matrix of  $\mathbf{y}$  becomes

$$\begin{aligned}
\mathbf{C}_y &= E(\mathbf{y}\mathbf{y}^H) & (3.41) \\
&= E\left\{\mathbf{V}^H \mathbf{x} (\mathbf{V}^T \mathbf{x})^H\right\} \\
&= E\left\{\mathbf{V}^H \mathbf{x} \mathbf{x}^H \mathbf{V}\right\} \\
&= \mathbf{V}^H E(\mathbf{x} \mathbf{x}^H) \mathbf{V} \\
&= \mathbf{V}^H \mathbf{C}_x \mathbf{V}
\end{aligned}$$

For no signal (H0) condition,  $\mathbf{C}_x = \sigma^2 \mathbf{I}_2$  and so  $\mathbf{C}_y = \mathbf{V}^H \sigma^2 \mathbf{I}_2 \mathbf{V} = \sigma^2 \mathbf{I}_2$ , and in the presence of signals (H1),  $\mathbf{C}_x = \mathbf{C}_s + \sigma^2 \mathbf{I}_2$ , one obtains

$$\begin{aligned}
\mathbf{C}_y &= \mathbf{V}^H \mathbf{C}_x \mathbf{V} & (3.42) \\
&= \mathbf{V}^H (\mathbf{C}_s + \sigma^2 \mathbf{I}_2) \mathbf{V} \\
&= \mathbf{V}^H \mathbf{C}_s \mathbf{V} + \mathbf{V}^H \sigma^2 \mathbf{I}_2 \mathbf{V} \\
&= \Lambda_s + \sigma^2 \mathbf{I}_2
\end{aligned}$$

which is a diagonal matrix that shows that  $\mathbf{y}$  is spatially white. It is noted here that the

eigen-decomposition of  $\mathbf{C}_s$  by using  $\mathbf{V} = [\mathbf{v}_0 \quad \mathbf{v}_1]$ , where  $\mathbf{v}_0 = \begin{bmatrix} \frac{1}{\sqrt{2}} & \frac{1}{\sqrt{2}} \end{bmatrix}^T$  and

$\mathbf{v}_1 = \begin{bmatrix} \frac{1}{\sqrt{2}} & -\frac{1}{\sqrt{2}} \end{bmatrix}^T$  are the eigenvectors of  $\mathbf{C}_s$ , results in the eigen-value matrix

$\Lambda_s = \begin{bmatrix} \lambda_{s_0} & 0 \\ 0 & \lambda_{s_1} \end{bmatrix}$ ,  $\lambda_{s_0}$  and  $\lambda_{s_1}$  being the eigen-values of  $\mathbf{C}_s$ , corresponding to first and

second antennas respectively.

The test statistic  $T(\mathbf{x})$ , after decorrelation processing with  $\mathbf{y} = \mathbf{V}^H \mathbf{x}$ , becomes

$$\begin{aligned}
T(\mathbf{x}) &= \mathbf{x}^H \hat{\mathbf{s}} & (3.43) \\
&= \mathbf{x}^H \mathbf{C}_s (\mathbf{C}_s + \sigma^2 \mathbf{I}_2)^{-1} \mathbf{x} \\
&= \mathbf{x}^H \mathbf{V} \mathbf{V}^H \mathbf{C}_s \mathbf{V} \mathbf{V}^H (\mathbf{C}_s + \sigma^2 \mathbf{I}_2)^{-1} \mathbf{V} \mathbf{V}^H \mathbf{x} \\
&= (\mathbf{V}^H \mathbf{x})^H (\mathbf{V}^H \mathbf{C}_s \mathbf{V}) [\mathbf{V}^H (\mathbf{C}_s + \sigma^2 \mathbf{I}_2) \mathbf{V}]^{-1} (\mathbf{V}^H \mathbf{x}) \\
&= (\mathbf{V}^H \mathbf{x})^H (\mathbf{V}^H \mathbf{C}_s \mathbf{V}) [\mathbf{V}^H \mathbf{C}_s \mathbf{V} + \sigma^2 \mathbf{I}_2]^{-1} (\mathbf{V}^H \mathbf{x}) \\
&= \mathbf{y}^H \Lambda_s (\Lambda_s + \sigma^2 \mathbf{I}_2)^{-1} \mathbf{y} \\
&= \frac{\lambda_{s_0}}{\lambda_{s_0} + \sigma^2} |y_0[k]|^2 + \frac{\lambda_{s_1}}{\lambda_{s_1} + \sigma^2} |y_1[k]|^2 \\
&= \frac{\lambda_{s_0} / \sigma^2}{\lambda_{s_0} / \sigma^2 + 1} |y_0[k]|^2 + \frac{\lambda_{s_1} / \sigma^2}{\lambda_{s_1} / \sigma^2 + 1} |y_1[k]|^2 \\
&= \frac{\lambda_0}{\lambda_0 + 1} |y_0[k]|^2 + \frac{\lambda_1}{\lambda_1 + 1} |y_1[k]|^2
\end{aligned}$$

where  $\lambda_0 = \lambda_{s_0} / \sigma^2$  and  $\lambda_1 = \lambda_{s_1} / \sigma^2$ . Equation (3.43) is the expression of the test statistic for the estimator-correlator (EC) for spatially correlated antennas. In order to find out the exact values of  $\lambda_{s_0}$  and  $\lambda_{s_1}$ , as mentioned earlier, we follow the eigen analysis procedure as

$$\begin{aligned}
\Lambda_s &= \mathbf{V}^H \mathbf{C}_s \mathbf{V} \tag{3.44} \\
&= \begin{bmatrix} \frac{1}{\sqrt{2}} & \frac{1}{\sqrt{2}} \\ \frac{1}{\sqrt{2}} & -\frac{1}{\sqrt{2}} \end{bmatrix}^H A^2 \sigma_h^2 \begin{bmatrix} 1 & \rho \\ \rho & 1 \end{bmatrix} \begin{bmatrix} \frac{1}{\sqrt{2}} & \frac{1}{\sqrt{2}} \\ \frac{1}{\sqrt{2}} & -\frac{1}{\sqrt{2}} \end{bmatrix} \\
&= A^2 \sigma_h^2 \begin{bmatrix} 1+\rho & 0 \\ 0 & 1-\rho \end{bmatrix}
\end{aligned}$$

which provides us with  $\lambda_{s_0} = A^2 \sigma_h^2 (1+\rho)$  and  $\lambda_{s_1} = A^2 \sigma_h^2 (1-\rho)$ . Finally it becomes

$$\begin{aligned}
\lambda_0 &= \frac{\lambda_{s_0}}{\sigma^2} = \frac{A^2 \sigma_h^2 (1+\rho)}{\sigma^2} = \Omega (1+\rho) \text{ and} \tag{3.45} \\
\lambda_1 &= \frac{\lambda_{s_1}}{\sigma^2} = \frac{A^2 \sigma_h^2 (1-\rho)}{\sigma^2} = \Omega (1-\rho)
\end{aligned}$$

where  $\Omega = \frac{A^2 \sigma_h^2}{\sigma^2}$  is the SNR per antenna in EC processing under the condition of

*uncorrelated* channels, as described earlier. On the other hand,  $\lambda_0$  and  $\lambda_1$  represent SNR at the first and second antennas respectively, under the condition of *correlated* channels, and  $\rho$  is the correlation coefficient ( $0 \leq \rho \leq 1$ ) between them. The case when  $\rho = 0$  indicates the *uncorrelated* channel condition. It is also understood that in case of fully correlated channels, i.e.  $\rho = 1$ , all the energy is carried by the first eigen value, and the second eigen value eventually becomes zero, i.e. *for fully uncorrelated channels*,  $\lambda_0 = \lambda_1 = \Omega$  and *for fully correlated channels*,  $\lambda_0 = 2\Omega$ ,  $\lambda_1 = 0$ .

In addition, the decorrelation process  $\mathbf{y} = \mathbf{V}^H \mathbf{x}$  can be written as

$$\mathbf{y} = \begin{bmatrix} y_0[k] \\ y_1[k] \end{bmatrix} = \mathbf{V}^H \mathbf{x} = \begin{bmatrix} \frac{1}{\sqrt{2}} & \frac{1}{\sqrt{2}} \\ \frac{1}{\sqrt{2}} & -\frac{1}{\sqrt{2}} \end{bmatrix} \begin{bmatrix} x_0[k] \\ x_1[k] \end{bmatrix} = \frac{1}{\sqrt{2}} \begin{bmatrix} x_0[k] + x_1[k] \\ x_0[k] - x_1[k] \end{bmatrix} \tag{3.46}$$

which results in

$$\begin{aligned} y_0[k] &= \frac{1}{\sqrt{2}} \{x_0[k] + x_1[k]\} \\ y_1[k] &= \frac{1}{\sqrt{2}} \{x_0[k] - x_1[k]\} \end{aligned} \quad (3.47)$$

Correspondingly, the EC test statistic  $T(\mathbf{x})$  becomes

$$\begin{aligned} T(\mathbf{x}) &= \mathbf{x}^H \hat{\mathbf{s}} \\ &= \frac{\lambda_0}{\lambda_0 + 1} |y_0[k]|^2 + \frac{\lambda_1}{\lambda_1 + 1} |y_1[k]|^2 \\ &= \frac{\Omega(1+\rho)}{\Omega(1+\rho)+1} \left| \frac{1}{\sqrt{2}} \{x_0[k] + x_1[k]\} \right|^2 + \frac{\Omega(1-\rho)}{\Omega(1-\rho)+1} \left| \frac{1}{\sqrt{2}} \{x_0[k] - x_1[k]\} \right|^2 \end{aligned} \quad (3.48)$$

Note that (3.43) expresses the test statistic for the EC combining processing for the correlated antenna condition in terms of the eigen values corresponding to the first and second antennas. However, (3.48) is the expression for the test statistic of the same in direct terms of antenna correlation and SNR per antenna.

Also, note that for the uncorrelated channel condition, i.e.  $\rho = 0$ , from (3.48) we have the following final test statistic:

$$T(\mathbf{x}) = \mathbf{x}^H \hat{\mathbf{s}} = \frac{\Omega}{\Omega + 1} \left\{ |x_0[k]|^2 + |x_1[k]|^2 \right\} \quad (3.49)$$

where the constant  $\Omega/(\Omega+1)$  indicates that this is an equal-gain condition. Therefore, for uncorrelated channel conditions, the estimator-correlator based combining readily becomes an equal-gain (EG) combining.

### 3.4 Performance evaluation

As detection performance of the spatial combining technique is a function of only the probability of false alarm  $P_{FA}$  and the probability of detection  $P_D$ , in this section, the

detection performance for single antenna and multiple antenna scenarios has been derived in the form of the probability of false alarm and the probability of detection. The single antenna case is discussed first, which is then followed by the equal-gain (EG) combining and estimator-correlator (EC) combining techniques.

(A) *Single-antenna case*

For the single-antenna case, since there is only one antenna, the detection statistic

$T(\mathbf{x})$  can be written as

$$z_0 = T(\mathbf{x}) = |x_0[k]|^2 = x_0[k]x_0[k]^H \quad (3.50)$$

which is a Chi-square two-degrees-of-freedom central pdf random variable for both  $H_0$  and  $H_1$  conditions. The distribution of  $z_0$  can be written as

$$H_0 : \frac{T(\mathbf{x})}{\sigma^2} \sim \chi_2^2 \quad (3.51)$$

$$H_1 : \frac{T(\mathbf{x})}{\sigma_s^2 + \sigma^2} \sim \chi_2^2$$

where  $\sigma^2$  and  $\sigma_s^2$  are the noise variance and signal variance, respectively. The signal variance  $\sigma_s^2$  is represented as  $\sigma_s^2 = A^2\sigma_h^2$  for both real and imaginary components combined. As a result, the probabilities of false alarm and detection can be written as

$$P_{FA} = Q_{\chi_2^2|H_0} \left( \frac{\lambda'}{\sigma^2} \right) = e^{-\frac{1}{2} \frac{\lambda'}{\sigma^2}} = e^{-\frac{\lambda''}{2}} \quad (3.52)$$

$$P_D = Q_{\chi_2^2|H_1} \left( \frac{\lambda'}{\sigma_s^2 + \sigma^2} \right) = e^{-\frac{1}{2} \frac{\lambda'}{(\sigma_s^2 + \sigma^2)}} = e^{-\frac{1}{2} \frac{\frac{\lambda'}{\sigma^2}}{\left(\frac{\sigma_s^2}{\sigma^2} + 1\right)}} = e^{-\frac{1}{2} \frac{\lambda''}{\left(\frac{A^2\sigma_h^2}{\sigma^2} + 1\right)}} = e^{-\frac{1}{2} \frac{\lambda''}{(\Omega+1)}}$$

where  $\lambda'' = \frac{\lambda'}{\sigma^2}$  is the threshold. In this way the false alarm and detection probabilities

can be derived as a function of the threshold  $\lambda''$ .

(B) *Multiple-antenna case:*

To discuss the detection performance of a multiple antenna system, the dual-antenna system with equal gain combining is first explained. Both uncorrelated and correlated channel conditions are described for the equal-gain (EG) combining technique. Finally, the detection performance for the estimator-correlator (EC) combining is developed.

(i) *Dual antenna with equal-gain combining (EGC)*

Considering the equal-gain (EG) combining with uncorrelated channels, i.e.  $\rho = 0$ , the test-statistic can be expressed as

$$T(\mathbf{x}) = \mathbf{x}^H \hat{\mathbf{s}} = \frac{\Omega}{\Omega + 1} \left\{ |x_0[k]|^2 + |x_1[k]|^2 \right\} \quad (3.53)$$

where  $\frac{\Omega}{\Omega + 1}$  is a constant and  $\Omega$  is the SNR per antenna and can be expressed as

$$\Omega = \frac{A^2 \sigma_h^2}{\sigma^2}. \text{ Since } x_0[k] \text{ and } x_1[k] \text{ are complex-normal random variables } |x_0[k]|^2 \text{ and}$$

$|x_1[k]|^2$  are Chi-square random variables with two degrees of freedom. As a result, the test

statistic  $T(\mathbf{x})$  is a Chi-square random variable with four degrees-of-freedom and can be

expressed as

$$H_0 : \frac{T(\mathbf{x})}{\sigma^2} \sim \chi_4^2 \Rightarrow T'(\mathbf{x}) \sim \chi_4^2 \quad (3.54)$$

$$H_1 : \frac{T(\mathbf{x})}{\sigma_s^2 + \sigma^2} \sim \chi_4^2 \Rightarrow \frac{T(\mathbf{x})}{\frac{\sigma_s^2}{\sigma^2} + 1} \sim \chi_4^2 \Rightarrow \frac{T'(\mathbf{x})}{\Omega + 1} \sim \chi_4^2.$$

The signal variance  $\sigma_s^2$  is represented as  $\sigma_s^2 = A^2\sigma_h^2$  for both real and imaginary components combined. The modified test statistic is  $T'(\mathbf{x}) = \frac{T(\mathbf{x})}{\sigma^2}$ . As a result, the probabilities of false alarm and detection can be written as

$$\begin{aligned}
 P_{FA} &= \int_{\lambda'}^{\infty} p_{\lambda'^2}(x | H_0) dx & (3.55) \\
 &= \int_{\lambda'}^{\infty} \frac{1}{4} x e^{-\frac{x}{2}} dx \\
 &= \left(1 + \frac{\lambda'}{2}\right) e^{-\frac{\lambda'}{2}}
 \end{aligned}$$

$$\begin{aligned}
 P_D &= \int_{\lambda'}^{\infty} p_{\lambda'^2}(x | H_1) dx & (3.56) \\
 &= \int_{\lambda'}^{\infty} \left\{ \frac{1}{\Omega+1} \cdot \frac{1}{4} \cdot \left(\frac{x}{\Omega+1}\right) e^{-\frac{x}{2(\Omega+1)}} \right\} dx \\
 &= \int_{\lambda'}^{\infty} \frac{1}{4} \cdot \frac{1}{(\Omega+1)^2} \left\{ x e^{-\frac{x}{2(\Omega+1)}} \right\} dx \\
 &= \frac{1}{4} \cdot \frac{1}{(\Omega+1)^2} \int_{\lambda'}^{\infty} x e^{-\frac{x}{2(\Omega+1)}} dx \\
 &= \left[ 1 + \frac{\lambda'}{2(\Omega+1)} \right] e^{-\frac{\lambda'}{2(\Omega+1)}}
 \end{aligned}$$

Let us now consider equal-gain combining (EGC) but assuming the signal at two receiving antennas being correlated, i.e.  $\rho \neq 0$ , i.e. the channel covariance matrix is now

$$\mathbf{C}_h = \sigma_h^2 \begin{bmatrix} 1 & \rho \\ \rho & 1 \end{bmatrix}.$$

Assuming the signal to be present (i.e. H1 hypothesis) and following

the formation of  $\mathbf{C}_x$  as in (3.40) above, the eigen-decomposition of  $\mathbf{C}_x$  yields

$\mathbf{V}^H \mathbf{C}_x \mathbf{V} = \mathbf{\Lambda}_x$  where the two eigen values corresponding to two antennas are

$$\lambda_{x_0} = (A^2 \sigma_h^2 + \sigma^2 + A^2 \sigma_h^2 \rho) \quad (3.57)$$

$$\lambda_{x_1} = (A^2 \sigma_h^2 + \sigma^2 - A^2 \sigma_h^2 \rho).$$

Referring to (3.48) and using a similar approach, the test statistic for this case can be written as

$$T(\mathbf{x}) = \mathbf{x}^H \hat{\mathbf{s}} = \frac{\lambda_{x_0}}{\lambda_{x_0} + 1} |y_0[k]|^2 + \frac{\lambda_{x_1}}{\lambda_{x_1} + 1} |y_1[k]|^2. \quad (3.58)$$

According to (3.58) and since  $y_0[k]$  and  $y_1[k]$  are both circularly normal, the test statistic  $T(\mathbf{x})$  in (3.58) is a sum of two scaled Chi-square random variables with two degrees-of-freedom,  $\chi_2^2$ , i.e.,

$$H_0 : \frac{\lambda_{x_0}}{\lambda_{x_0} + 1} |y_0[k]|^2 \sim \chi_2^2 \quad (3.59)$$

$$H_0 : \frac{\lambda_{x_1}}{\lambda_{x_1} + 1} |y_1[k]|^2 \sim \chi_2^2.$$

The pdf of  $T(\mathbf{x})$  will be determined from the convolution of the two individual pdf's of

$|y_0[k]|^2$  and  $|y_1[k]|^2$ . The pdf of two scaled Chi-square random variables is derived in

Appendix A (Nielsen 2008a). Referring to Appendix A,

$$p_{T(\mathbf{x})}(z) = \frac{1}{\left( \frac{\lambda_{x_1}}{\lambda_{x_1} + 1} - \frac{\lambda_{x_0}}{\lambda_{x_0} + 1} \right)} \left\{ e^{\frac{-z}{\lambda_{x_1} + 1}} - e^{\frac{-z}{\lambda_{x_0} + 1}} \right\} u(z) \quad (3.60)$$

where  $u(z)$  is a *step* function of  $z$  showing  $p_{T(\mathbf{x})}(z) = 0$  for any value of  $z$  in the region

$z < 0$ . The corresponding probability that  $T(\mathbf{x}) > \lambda$  is then found is

$$\Pr(T(\mathbf{x}) > \lambda') = \int_{\lambda'}^{\infty} p_{T(\mathbf{x})}(z) dz = \frac{1}{\left( \frac{\lambda_{x_1}}{\lambda_{x_1} + 1} - \frac{\lambda_{x_0}}{\lambda_{x_0} + 1} \right)} \left\{ \frac{\lambda_{x_1}}{\lambda_{x_1} + 1} e^{-\frac{z}{\lambda_{x_1} + 1}} - \frac{\lambda_{x_0}}{\lambda_{x_0} + 1} e^{-\frac{z}{\lambda_{x_0} + 1}} \right\}. \quad (3.61)$$

Since  $T(\mathbf{x})$  is the sum of two scaled Chi-square random variables,  $|y_0[k]|^2$  and  $|y_1[k]|^2$ , putting the appropriate eigen values corresponding to two antennas  $\lambda_{x_0}$  and  $\lambda_{x_1}$  in the above equation for  $\Pr(T(\mathbf{x}) > \lambda')$  at  $H_0$  results in the probability of false alarm  $P_{FA}$  and, in a similar way, putting the eigen values  $\lambda_{x_0}$  and  $\lambda_{x_1}$  at  $H_1$  results in the probability of detection for the spatial combining in this case.

(ii) *Dual antenna with estimator-correlator (EC) combining*

As mentioned earlier, the test statistic for estimator-correlator (EC) combining can be expressed as (Kay 1998, Nielsen 2008a)

$$T(\mathbf{x}) = \mathbf{x}^H \hat{\mathbf{s}} = \mathbf{x}^H \mathbf{C}_s (\mathbf{C}_s + \sigma^2 \mathbf{I})^{-1} \mathbf{x} = \mathbf{x}^H \mathbf{C} \mathbf{x} \quad (3.62)$$

where  $\mathbf{C} = \mathbf{C}_s (\mathbf{C}_s + \sigma^2 \mathbf{I})^{-1}$  and the correlation coefficient  $\rho$  between the antennas are taken into consideration. The EC combining takes the estimation of antenna correlation  $\rho$  into account. This results in that the first and foremost objective of EC combining technique is to estimate the covariance matrix  $\mathbf{C}_x$ . This covariance matrix will be different depending on whether the signal processing that takes place involving  $\mathbf{C}_x$  can conclude that, once the eigen values of  $\mathbf{C} \mathbf{C}_x$  are obtained, following the derivation of the pdf of sum of two scaled Chi-square random variable in Appendix-A,  $P_{FA}$  and  $P_D$  can be correspondingly computed. In the following, the necessary signal processing steps to reach the above conclusion are shown in detail.

Let us first consider the eigen-decomposition of the covariance matrix of

$\mathbf{x} = [x_0[k] \ x_1[k]]^T$ , i.e.  $\mathbf{C}_x$  as

$$\mathbf{C}_x = \mathbf{V}_x^H \Lambda_x \mathbf{V}_x = \mathbf{V}_x^H \Lambda_x^{\frac{1}{2}} \Lambda_x^{\frac{1}{2}} \mathbf{V}_x \quad (3.63)$$

where symbols are as described previously. This results in the eigen value matrix of  $\mathbf{C}_x$  as

$$\Lambda_x = \begin{bmatrix} \lambda_{x_0} & 0 \\ 0 & \lambda_{x_1} \end{bmatrix}. \quad (3.64)$$

Here  $\lambda_{x_0}$  and  $\lambda_{x_1}$  are the eigen values of  $\mathbf{C}_x$  corresponding to the first and second

antennas respectively. The eigenvectors are orthonormal and  $\mathbf{V}_x^H = \mathbf{V}_x^{-1}$ . It can therefore

be written that

$$\mathbf{C}_x = \mathbf{V}_x^H \Lambda_x \mathbf{V}_x = \mathbf{V}_x^H \Lambda_x^{\frac{1}{2}} \Lambda_x^{\frac{1}{2}} \mathbf{V}_x = \mathbf{V}_x^H \Lambda_x^{\frac{1}{2}} (\mathbf{V}_x \mathbf{V}_x^{-1}) \Lambda_x^{\frac{1}{2}} \mathbf{V}_x = \mathbf{A} \mathbf{A}^H \quad (3.65)$$

where  $\mathbf{A} = \mathbf{V}_x^H \Lambda_x^{\frac{1}{2}} \mathbf{V}_x = \mathbf{A}^H$ . Note that  $\mathbf{A}$  is obtained from the signal processing of  $\mathbf{x}$

only. Since it is assumed that the channel noise is white between the two antennas,  $\mathbf{A}$  is

assumed to be full-rank, and so  $\mathbf{A}$  is invertible such that the test statistic in (3.62)

becomes

$$\begin{aligned} T(\mathbf{x}) &= \mathbf{x}^H \hat{\mathbf{s}} \\ &= \mathbf{x}^H \mathbf{C}_x \mathbf{x} \\ &= \mathbf{x}^H \mathbf{C}_s (\mathbf{C}_s + \sigma^2 \mathbf{I})^{-1} \mathbf{x} \\ &= \mathbf{x}^H (\mathbf{A}^{-1} \mathbf{A}) \mathbf{C} (\mathbf{A}^{-1} \mathbf{A})^H \mathbf{x} \\ &= \mathbf{x}^H \mathbf{A}^{-1} \mathbf{A} \mathbf{C} \mathbf{A}^H \mathbf{A}^{-1,H} \mathbf{x} \\ &= \mathbf{x}^H \mathbf{A}^{-1} \mathbf{Q} \mathbf{A}^{-1,H} \mathbf{x} \end{aligned} \quad (3.66)$$

where  $\mathbf{Q} = \mathbf{A} \mathbf{C} \mathbf{A}^H$  is symmetric and real and  $\mathbf{Q}$  can be decomposed into eigenvalues

such that  $\mathbf{Q} = \mathbf{V}_Q \Lambda_Q \mathbf{V}_Q^H$  and, as a result, defining  $\mathbf{m} = \mathbf{V}_Q^H \mathbf{A}^{-1,H} \mathbf{x}$ , one obtains

$$\begin{aligned}
T(\mathbf{x}) &= \mathbf{x}^H \mathbf{A}^{-1} \mathbf{V}_Q \Lambda_Q \mathbf{V}_Q^H \mathbf{A}^{-1,H} \mathbf{x} \\
&= \mathbf{m}^H \Lambda_Q \mathbf{m} \\
&= \begin{bmatrix} m_0[k] \\ m_1[k] \end{bmatrix}^H \begin{bmatrix} \lambda_{Q_0} & 0 \\ 0 & \lambda_{Q_1} \end{bmatrix} \begin{bmatrix} m_0[k] \\ m_1[k] \end{bmatrix} \\
&= \lambda_{Q_0} |m_0[k]|^2 + \lambda_{Q_1} |m_1[k]|^2
\end{aligned} \tag{3.67}$$

where  $\lambda_{Q_0}$  and  $\lambda_{Q_1}$  are the two eigen values of  $\mathbf{Q}$  corresponding to the first and second antennas respectively. This states that for estimator-correlator (EC) combining of GNSS signals the signals coming out of the two GNSS antennas are multiplied by the eigen

values of the  $\mathbf{Q} = \mathbf{A} \mathbf{C} \mathbf{A}^H$  matrix, where  $\mathbf{C} = \mathbf{C}_s (\mathbf{C}_s + \sigma^2 \mathbf{I})^{-1}$  and  $\mathbf{A} = \mathbf{V}_x^H \Lambda_x^{\frac{1}{2}} \mathbf{V}_x$ .

As shown in (3.67) above, assuming that  $m_0[k]$  and  $m_1[k]$  as circularly normal, the test statistic is a sum of two Chi-square random variables with two degrees-of-freedom, the scaling factors being  $\lambda_{Q_0}$  and  $\lambda_{Q_1}$ , i.e. the eigen values of  $\mathbf{Q}$ . As an alternative way of dealing with  $\mathbf{Q}$  it has been shown in the following that the eigen values are the same for  $\mathbf{Q}$  and  $\mathbf{C} \mathbf{C}_x$ , so the eigen values of  $\mathbf{C} \mathbf{C}_x$  can be used as the scaling factors as well (Nielsen 2008a). In order to calculate the eigen values  $\lambda_{Q_i}$  where  $i = 0,1$  non-trivial solutions of  $\mathbf{Q} \mathbf{v}_i = \lambda_i \mathbf{v}_i$ ,  $i = 0,1$  have to be found. Since

$$\begin{aligned}
\mathbf{Q} \mathbf{v}_i - \lambda_i \mathbf{v}_i &= \mathbf{0} \\
\Rightarrow (\mathbf{Q} - \lambda_i \mathbf{I}_2) \mathbf{v}_i &= \mathbf{0}
\end{aligned} \tag{3.68}$$

non-trivial solutions would occur if and only if  $(\mathbf{Q} - \lambda_i \mathbf{I}_2)$  is a singular matrix, i.e.

$$\begin{aligned}
\det(\mathbf{Q} - \lambda_t \mathbf{I}_2) &= 0 & (3.69) \\
\Rightarrow |\mathbf{Q} - \lambda_t \mathbf{I}_2| &= 0 \\
\Rightarrow |\mathbf{A} \mathbf{C} \mathbf{A}^H - \lambda_t \mathbf{I}_2| &= 0 \\
\Rightarrow |\mathbf{A} \mathbf{C} \mathbf{A}^H - \lambda_t \mathbf{A}^{-1} \mathbf{A}| &= 0 \\
\Rightarrow |\mathbf{C} \mathbf{A}^H - \lambda_t \mathbf{A}^{-1}| |\mathbf{A}| &= 0 \\
\Rightarrow |\mathbf{C} \mathbf{A}^H - \lambda_t \mathbf{A}^{-1}| &= 0 \quad \because |\mathbf{A}| \neq 0, \text{ as } \mathbf{A} = \text{invertible} \\
\Rightarrow |\mathbf{C} \mathbf{A}^H \mathbf{A} - \lambda_t \mathbf{I}_2| &= 0 \\
\Rightarrow |\mathbf{C} \mathbf{C}_x - \lambda_t \mathbf{I}_2| &= 0 \quad \because \mathbf{C}_x = \mathbf{A}^H \mathbf{A}
\end{aligned}$$

The above simplification is necessary because it ultimately shows that the eigen values of  $\mathbf{Q} = \mathbf{A} \mathbf{C} \mathbf{A}^H$  and  $\mathbf{C} \mathbf{C}_x$  are the same and thus the computations become easier. In dealing with EC combining, the eigen values of  $\mathbf{C} \mathbf{C}_x$  can now be used in the following way:

For H0, i.e. 'no signal' case,

$$\mathbf{C}_x = \sigma^2 \mathbf{I}_2 \text{ and}$$

$$\begin{aligned}
\mathbf{C} \mathbf{C}_x &= \mathbf{C}_s (\mathbf{C}_s + \sigma^2 \mathbf{I}_2)^{-1} \sigma^2 \mathbf{I}_2 & (3.70) \\
&= \mathbf{V}_s^H \Lambda_s \mathbf{V}_s (\mathbf{V}_s^H \Lambda_s \mathbf{V}_s + \sigma^2 \mathbf{I}_2)^{-1} \sigma^2 \mathbf{I}_2 \\
&= \mathbf{V}_s^H \Lambda_s \mathbf{V}_s (\mathbf{V}_s^H \Lambda_s \mathbf{V}_s + \sigma^2 \mathbf{I}_2 \mathbf{V}_s^H \mathbf{V}_s)^{-1} \sigma^2 \mathbf{I}_2 \\
&= \mathbf{V}_s^H \Lambda_s \mathbf{V}_s \left\{ \mathbf{V}_s^H (\Lambda_s + \sigma^2 \mathbf{I}_2) \mathbf{V}_s \right\}^{-1} \sigma^2 \mathbf{I}_2 \\
&= \mathbf{V}_s^H \Lambda_s \mathbf{V}_s \mathbf{V}_s^H (\Lambda_s + \sigma^2 \mathbf{I}_2)^{-1} \mathbf{V}_s \sigma^2 \mathbf{I}_2 \\
&= \mathbf{V}_s^H \Lambda_s (\Lambda_s + \sigma^2 \mathbf{I}_2)^{-1} \sigma^2 \mathbf{I}_2 \mathbf{V}_s \\
&= \mathbf{V}_s^H \begin{bmatrix} \frac{\lambda_{s_0} \sigma^2}{\lambda_{s_0} + \sigma^2} & 0 \\ 0 & \frac{\lambda_{s_1} \sigma^2}{\lambda_{s_1} + \sigma^2} \end{bmatrix} \mathbf{V}_s
\end{aligned}$$

This results in the eigen values

$$\lambda_0 = \frac{\lambda_{s_0} \sigma^2}{\lambda_{s_0} + \sigma^2} \text{ and } \lambda_1 = \frac{\lambda_{s_1} \sigma^2}{\lambda_{s_1} + \sigma^2} \quad (3.71)$$

corresponding to the first and second antennas respectively. According to (3.67), the test statistic  $T(\mathbf{x})$  is a sum of two scaled Chi-square pdf's. As mentioned earlier, the pdf of the sum of two Chi-square random variables has been derived in Appendix A (Nielsen 2008a). Referring to that, the probability of false alarm is written as

$$\begin{aligned} P_{FA} &= \Pr(T(\mathbf{x}) | H_0 > \lambda') \quad (3.72) \\ &= \int_{\lambda'}^{\infty} p_{T(\mathbf{x})|H_0}(z) dz \\ &= \frac{1}{\left( \frac{\lambda_{s_1} \sigma^2}{\lambda_{s_1} + \sigma^2} - \frac{\lambda_{s_0} \sigma^2}{\lambda_{s_0} + \sigma^2} \right)} \left\{ \frac{\lambda_{s_1} \sigma^2}{\lambda_{s_1} + \sigma^2} e^{-\frac{z}{\frac{\lambda_{s_1} \sigma^2}{\lambda_{s_1} + \sigma^2}}} - \frac{\lambda_{s_0} \sigma^2}{\lambda_{s_0} + \sigma^2} e^{-\frac{z}{\frac{\lambda_{s_0} \sigma^2}{\lambda_{s_0} + \sigma^2}}} \right\} \end{aligned}$$

Similarly, for the H1 condition, i.e. when there is signal present,  $\mathbf{C}_x = (\mathbf{C}_s + \sigma^2 \mathbf{I}_2)$ , and

$$\begin{aligned} \mathbf{C} \mathbf{C}_x &= \mathbf{C}_s (\mathbf{C}_s + \sigma^2 \mathbf{I}_2)^{-1} (\mathbf{C}_s + \sigma^2 \mathbf{I}_2) \quad (3.73) \\ &= \mathbf{C}_s \\ &= \mathbf{V}_s^H \Lambda_s \mathbf{V}_s \\ &= \mathbf{V}_s^H \begin{bmatrix} \lambda_{s_0} & 0 \\ 0 & \lambda_{s_1} \end{bmatrix} \mathbf{V}_s \end{aligned}$$

So, the probability of detection is

$$\begin{aligned} P_D &= \Pr(T(\mathbf{x}) | H_1 > \lambda') \quad (3.74) \\ &= \int_{\lambda'}^{\infty} p_{T(\mathbf{x})|H_1}(z) dz \\ &= \frac{1}{(\lambda_{s_1} - \lambda_{s_0})} \left\{ \lambda_{s_1} e^{-\frac{z}{\lambda_{s_1}}} - \lambda_{s_0} e^{-\frac{z}{\lambda_{s_0}}} \right\} \end{aligned}$$

Referring back to (3.62), this is how the detection performance can be derived for the EC processing.

### **3.5 Conclusions**

In this chapter, the system has been described and the concept of spatial combining has been illustrated for GNSS signals (Nielsen 2008a, Shanmugam 2008). Different channel conditions in terms of antenna correlation are considered. Spatial combining techniques based on equal-gain (EG) and estimator-correlator (EC) schemes have been illustrated and their detection performance in the form of probabilities of false alarm and detection are derived. These theoretical formulations are important in the sense that the effect of signal combining on the detection of GNSS signals will be presented on an empirical basis with several test setups with real GPS data in Chapter 4 and 5. Finally, this chapter acts as the theoretical part of the proposed spatial combining algorithms.

## **CHAPTER 4: Test Methodology and GNSS Signal Processing**

Spatial diversity and its applicability to GNSS signals have been reviewed in Chapter 2, where spatial correlation between antenna elements as well as diversity combining techniques were also discussed. Chapter 3 has described the signal and system model and developed mathematical formulations for spatial diversity combining of weak GNSS signals. While Chapter 3 contains the theoretical contributions of this research, this chapter describes the test methodology and the subsequent GNSS signal processing techniques. The experimental setup is explained. The chapter also presents some of the results in terms of multiple antenna GNSS signal processing including enhanced GNSS signal acquisition and tracking.

### **4.1 GPS Signal Structure**

GPS uses a Direct Sequence-Code Division Multiple Access (DS-CDMA)-based signaling technique for transmission from the satellite. This is designed to allow all satellites to transmit different information in the same frequency band using different pseudo-random noise (PRN) codes to facilitate efficient receiver design. Each PRN code is unique for each satellite transmitting the signal and there is low cross-correlation between any two PRN codes. The codes transmitted from the satellites are known to the receiver and the receiver correlates the received signal with a replica of the locally generated code to obtain the code start time (or code phase). The code phase provides an estimation of the transmit time of the signal traveling from the satellite to the receiver. The civilian code of GPS is of length 1023 in chips and is derived from the family of Gold codes known as coarse/acquisition (C/A) codes. The basic chipping rate is 1.023

MHz, resulting in a code repetition time of 1 ms. The navigation data bits are transmitted at 50 Hz rate, which corresponds to 20 code periods. The data bits contain information such as absolute time and orbital parameters. Finally, the signal is binary-phase-shift-keying (BPSK) modulated on a carrier wave (sinusoid) at 1575.42 MHz prior to transmission via onboard antenna. Thus, when the transmitted GPS signal is received by a GPS receiver, as shown in Section 3.2, the down-converted discrete time sampled received signal can be represented by

$$y(n) = \sum_{j=0}^{J-1} h_j(n) A_j g_j(n) + w(n) \quad (4.1)$$

where symbols bear the meanings described in Section 3.2 pertaining to satellite “*j*”. Signals from other GPS satellites and those from multipath reflections finally make the received signal a composite signal. It should be noted here that the noise  $w(n)$  also includes thermal background noise of the receiver, in-band interference and signals from other satellites. Due to the substantial signal attenuation, the received GPS signal is typically buried under the noise. Hence, the receiver requires extensive signal processing to extract the signal information from the weak GPS signal. Signal demodulation and estimation of code-delay and Doppler frequency requires successful signal detection and continuous tracking. The following sections describe the GPS signal conditioning techniques that accomplishes the above mentioned tasks.

## 4.2 GNSS Receiver Signal Processing

This section provides a brief description of receiver signal processing in the context of GPS. The readers are further referred to Misra & Enge (2006), Kaplan & Hegarty (2006) and Parkinson & Spilker (1996) for a more detailed treatment of the same. It should be

emphasized here that the following analysis although based on GPS can readily be extended to other GNSS such as GLONASS, Galileo and COMPASS.

#### **4.2.1 Signal conditioning: Antenna Element**

As discussed earlier, the receiver necessitates the estimation of code phase, carrier Doppler and phase for navigation data demodulation and position solution. Figure 4.1 shows a generic GPS receiver operation chain. The receiver antenna is the first element that captures the right hand circularly polarized (RHCP) transmitted GPS signal. The test methodology developed herein utilizes a U-blox active patch antenna for all GPS IF data collection (U-blox 2008). The receiver front-end is the first signal processing block inside a GPS receiver. The cable length for the U-blox patch antenna is 5 m. The gain provided by the preamplifier in the patch antenna is around 27 dB with a noise figure of 3 dB.

#### **4.2.2 RF Down-conversion and Sampling**

The received RF signal is *conditioned* through band-pass filtering, low-noise amplification and down-conversion process before it is converted into digital samples. The RF signal is beaten with a locally generated signal with frequency equal to  $f_L - f_{IF}$ , where  $f_{IF}$  is the intermediate frequency,  $f_L$  is the GPS L1 band frequency and the signal output is filtered with a band-pass filter that allows signals near  $f_{IF}$  only to pass. This process of multiplying and filtering of signals is known as *mixing*.

The down-conversion process can be performed directly using a single stage only known as *direct down-conversion* or through multiple stages (typically two stages) prior to sampling and digitization. However, *direct down-conversion* requires the receiver to be designed with great care because high power and low power signals co-exist at one frequency and there is a potential possibility of oscillation instead of amplification if the

strong output leaks back into the input side (Misra & Enge 2006). As a result, *multi-stage down-conversion* is recommended rather than *direct down-conversion*. Multistage down-conversion typically translates the received RF signal close to baseband ( $\leq 5$  MHz). It also suppresses image frequencies by intermediate filtering.

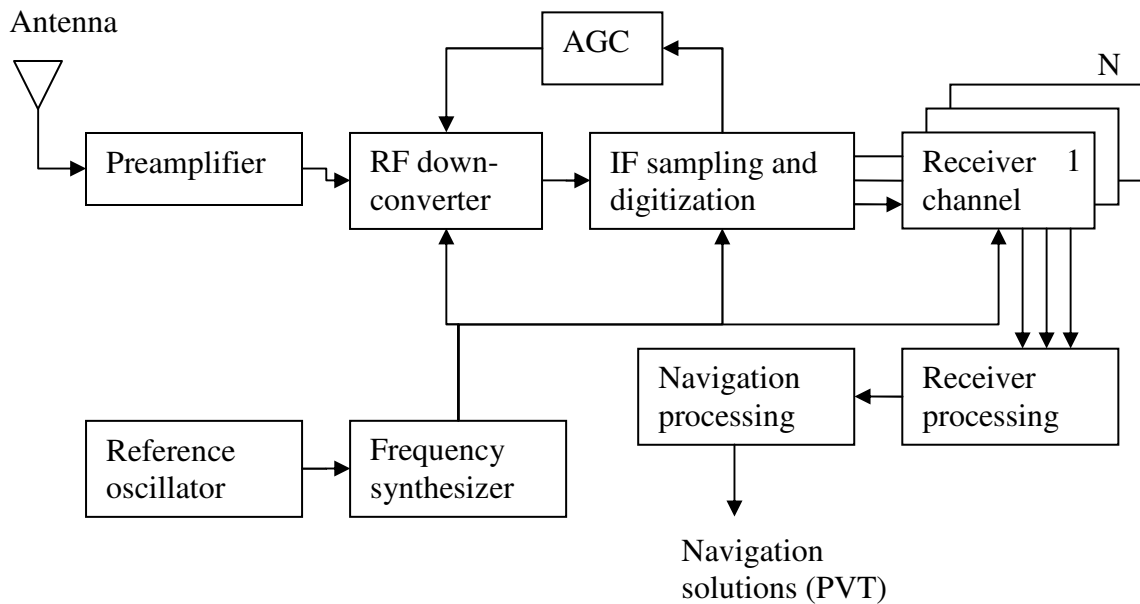


**Figure 4.1 Generic GPS digital receiver block diagram**

### 4.2.3 Baseband Signal Processing

Baseband signal processing primarily consists of pre-correlation sampling, code removal and Doppler removal, post-correlation filtering, receiver clocks and finally navigation processing.

**Pre-correlation sampling** - Modern GPS receivers involves digital processing for code correlation and Doppler removal. The baseband conversion is achieved as part of the sampling process known as *IF sampling* or *pre-correlation sampling*. The process of IF

sampling is to sample the IF signal at a rate at which the  $I$  and  $Q$  signals are obtained directly (Parkinson & Spilker 1996, p.348).

**Doppler removal** - The next step is Doppler removal, which involves the phase-rotation of the received  $I$  and  $Q$  samples. Doppler removal process is used by the carrier tracking loops to track either the phase or the frequency of the incoming signal samples (Parkinson & Spilker 1996, p.356). The carrier tracking loop controls the numerically controlled oscillator (NCO) to generate the inphase and quadrature phase signal outputs for Doppler removal operation.

**Code removal** - After Doppler removal processing is complete, the received  $I$  and  $Q$  samples are correlated with three versions of locally generated PRN code samples to form corresponding correlator outputs. The three versions of the locally generated code are named as *early*, *prompt*, and *late* correlators. This process of correlation of received samples with local code is known as *code removal*. The PRN code tracking process is maintained through *Delay Lock Loop (DLL)*. The output error signal of the DLL is obtained by the difference of the correlator output functions of *early (E)* and *late (L)* correlators. When navigation bit synchronization is obtained, the coherent integration can be extended up to 20 ms for both code and carrier tracking algorithms.

**Discriminator outputs** - The code phase and carrier phase discriminator outputs are fed into the code and carrier numerically controlled oscillators (NCOs) such that loops are maintained properly. The discriminator outputs are computed by the digital computer from respective code phase and carrier phase measurements. As mentioned earlier, the receiver has to estimate the code phase and carrier phase from the received signals, and these estimates are further processed to estimate the position-velocity-time (PVT)

navigation solutions for the receiver. The reader is further referred to Kaplan & Hegarty (2006), Parkinson & Spilker (1996), and Misra & Enge (2006) for a detailed treatment of signal acquisition and tracking algorithms.

### **4.3 GPS Signal Acquisition**

#### **4.3.1 Correlation**

The GPS signal acquisition is the initial operation that deals with the detection and coarse estimation of Doppler and code phase. This is essentially accomplished through a two-dimensional discretized maximum likelihood search in the code phase and Doppler domain.

For the GPS L1 frequency, the Doppler shift due to satellite motion causing a satellite to user distance rate of change is typically on the order of  $\pm 4$  kHz. An unknown frequency error of the local clock typically adds another uncertainty. As a result, an overall total Doppler search space of typically  $\pm 10$  kHz should be used. On the other hand, the code phase can assume almost any value, but as the code repeats every 1 ms, the search for code phase estimate is restricted to within 1 ms of duration. Since baseband signal at this stage still has the Doppler frequency in it, it is named *pseudo-baseband* signal. As a result, the search is performed by mixing the pseudo-baseband signal and correlating it with a known locally generated PRN code. Figure 4.2 shows the inphase and quadrature phase complex correlation. As described in Section 3.2, having defined  $\Delta F$  and  $\phi_0$  as the initial frequency and phase offset, the correlation output can thus be expressed as

$$\begin{aligned}
x &= \frac{1}{N} \sum_{n=0}^{N-1} y(n)g^*(n) \\
&= R(\Delta\tau) \frac{\sin(\pi N \Delta f_D)}{\pi N \Delta f_D} \exp(j\phi_{err}) \left( \frac{1}{N} \sum_{n=0}^{N-1} h(n) \right) + \frac{1}{N} \sum_{n=0}^{N-1} w(n) g^*(n)
\end{aligned}$$

where  $R(\Delta\tau)$  is the correlation function and  $\phi_{err}$  is the relative phase difference between the reference and receiver signal,  $N$  is the total number of samples pertaining to the coherent integration period and is related to the sampling duration as  $N = T_{coh} T_s^{-1}$ .

The time taken by the transmitted signal to reach the receiver is indicated by the time delay of  $\tau$  seconds and so known as the code-delay. The  $\Delta\tau$  is the code-phase error of the signal. The output  $\tilde{S}$  is the representation of the ambiguity function. As explained in detail in Misra & Enge (2006), the ambiguity function relates to the correlation function  $R(\Delta\tau)$  and incorporates the Doppler frequency error  $\Delta f_D$  as well. As a result, the ambiguity function  $\tilde{S}$  can be represented as  $\tilde{R}(\Delta\tau, \Delta f_D)$ , where  $\tilde{R}(\Delta\tau, \Delta f_D)$  is a function of  $R(\Delta\tau)$  and  $\Delta f_D$ , i.e.  $\tilde{R}(\Delta\tau, \Delta f_D) = f\{R(\Delta\tau), \Delta f_D\}$ . As a result, the correlation output is dependent on the estimation accuracies of Doppler and code-phase errors. To estimate  $(\Delta\tau, \Delta f_D)$  and to suppress the effect of navigation data modulation and residual carrier, the GPS receiver takes the magnitude of  $\tilde{S}$ . Figure 4.2 shows how the IF and Doppler frequency  $f_{Doppler}$  removal process takes place and subsequently how the local code correlation is done at the GPS receiver. The symbols in Figure 4.2 bear the usual meanings as defined previously. Symbols marked with a hat represent corresponding

estimated values.

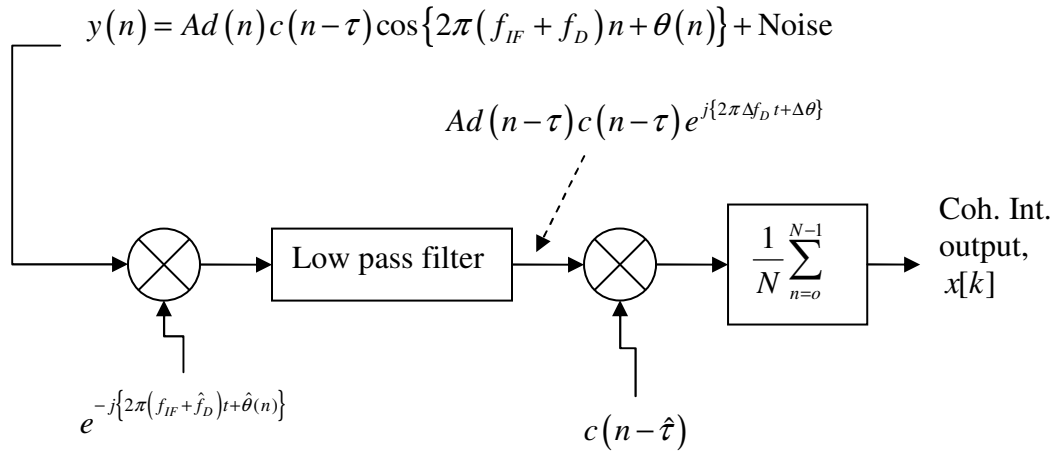


**Figure 4.2 Doppler removal and code correlation**

### 4.3.2 Non-Coherent Combining Detector

Non-coherent combining is a popular technique for increasing the probability of detection  $P_D$  for a given probability of false alarm,  $P_{FA}$ , in the presence of a randomly varying phase offset due, for example, to a carrier Doppler offset, or data modulation effects. The approach of non-coherent combining detector (NCCD) dates back to radar detection theory and in general in the detection of unknown signal in noise (O’Driscoll 2007). The NCCD is a standard detection technique for GPS signals and has been employed during the analysis. Figure 4.3 shows a conventional non-coherent detector applicable for GPS signals. In principle, the NCCD is an energy detector and operates by accumulating a number of  $N_{NCH}$  outputs obtained from coherent averaging of  $N$  time samples as shown in Figure 4.3. The carrier removal and the code removal parts are taken care of by the carrier NCO and code generator respectively, as shown. However, a major disadvantage of non-coherent combining detector is the SNR degradation (i.e. *squaring loss*) due to

envelope detection (Lachapelle 2006). By squaring the received signal after coherent integration as shown in Figure 4.3, the navigation data bit effect is stripped off. While it achieves the intended purpose of removing the data modulation, it also squares the received noise. This squaring of noise introduces *squaring loss*. The effect of the *squaring loss* is significant in low signal environment. The details on squaring loss are available in Misra & Enge (2006, pp. 388, 480) and Shanmugam et al (2005).

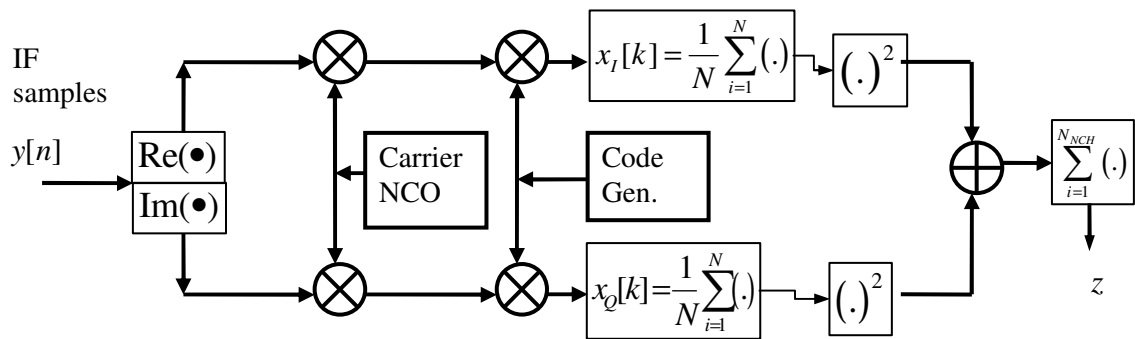


**Figure 4.3 Non-coherent combining detector for GPS signal acquisition**

#### 4.4 Software Implementation of Dual-Antenna Array GPS Receiver

The developed test setup involved a commercial multi-channel front-end for RF down conversion and subsequent signal conditioning. The raw IF samples from the commercial front-end were stored in a PC memory for post-mission signal processing.

For synthetic array setup, the indoor antenna was mounted on a linear motion table and moved at a constant slow velocity. The linear motion table was set to a pre-defined motion of 0.012 m/sec or  $\lambda/16$  per second, where  $\lambda$  is the wavelength of the GPS L1 carrier and  $\lambda$  is approximately equal to 19 cm. The antenna was moving back and forth across the linear motion table, whose length was approximately 1.4 m.

In addition to the indoor data collection, an outdoor reference antenna was utilized for assisting the signal demodulation. The output of the outdoor reference antenna as well as the indoor antenna were connected to the commercial front-end to allow for synchronized data collection. Approximately one hour of data was collected using the front-ends. Finally, a *NovAtel* reference antenna and an OEM receiver were utilized to obtain approximate Doppler to reduce the search space during signal acquisition. The two selected indoor locations were inside a commercial office building, namely the CCIT building of the University of Calgary. The first location was in a corridor and the other location was inside a room of the 3<sup>rd</sup> floor. Both the test locations had window panes but exhibited substantial signal attenuation due to protective coating. Figures 4.4 and 4.5 below show the schematic diagram of the overall test setup and the mounting of dual-antenna setup on the linear motion table respectively. Figure 4.6 shows the plan-view of the third floor of the building and the indoor test locations. Regarding the experimental data collection, it is noted that two different types of data collection modes were considered and are summarized below

- Mode – 1: Outdoor reference antenna and indoor synthetic array antenna
- Mode – 2: Two indoor antennas

In the first mode of operation, the reference antenna is used to estimate the Doppler frequency, code phase and navigation data bits and these estimates were then used for the demodulation of the GPS IF data pertaining to the indoor antenna. The use of the synthetic array readily eliminates the issues such as mutual coupling and antenna leakage and allows for overcoming the limitation in physical separation. However, the results

were further verified with dual antenna indoor data collection with a reduced number of antenna separations.

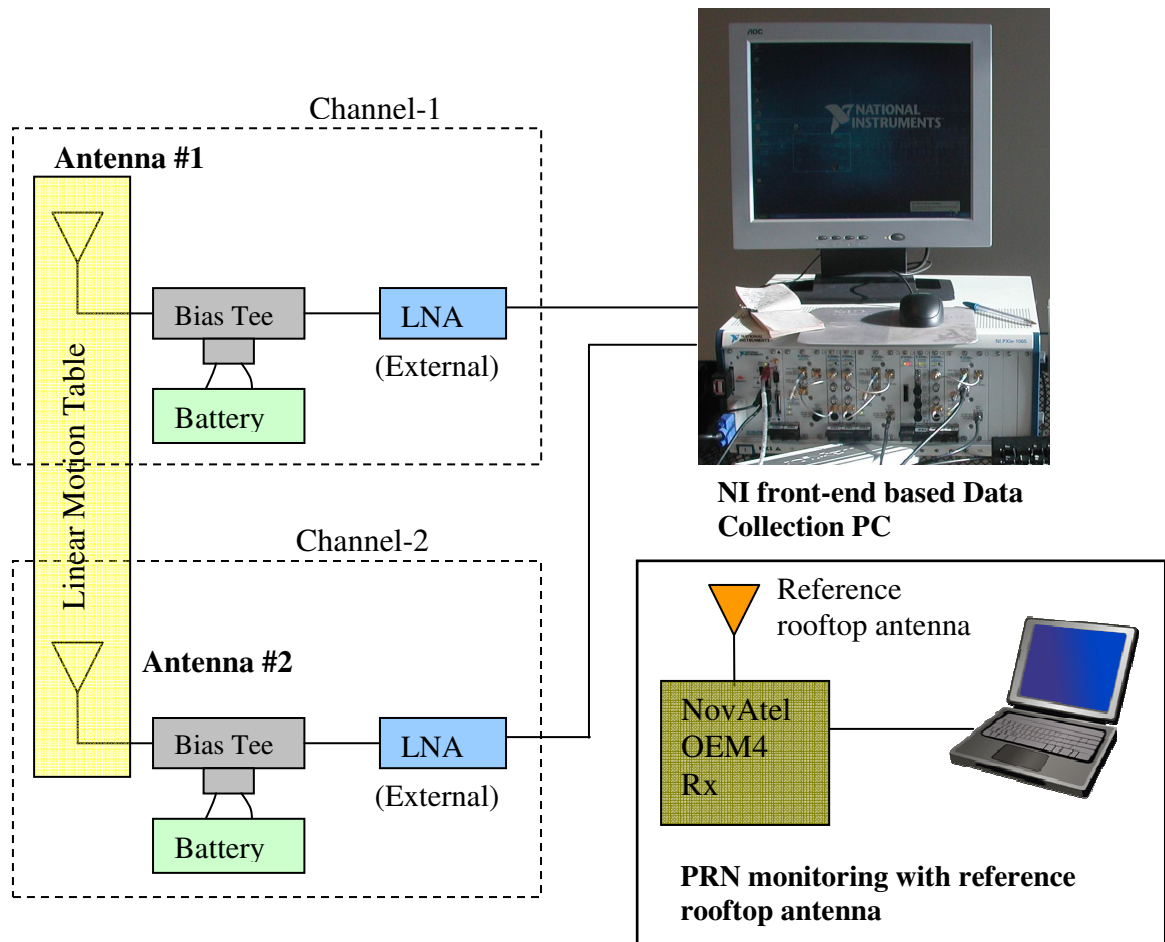


Figure 4.4 Schematic diagram of the test setup

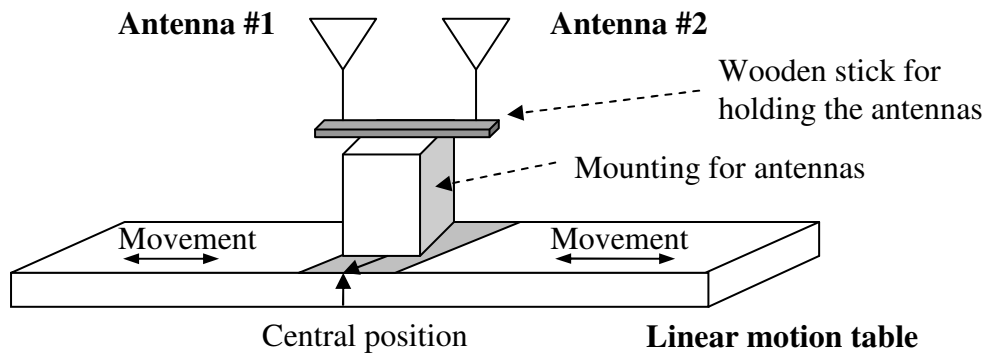


Figure 4.5 Schematic diagram of the dual antenna system with linear motion table

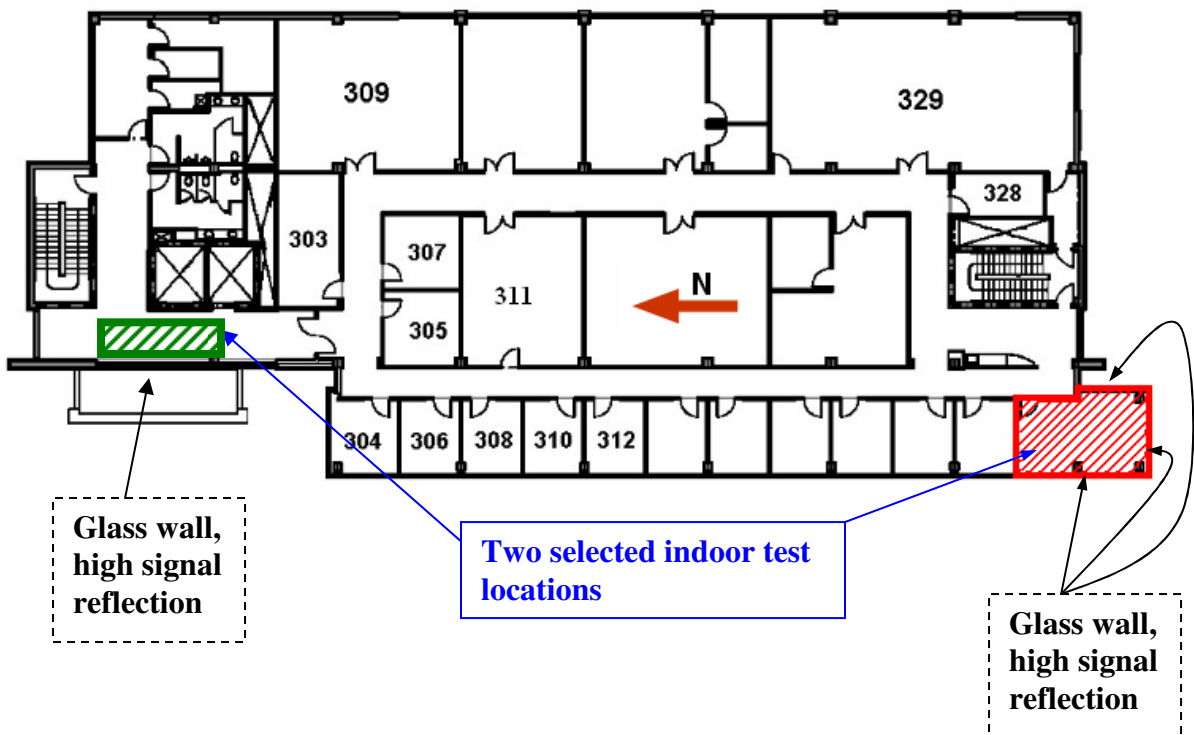
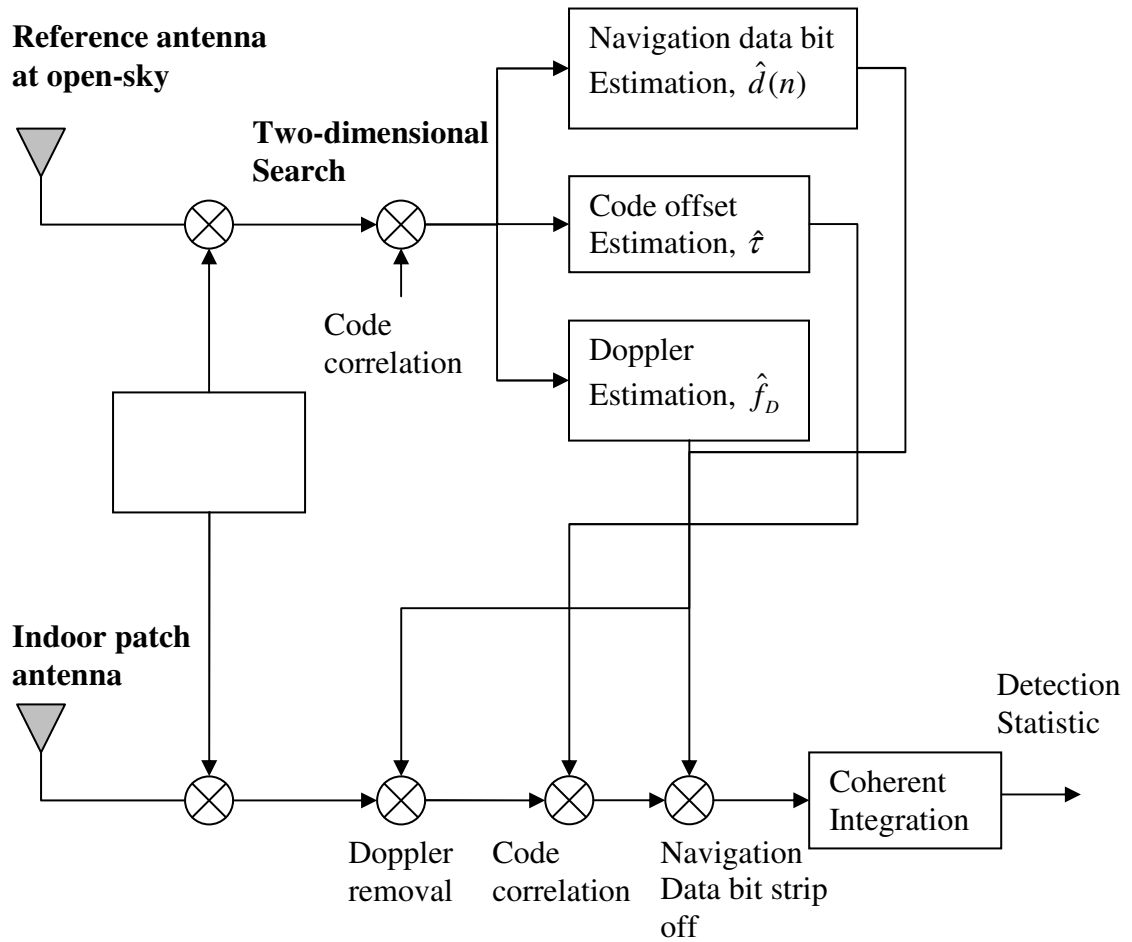
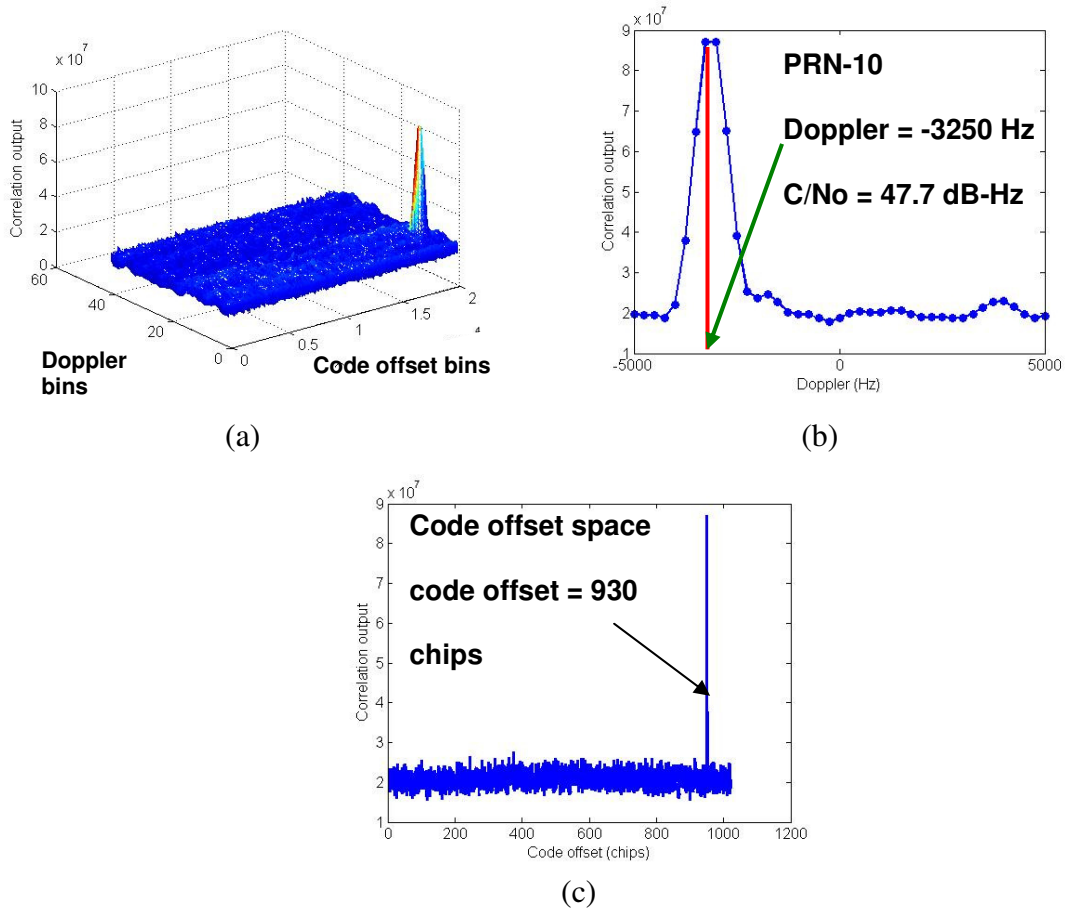


Figure 4.6 Plan view of the test locations in CCIT building, University of Calgary



**Figure 4.7 Software signal processing of GNSS signal acquisition**

Figure 4.7 shows the receiver signal processing stages for the post-mission processing of dual-antenna GPS IF data. The reference antenna was used to estimate the Doppler, code phase and navigation data bits. Those estimated parameters were then used for the data set collected with the indoor patch antenna.



**Figure 4.8 Acquisition results of a strong GPS signal (a) Full search space (b) Doppler frequency space (c) Code offset space**

#### 4.4.1 Signal Acquisition Results

Figure 4.8 shows the acquisition of a strong GPS signal, where the correlation peak is also zoomed in plots of Doppler frequency and for code offset. The Doppler space of  $\pm 5$  kHz and code offset space of 1 ms were considered in this figure. Figure 4.8(a) shows the two-dimensional search space for GPS signal acquisition. The FFT based correlation technique (Tsui 2005) was used to correlate the received signal with the locally generated code.

#### 4.4.2 Signal Tracking Results

To investigate the feasibility of the dual-antenna system proposed herein for spatial combining of GPS signals, it is important to analyze the inherent channel biases. During the preliminary analysis, acquisition results in terms of Doppler estimation and code phase estimation were analysed to determine the significance of inter-channel biases in the dual-antenna system. Figures 4.9 and 4.10 show the fine Doppler and code-offset searches respectively of two U-blox patch antennas under open-sky condition for an antenna spacing of  $2\lambda$  ( $\lambda=19$  cm). The data sets corresponding to these two plots were collected using two *Euro-3M* front-ends (NovAtel 2004). The Doppler estimation utilized was a FFT-based technique, which allowed for a fine resolution of 1 Hz. Both the Doppler and code phase results readily corroborates the stability and the feasibility of the proposed dual-antenna system.

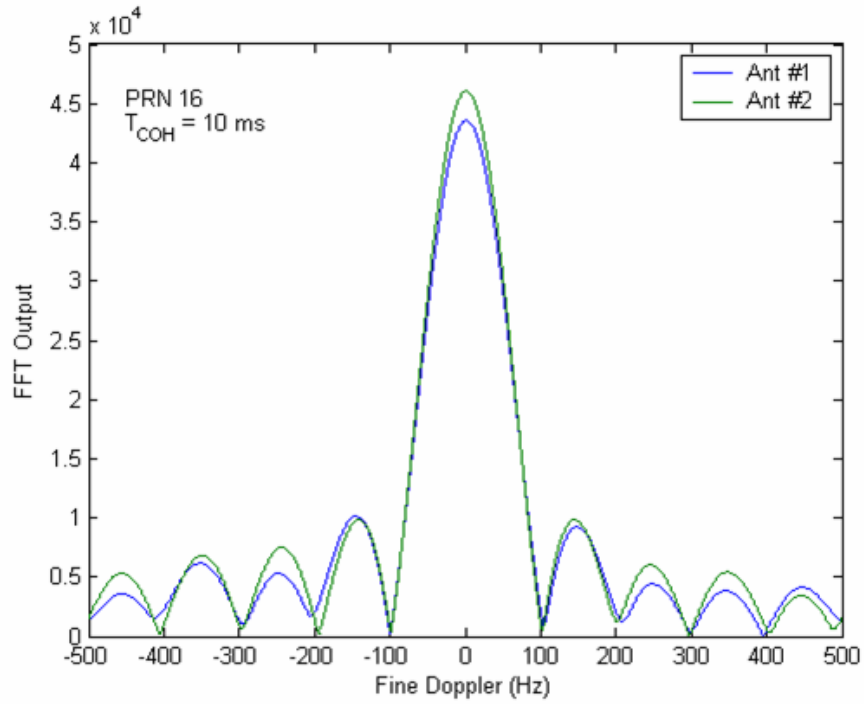


**Figure 4.9** Fine Doppler search for Rx1 and Rx2, PRN-16,  $T_{coh}=10$  ms,  $d=2\lambda$

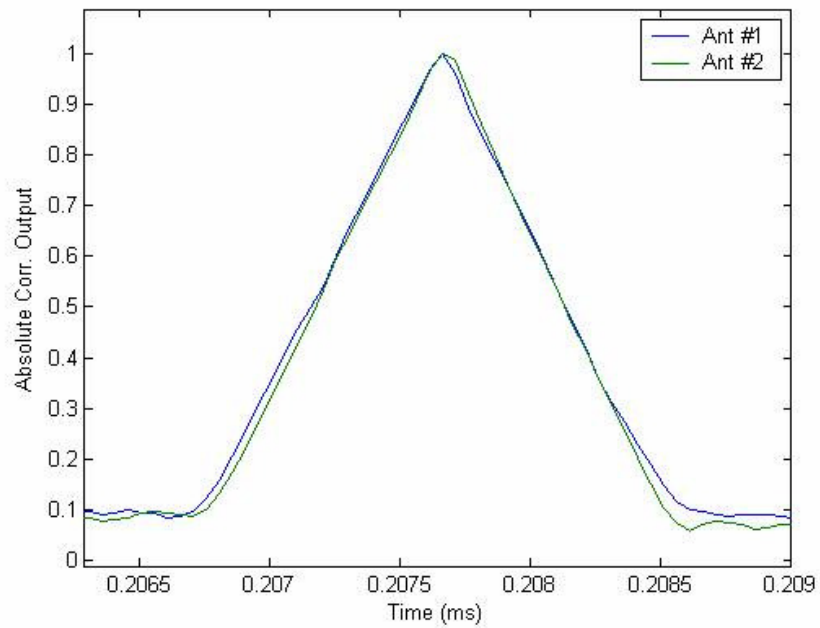


**Figure 4.10** Code-offset search for Rx1 and Rx2,  $T_{coh}=1$  ms,  $N=10$ ,  $T=10$  ms,  $d=2\lambda$

For an antenna spacing of  $2\lambda$ , the inphase and quadrature correlation outputs for the first and second receiver antennas for the case of PRN-16 are shown in Fig. 4.11. The sharp changes in inphase and quadrature phase correlation outputs at 20 ms, 40 ms, 275 ms and 295 ms are caused by the data bit transitions.

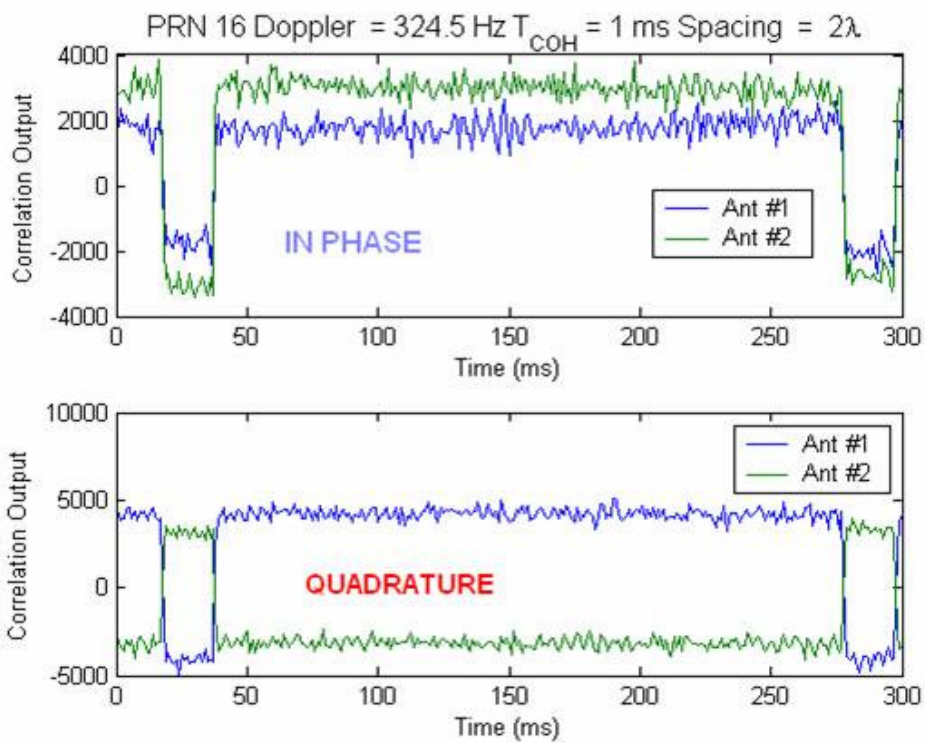


**Figure 4.11 Inphase and quadrature correlation outputs for Rx1 and Rx2 sampled at 1 kHz rate, PRN-16,  $T_{coh}=1$  ms,  $d=2\lambda$**

Figure 4.12 shows the accumulated phase in radians for the two receiver channels over the duration. The phase difference between the two receiver channels can readily be noticed in the plot. The phase difference essentially arises from the initial phase ambiguity caused by the individual phase locked loops in the RF down conversion stages. Note that the phase offset should be estimated separately and be removed prior to any

subsequent analysis. Moreover, the stability of this phase is also critical in terms of subsequent analysis.

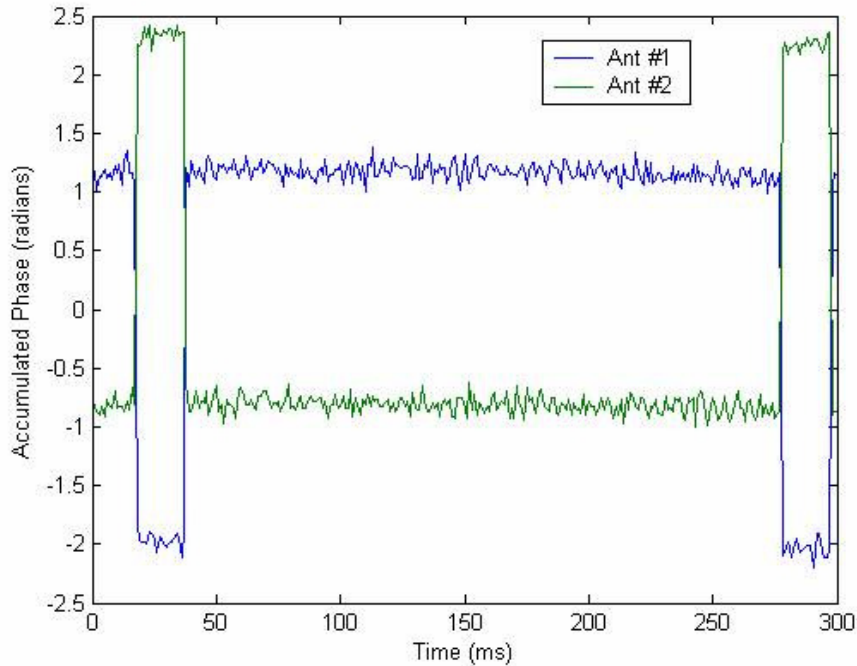


**Figure 4.12 Accumulated phase in radians for Rx1 and Rx2 sampled at 1 kHz rate, PRN-16,  $T_{\text{coh}}=1$  ms,  $d=2\lambda$**

Figure 4.13 shows the results for Doppler and code-phase tracking for one patch antenna located in an indoor location (Room-326, CCIT building) when the indoor patch antenna was simultaneously assisted by one reference GPS receiver located on the rooftop under LOS conditions. Figure 4.13(a) shows the code tracking and Figure 4.13(b) shows the carrier tracking respectively, for this assisted indoor patch antenna, the raw data samples being collected with a *National Instruments (NI)* hardware setup as shown in Figure 4.4.

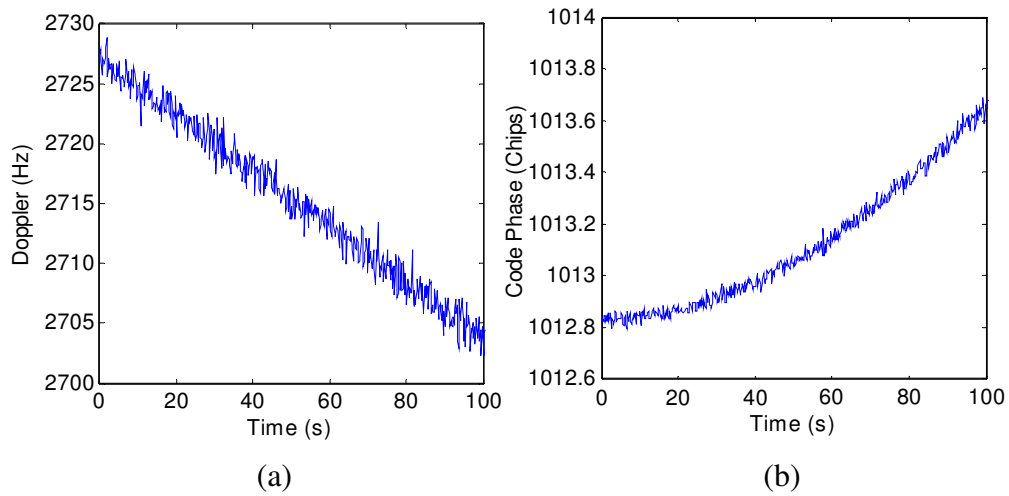
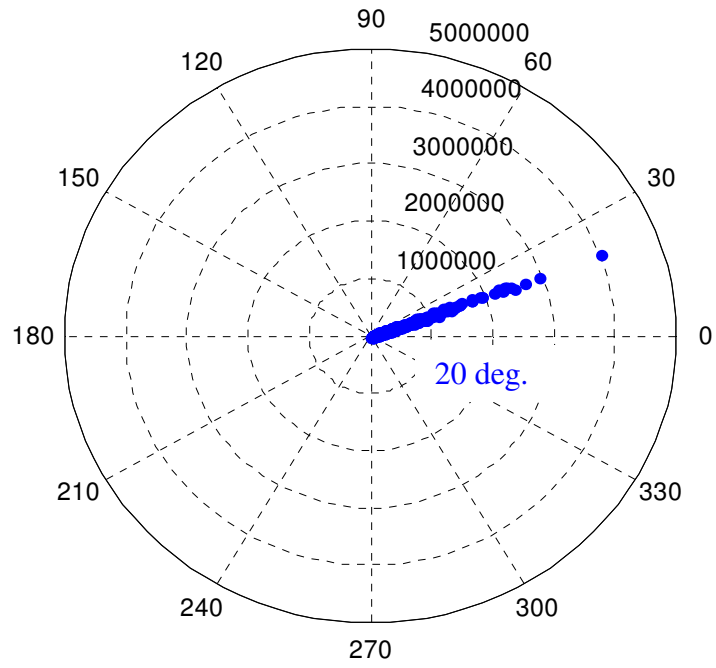


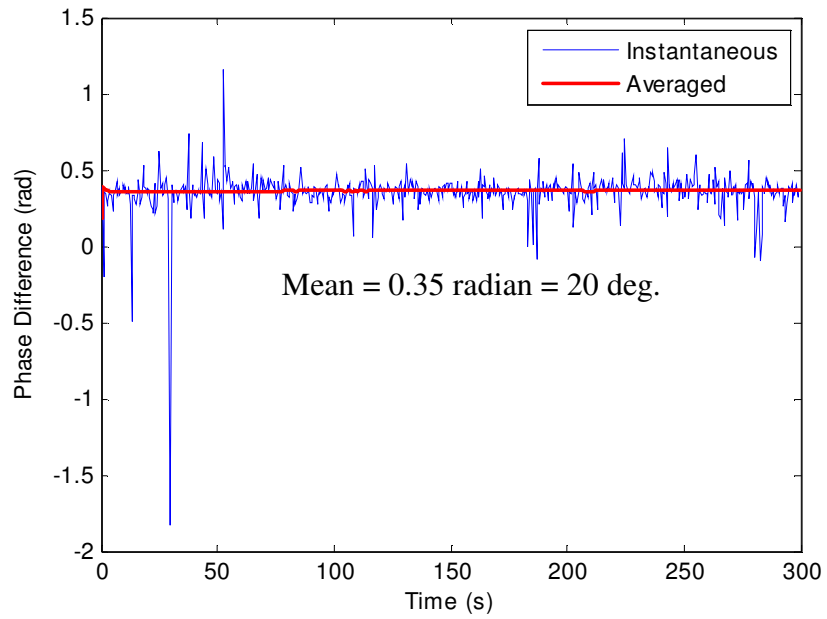
**Figure 4.13 Signal tracking results (a) Doppler tracking (b) Code tracking (System parameters: Sampling frequency  $F_S = 10$  MHz,  $F_C = 3.42$  MHz, selected indoor location)**

#### 4.4.3 Phase stability

Phase stability among the channels is critical in terms of subsequent analysis for spatial combining. Figure 4.14 shows the phase difference, due to PLL ambiguity, between the two receivers for PRN-26 over a duration of five minutes. Figure 4.14(a) shows the polar plot of phase difference and Figure 4.14(b) shows the instantaneous phase difference between the two receivers over a duration of five minutes. The phase difference was almost constant over the observation period hence it can be averaged out during post-mission processing. The resulting covariance matrix is used for finding the antenna correlation.



(a) Polar plot



(b) Over time

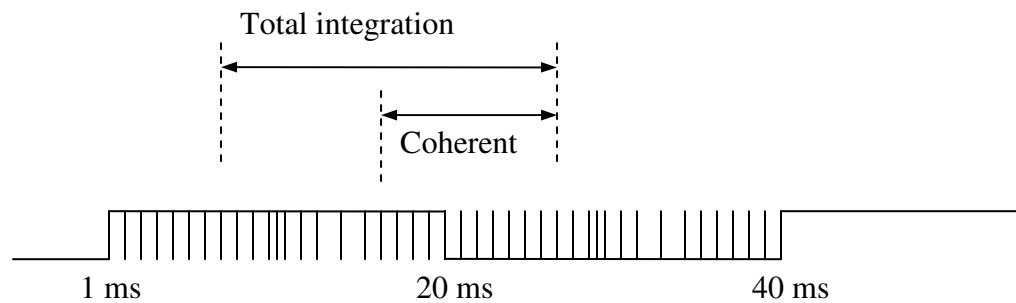
**Figure 4.14 Phase difference of PRN-26 over 5 mins, due to PLL ambiguity, between two antennas at open-sky-condition**

#### **4.4.4 Navigation Bit Synchronization**

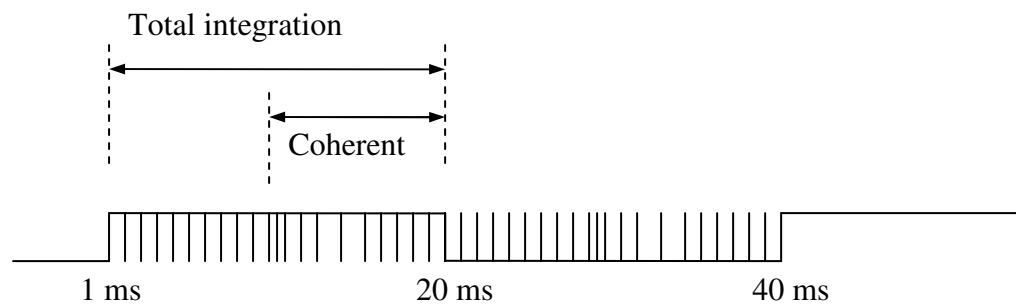
The navigation message contains information in the form of bits at the rate of 50 Hz. This results in a bit interval of 20 ms, whereas it is mentioned earlier that the C/A code repetition period is 1 ms. Data bit synchronization means detection of data bit boundary and synchronization of coherent integration with that boundary. This is essential for navigation data bit extraction, especially under weak signal tracking conditions. This is because for weak signal acquisition and tracking case, the coherent integration time necessarily has to be extended beyond 20 ms bit intervals of the navigation message. If the bit boundaries are not synchronized, the correlation output after coherent integration will be low because of opposite polarity of the data bits. As a result, it becomes evident that data bit boundaries must be synchronized for weak signal tracking e.g. indoors.

Figure 4.15 shows the effects of data bit changes on coherent integration output of the received signal. Since C/A code repeats every 1 ms, the correlation output value after coherent integration of 1 ms is calculated. If there is a bit transition, the phase of the coherently integrated correlated output has a shift of  $\pi$  radians, i.e. the sign of in-phase and quadrature-phase correlation values reversed. In the following a technique of navigation bit synchronization, referred to as *hard decision* calculating the phase of the correlation output, is explained. A vector of length 20 is considered and the variable is synchronized with the integration timer. An index counter is assumed to take on values from 0 to 19, where 0 refers to first element in the vector and 19 refers to the 20<sup>th</sup> element of the vector, respectively. To detect the data bit synchronization, the phase of correlation

output is sensed after every 1 ms. For each sign change of the correlation output, a 1 is added to the element in the vector pointed by the index counter. When any element corresponding to an index vector exceeds all other 19 elements by a pre-specified amount, then the bit synchronization is declared successful and then the C/A code epoch count is reset to the correct value. Figure 4.16 shows the hard decision navigation data bit synchronization principle. Figure 4.17 shows the extraction of navigation data bits from the correlation output values.



**(a) Before bit synchronization**



**(a) After bit synchronization**

**Figure 4.15 Effect of bit synchronization on coherent integration output**

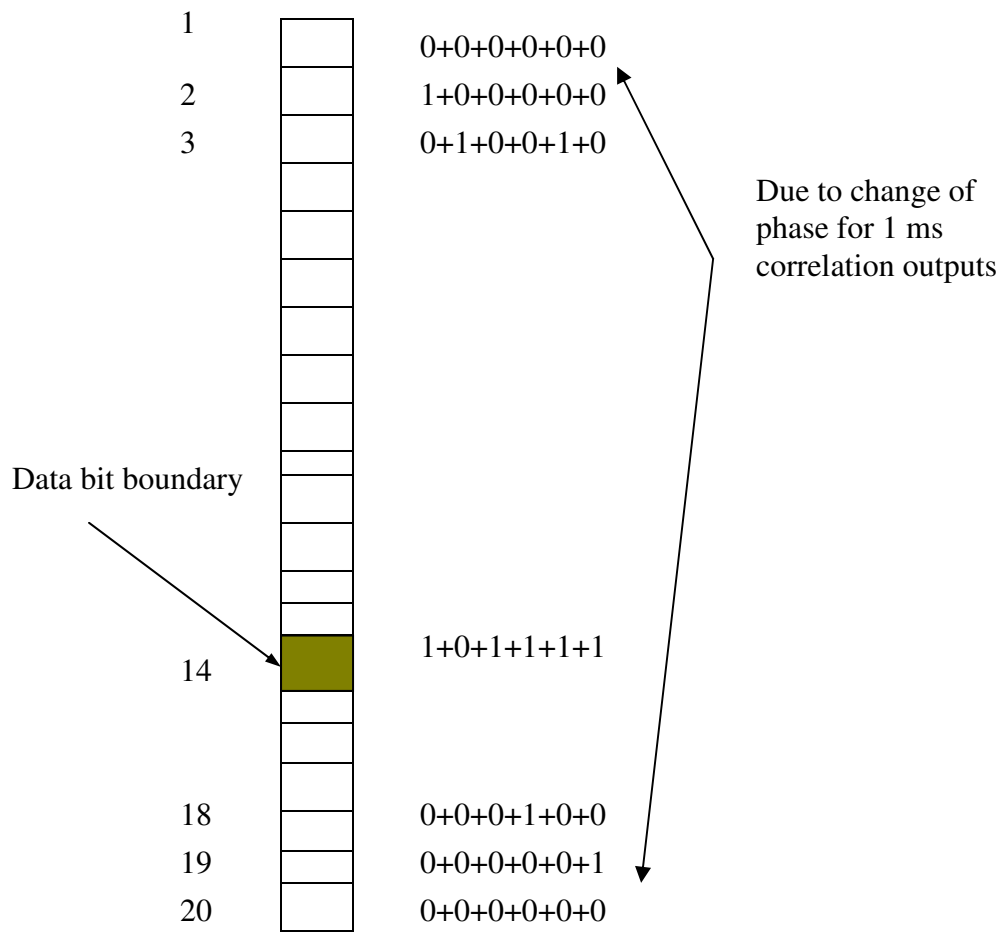


**Figure 4.16 Hard decision technique for navigation bit synchronization**

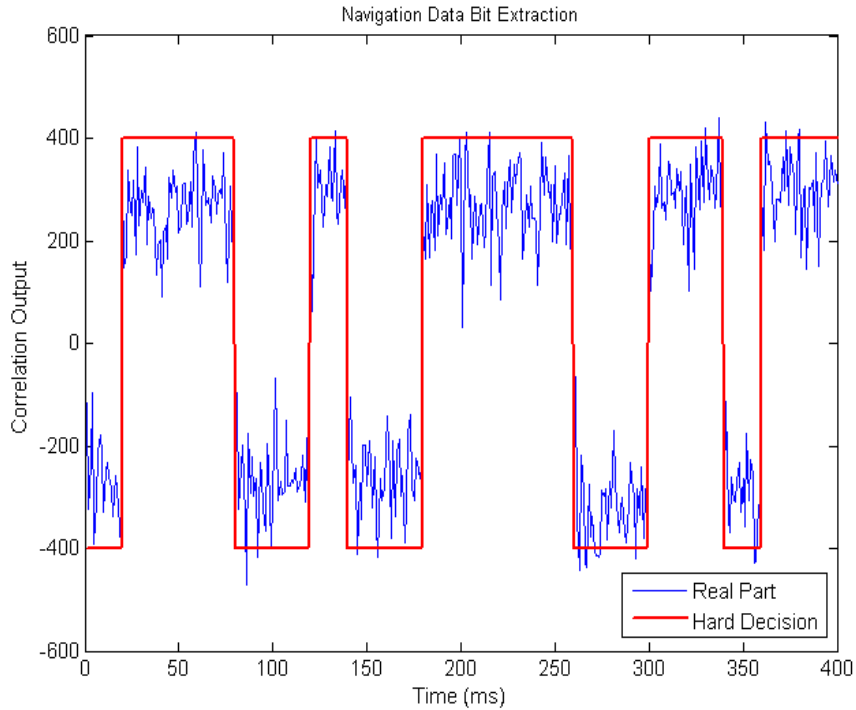
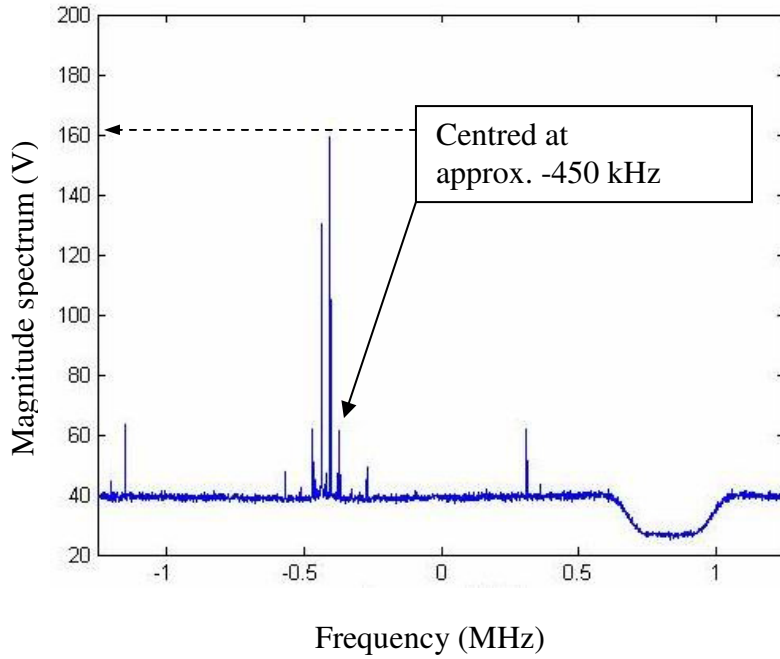


**Figure 4.17** Navigation data bit extraction from correlation output values,  $T_{coh} = 1$  ms,  $C/N_0 = \text{approx. } 40 \text{ dB-Hz}$

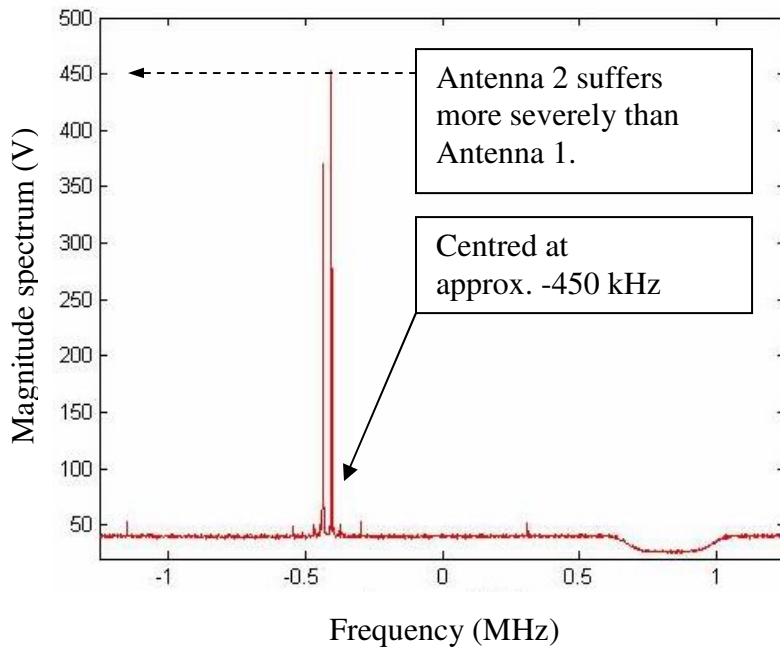
#### 4.4.5 Continuous Wave Interference Issues and Frequency excision

During the data collection campaign, the NI-based data collection setup itself acted as a source of spurious signals that contributed to an undesired continuous wave interference (CWI) at approximately -450 kHz. The effect of this CWI was severe because the antennas were close to the main data collection system. Figure 4.18 (a) and (b) show the spectrum of the received signal at both antennas. It is clear that both channels were affected by the CWI, the effect on the second antenna being more severe. Though the correlation outputs were also severely affected by the CWI from the system, in order to remove the interference, the data collection PC and front-ends were taken a distance

away from the antennas. To further mitigate the unwanted CWI effects from the correlation outputs, a FFT-based frequency excision technique was adopted. The effects of CWI on correlation output before and after applying the frequency excision technique is shown in Figure 4.19, which shows that antenna 2 was more affected by the CWI. However, using the frequency excision technique, the unwanted frequencies were removed. In addition to Figures 4.18 and 4.19, Figure 4.20 shows that the code-phase and Doppler estimates contain a lower amount of outliers after frequency excision is applied.

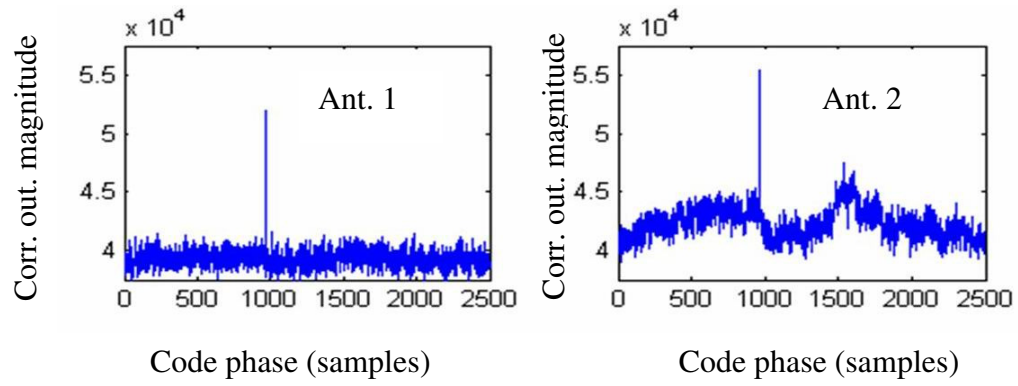


(a) Antenna 1

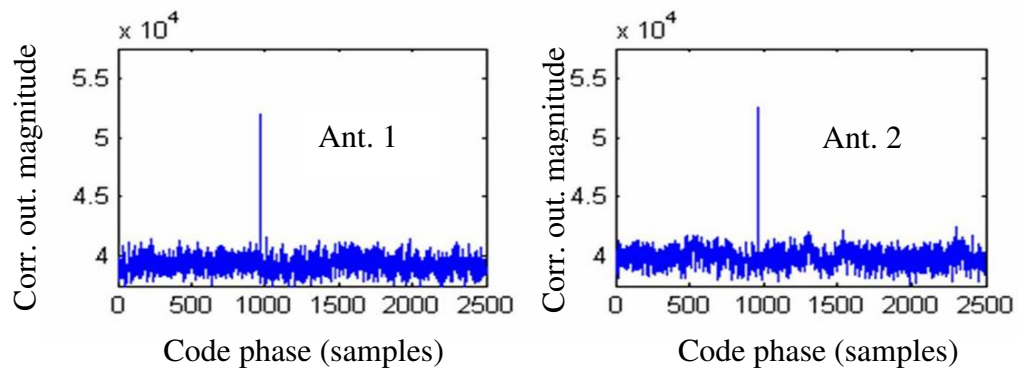


(b) Antenna 2

**Figure 4.18 Observed continuous wave interference (CWI)**



(a)



(b)

**Figure 4.19 Effects of CWI on antenna correlation outputs (a) before and (b) after frequency excision is applied.**

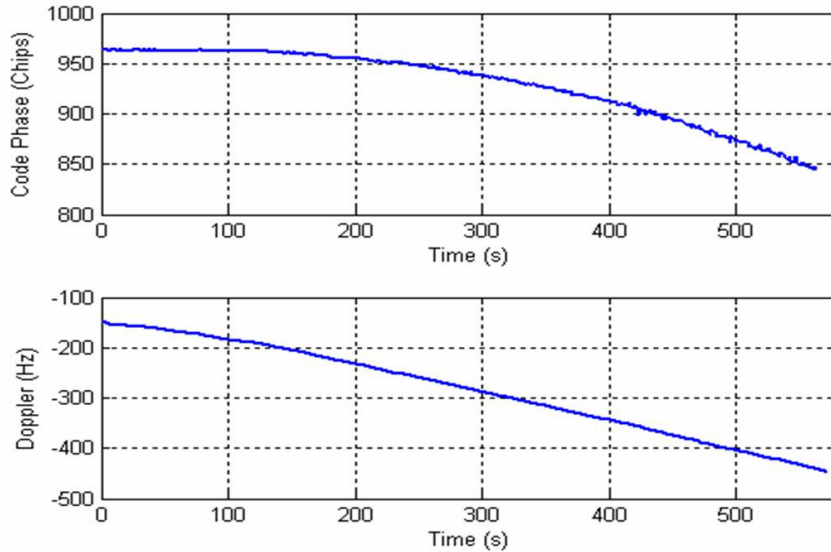


**Figure 4.20 Code phase and Doppler tracking after frequency excision. The outliers are removed after frequency excision.**

#### **4.4.6 High-Sensitivity Performance with Extended Coherent Integration**

Due to weak and severe NLOS signal conditions indoors, high-sensitivity operation with extended coherent integration time is necessary. In this section, a few indoor results are presented. Coherent integration times of 100 ms, 200 ms, and 400 ms have been considered and the corresponding detection outputs are shown in Figures 4.21, 4.22 and 4.23, respectively. Non-coherent summations are also considered. It is clear that there exists a PSNR improvement for extended coherent integration time. Another significant point is the effect of data bit synchronization on the detection output of the signal. Figure 4.24 shows one particular condition when the extended coherent integration operation has been performed without the assistance of data bit synchronization from the reference receiver. As expected, there is no peak detection without data bit information. As shown in Figure 4.25, this is reasonable to show the PSNRs of 20 ms coherent integration over a

total observation period of 6 s. As shown in Figure 4.25, with data bit synchronization, the PSNR is improved over the entire observation period.

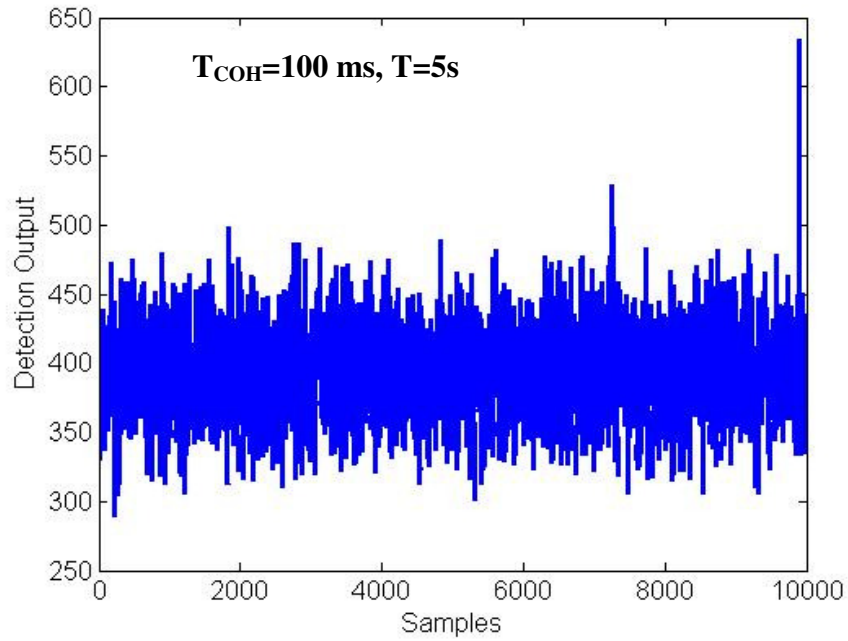


**Figure 4.21** Extended integration detection output for  $T_{\text{coh}}=100$  ms,  $T=5$  s

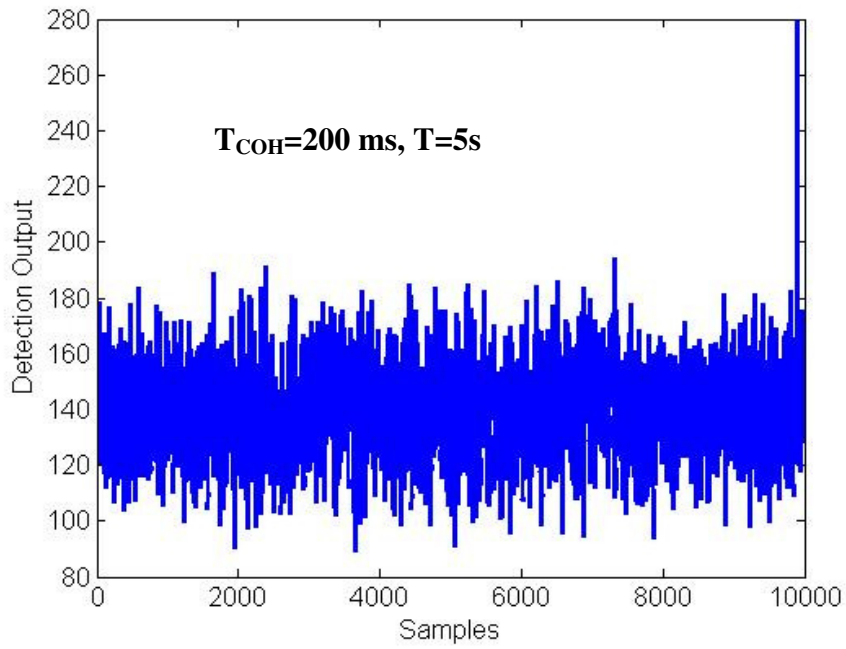


**Figure 4.22** Extended integration detection output for  $T_{coh}=200$  ms,  $T=5$  s

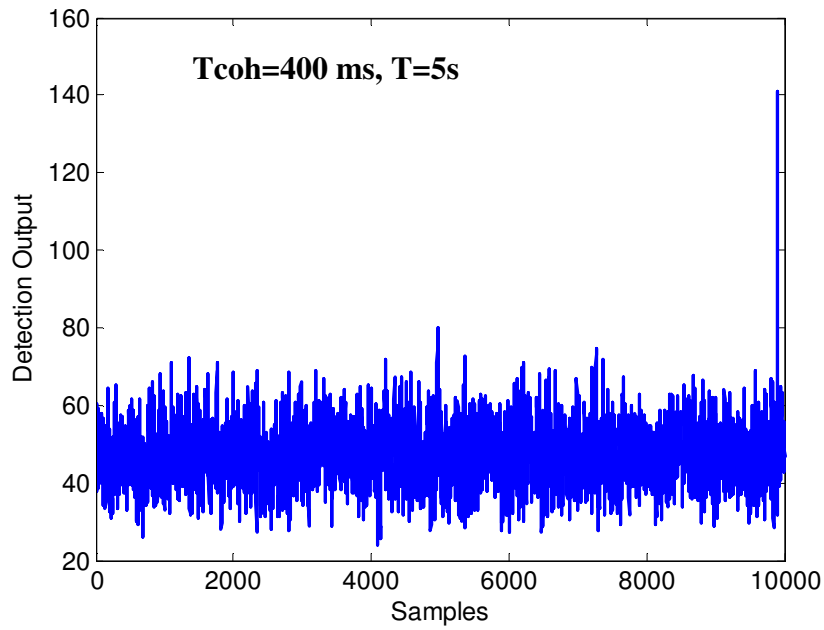


**Figure 4.23** Extended integration detection output for  $T_{coh}=400$  ms,  $T=5$  s

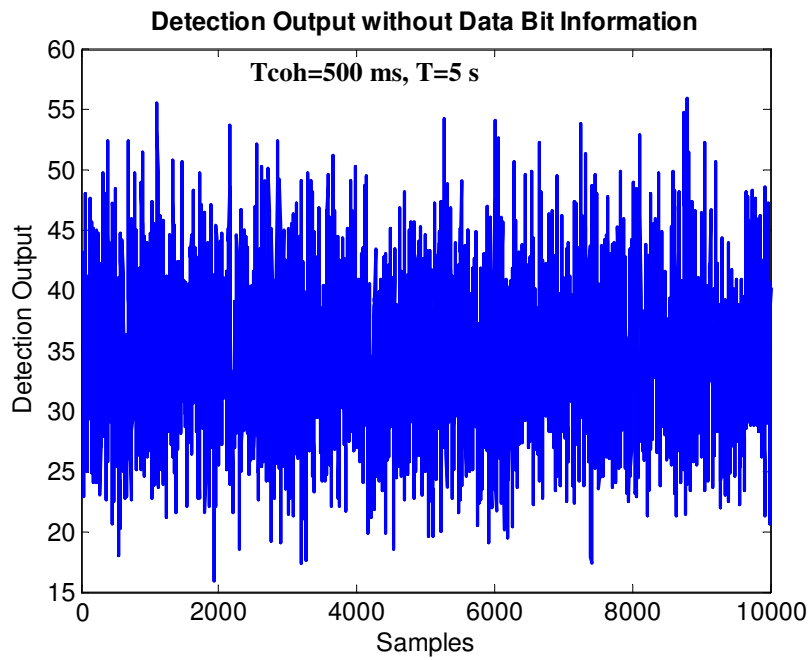


Figure 4.24 Detection output without data bit information,  $T_{coh}=500$  ms,  $T=5$  s

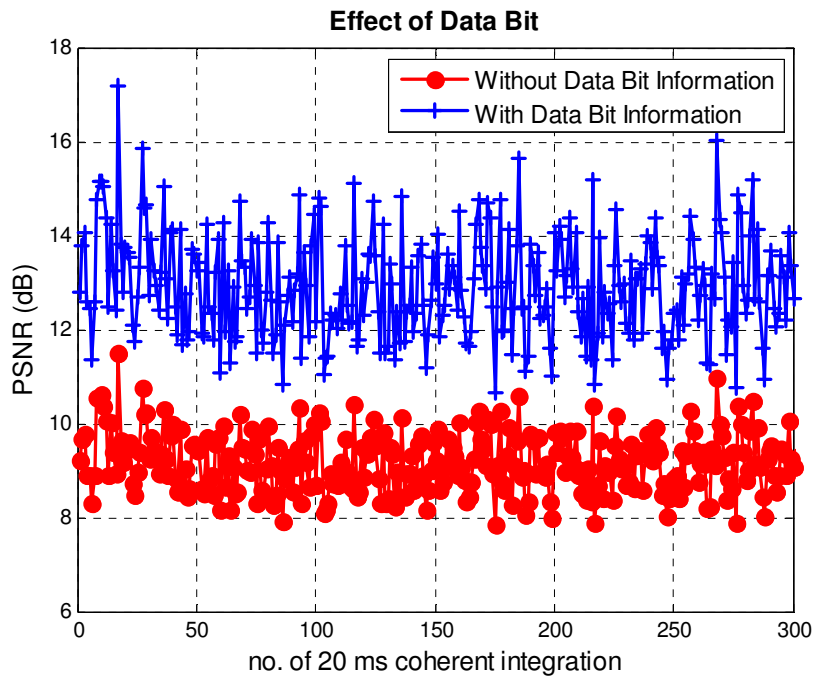


Figure 4.25 PSNR sampled at 20 ms over an interval of  $T=6$  s. Total points=300

## **4.5 Conclusions**

In this chapter of the thesis, the test methodology has been described in relation to the GPS digital receiver signal processing. The test setup is first described, which is then followed by the software dual-antenna GPS signal processing and implementation. A brief description of the received GPS signal, signal search space and the acquisition process was also illustrated. Several intermediate results have been included in order to verify some important aspects of the implemented dual-antenna receiver system. This chapter mainly explained the experimental procedures for multiple GPS antenna signal processing as well as the accuracy of the test methodology that has been developed at the hardware level to collect raw data from multiple GPS receivers. Extended coherent integration times and phase stability are thereby of critical importance. A brief note on the data sets and some pictures of the indoor test location have been included in the next chapter where the remaining results as well as the main contribution of GPS spatial signal combining gains and improvement of detection performance with dual-antenna receiver setup are provided.

## CHAPTER 5: Experimental Analysis and Seminal Results

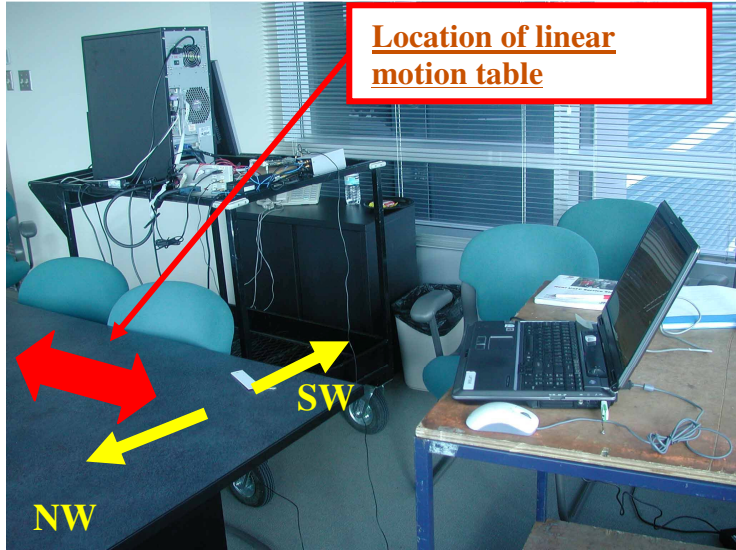
This chapter discusses the major results obtained with spatial combining of GPS signals. The performance of SNR gain and improvement in detectability of GPS signals in degraded signal environments is demonstrated. The detection performance of single antenna and multiple antenna performances are compared under real indoor situations. The performance of spatial combining schemes such as the equal-gain (EG) combining and estimator-correlator (EC) combining are also reported. The test results of antenna correlation, spatial combining gain in terms improvement in SNR and detection performance are demonstrated.

### 5.1 Overview of the Recorded Data Sets and Data Processing

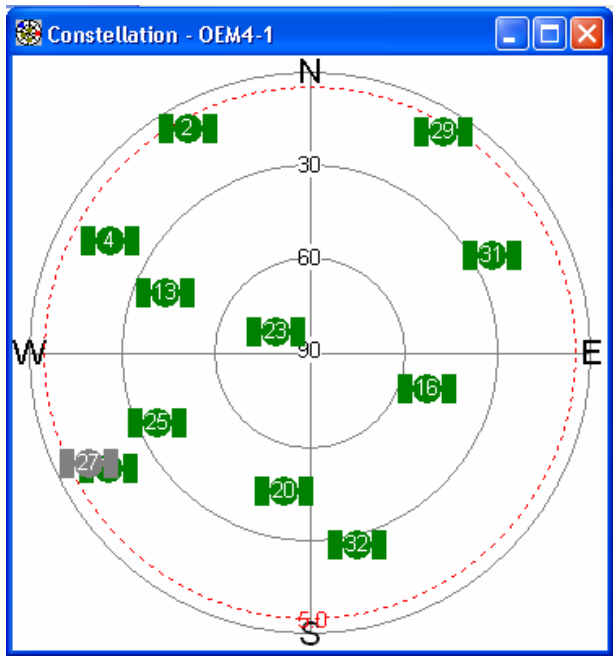
As discussed in Section 4.4 there are two selected locations where raw indoor GPS data were collected using the dual-antenna GPS receiver system. The GPS L1 samples were collected at a sampling rate of 10 MHz. The collected data samples were first amplified by the respective LNAs and processed with down-conversion. However, the LNAs for the two receiver front-ends were independent, but of the same type, so their amplification characteristics are expected to be similar and not affecting the analysis significantly.

In the indoor location test, the linear motion table was placed inside the designated room and one GPS patch antenna was mounted on it. The test strategy was to place one antenna on the linear motion table and collect raw data for a period of one hour. The reason for using one antenna was that the NI system had two available front-end receivers, of which one was used for tapping real LOS GPS signals with a reference GPS antenna located on

the rooftop. The linear motion table was moving at a speed of 1.2 cm/sec or approximately  $\lambda/16$  per second, where  $\lambda$  is the carrier wavelength for GPS L1 band signal and is equal to approximately 19 cm. The indoor antenna inside the office room had its north side view blocked with the building wall, but the southern side of the antenna was open through the glass windows. While the GPS antenna was moving on the linear table, the concept of synthetic GPS antenna was tested using the data at several antenna spacing. Figure 5.1(a) shows the test location inside the room and the position of the linear motion table, and the sky-view plot at that time as recorded by the reference antenna is shown in Figure 5.1(b).



(a) Indoor test location:



(b) Skyview at one particular instant

**Figure 5.1 Selected indoor data collection site (a) indoor (b) skyview plot of reference antenna**

For verification purposes, a second location on the same floor of the same building was also investigated. As seen in Figure 5.2, the patch antenna indoors was facing the glass

window panes towards the north-west (NW) direction. The reference antenna was placed on the roof of the same building with an unobstructed view. The roof reference antenna was stationary; the indoor patch antennas were mounted on a linear motion table. The linear motion table carried the antennas and moved back and forth at a speed of 0.012 m/s i.e.  $\lambda/16$  /s. Figure 5.2(a) shows the orientation of patch antennas indoors and Figure 5.2(b) shows the sky-view plot from the reference receiver during that time of data collection. The red blocks in Figure 5.2(b) show the available PRNs in NW and NE directions.

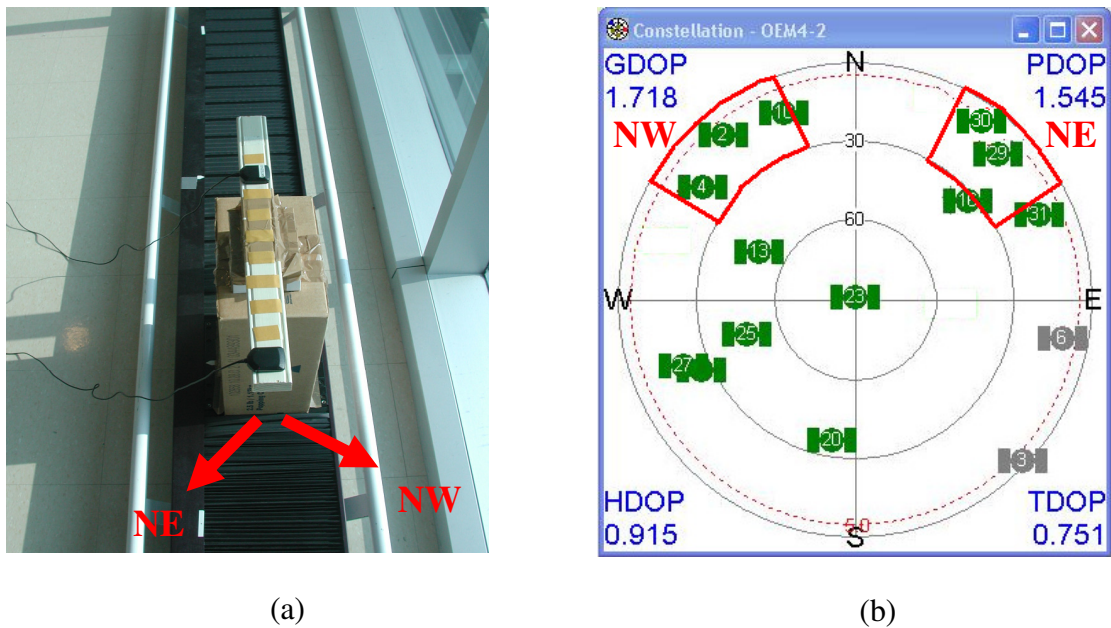


**Figure 5.2 Orientation and skyview plot of the dual-antenna system**

The data collected using the NI based front-ends was first stored in a PC hard drive for post-mission processing. Using conventional FFT-based correlation techniques in two-dimensional search space, the code-phase and Doppler were determined, however, the search space is reduced from 10 kHz to only 500 Hz by using the rough estimates of Doppler from the *NovAtel* OEM4 reference receiver antenna located at the rooftop.

Additionally, the frequency estimates were obtained through a discrete open-loop FFT-based tracking. The code phase and Doppler tracking outputs obtained through block FFT-based processing have been already shown in Chapter 4. The system parameters utilized during the data collection are summarized in Table 5.1. The digitized samples were obtained at a rate of 10 MHz.

**Table 5.1 System parameters**

Parameter	Front-end Bandwidth	Sampling Frequency	Intermediate Frequency	Coh. Int. Period	PRN Code Length	Sampling Factor
Value	<b>20 MHz</b>	<b>10 MHz</b>	<b>3.42 MHz</b>	<b>100 ms</b>	<b>1023 chips</b>	<b>≈10</b>

## 5.2 Experimental Results

The results of the spatial combining of GPS signals as obtained herein are described in three major steps.

Firstly, the fading behaviour indoors for both of the antennas has been shown, where the  $C/N_0$  distribution characteristics indicate the indoor fading behaviour in terms of envelope correlation and Ricean factor. The envelope correlation is compared with the theoretical correlation coefficient as the antenna spacing is varied.

Secondly, the effects of spatial combining are illustrated. In particular, the effects of equal-gain combining (EGC) and estimator-correlator combining (ECC) are illustrated and compared. A comparison with single antenna case is also made. PSNR improvements for EGC and ECC are also shown.

Finally, the detection performance for a single antenna and diversity combining are compared. Analyses with receiver operating characteristics (ROC) curves in terms of

improvement in detection probability as compared to that of single antenna processing are illustrated.

### 5.2.1 Indoor Fading Characteristics

For the selected indoor locations, coherent integration times of 2 ms, 4 ms and 8 ms along with subsequent non-coherent integration were considered. As an example of indoor fading characteristics  $C/N_o$  characteristics over time for PRN-29 corresponding to the dataset with  $1 \lambda$  antenna spacing is shown in Figure 5.3.

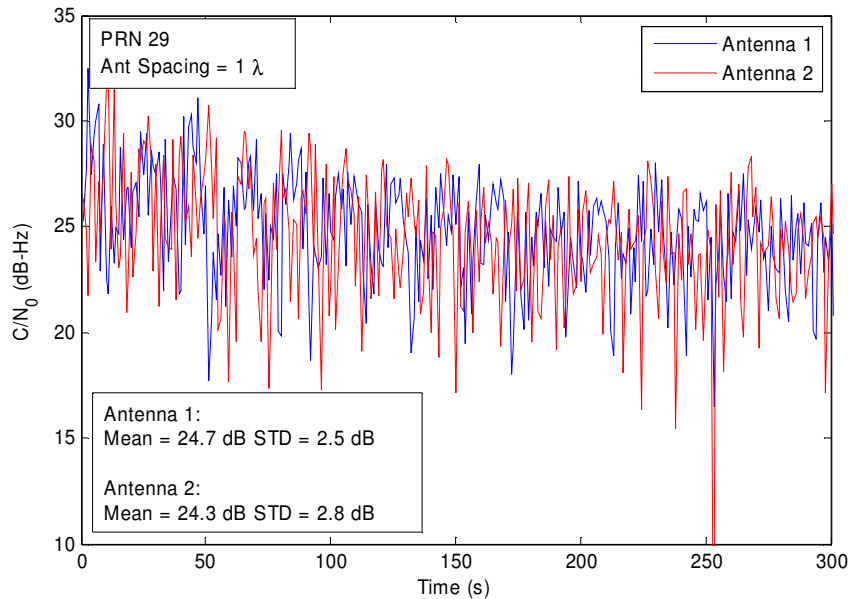


**Figure 5.3  $C/N_o$  fading plots for two antennas at the indoor location using a synthetic antenna configuration**

With a coherent integration time  $T_{\text{coh}} = 2$  ms and a total non-coherent sum of  $T=300$  ms, the average  $C/N_o$  for both of the antennas is approximately 24.5 dB-Hz for  $1\lambda$  spacing.

However, the  $C/N_o$  characteristics have been further investigated with the help of a

probability cumulative distribution function (cdf) as shown in Figure 5.4. The propagation channel and its probability distribution are well explained in several textbooks in the communication engineering area, for example, in Stüber (2000). When signal propagation is concerned, some types of propagation environments have a specular or LOS component. Ricean fading occurs when one of the propagation paths, typically a LOS propagation signal, is much stronger than the others. The LOS signal strength is characterized by the Ricean factor,  $K$ , which is defined as the ratio of the specular power to scattered power (Stüber 2000). This means that, when  $K = 0$  the channel exhibits Rayleigh fading and when  $K = \infty$  the channel does not exhibit any fading at all. That is, when  $K = \infty$  the channel is Gaussian. In Ricean fading, the amplitude gain of the propagation channel is characterized by a Rician distribution. On the other hand, Rayleigh fading is a special fading model for the propagation scenarios when there is no LOS signal. This is sometimes considered as a special case of the more generalized concept of the Ricean fading model. In Rayleigh fading, the amplitude gain is characterized by a Rayleigh distribution. However, the results shown in Figure 5.4 indicate that the signals at the two antennas show a Ricean pdf fit with a very low Ricean factor of  $K = -28$  dB. This low value indicates that the two antennas experience Rayleigh fading and after subsequent analyses it was found that the envelope correlation coefficient between the two antennas was low (approximately 0.07 in this case). Figure 5.5 shows the fading histogram for weak GNSS signal acquisition for an extended coherent integration time of  $T_{\text{coh}}=200$  ms with non-coherent summation of  $T=1$  s. As shown in Figure 5.5(b), with the given scenario the GPS signal indoor suffers approximately 30 dB mean attenuation with respect to nominal LOS signal power.

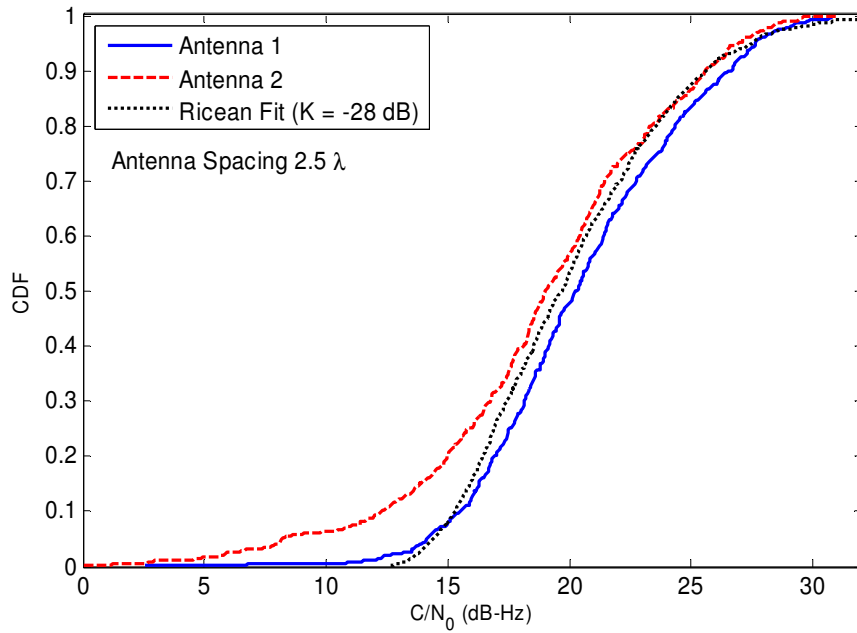
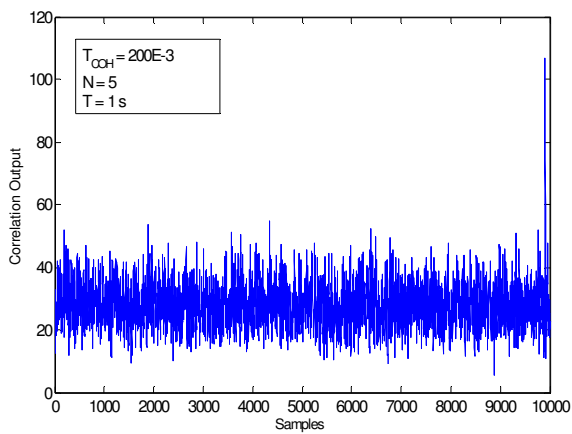
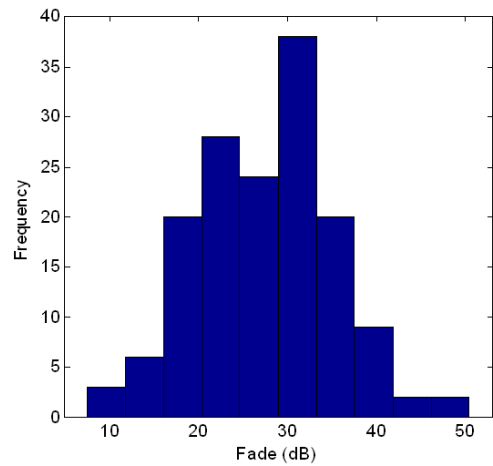


**Figure 5.4 Cumulative distribution function for two antennas in a synthetic array configuration (with best fit Ricean pdf of  $K=-28$  dB and  $\rho=0.07$ , indoor location inside,  $d=2.5\lambda$ , PRN-4)**



(a)



(b)

**Figure 5.5 Fading histogram during weak GNSS signal acquisition. (a) Correlation output with extended coherent integration,  $T_{\text{coh}} = 200$  ms,  $T = 1$  s (b) Fading histogram, indoor**

### 5.2.2 Envelope Correlation

The envelope correlation between the two receiver channels has been calculated and compared with theoretical values found by Jakes (1994). After code and carrier removal, the resulting output is coherently integrated prior to any kind of temporal or spatial processing. Let a coherent integration output of  $T_{\text{Coh}}$  seconds for first and second antennas be  $x_0[k] = I_0 + jQ_0$  and  $x_1[k] = I_1 + jQ_1$  respectively, in which case their envelopes are  $x_0 = |x_0[k]| = \sqrt{I_0^2 + Q_0^2}$  and  $x_1 = |x_1[k]| = \sqrt{I_1^2 + Q_1^2}$  respectively, then the envelope correlation between the two antennas is expressed in terms of mean-removed versions of  $x_0$  and  $x_1$  as

$$\begin{aligned} \rho &= \frac{E\{(x_0 - \bar{x}_0)(x_1 - \bar{x}_1)\}}{\sqrt{\text{var}(x_0 - \bar{x}_0)} \cdot \sqrt{\text{var}(x_1 - \bar{x}_1)}} \\ &= \frac{E\{(x_0 - \bar{x}_0)(x_1 - \bar{x}_1)\}}{\sqrt{E\{(x_0 - \bar{x}_0)^2\}} \cdot \sqrt{E\{(x_1 - \bar{x}_1)^2\}}} \end{aligned} \quad (5.1)$$

However, Jakes (1994) showed that the theoretical correlation value between two receiving antennas depends on the spacing between them, which can be written in terms of a zero-order Bessel function of the first kind as

$$\rho = J_0^2\left(2\pi \frac{d}{\lambda}\right). \quad (5.2)$$

The expression in (5.2) holds good for a uniform angle of arrival distribution in azimuth and omni-directional receiving antennas that are matched to the polarization of the incoming radio wave. It should also be noted here that the envelope correlation of signals received by two antennas can be influenced by several factors, such as the radiation pattern, mutual coupling, direction of arrival of the radio wave and antenna gain. A detailed discussion of antenna correlation was provided in Chapter 2. To overcome these issues, the proposed test methodology utilized a single antenna with linear motion such that a linear array is emulated. Figure 5.6 shows the squared magnitude envelope correlation as a function of antenna spacing and the theoretical curve. In addition to this, antenna correlation results for two indoor patch antennas for selected antenna separation is also plotted in Figure 5.6. As shown in Figure 5.6, the measured antenna envelope correlation is generally lower than the theoretical correlation curve, especially for a smaller antenna spacing. This is because the indoor patch antenna used in this research is not an ideal antenna; also the radiation pattern of the indoor patch antenna is not omni-directional (Clarke 1968). As seen in Figure 5.6, the measured squared magnitude envelopes maintained a similar shape for all of the available PRNs but they differed in terms of actual correlation value. This is because the actual antenna envelope correlation significantly depends on the angular multipath spread besides antenna characteristics (Durgin & Rappaport 1999).

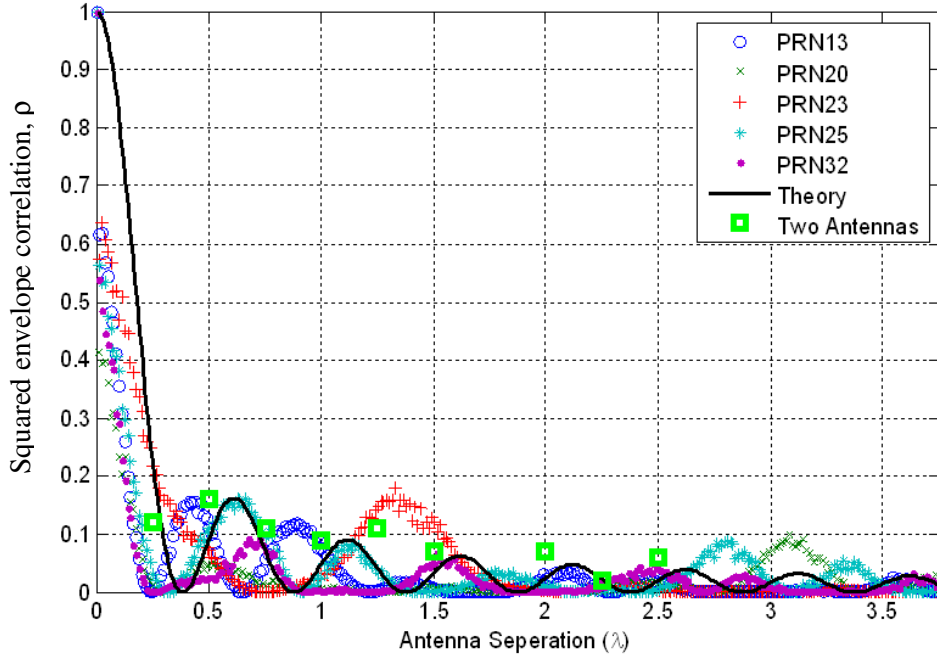


**Figure 5.6 Squared envelope correlation as a function of antenna spacing, indoor location**

As shown in Figure 5.6, the average antenna correlation obtained through experimental measurements readily validates the theoretical envelope correlation prediction shown in Eq. (5.2).

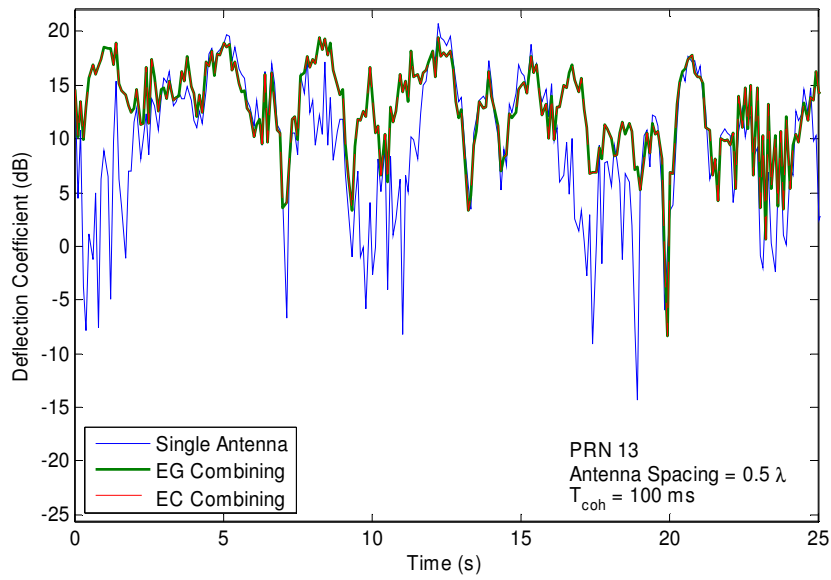
### 5.2.3 Diversity Gain

The diversity gain measurements initially involve the estimation of SNR at the output of the coherent integration. Here the post-correlation SNR for the single and dual antenna channel combining schemes has been evaluated in terms of the *deflection coefficient*  $d^2$  defined as (Kay 1998)

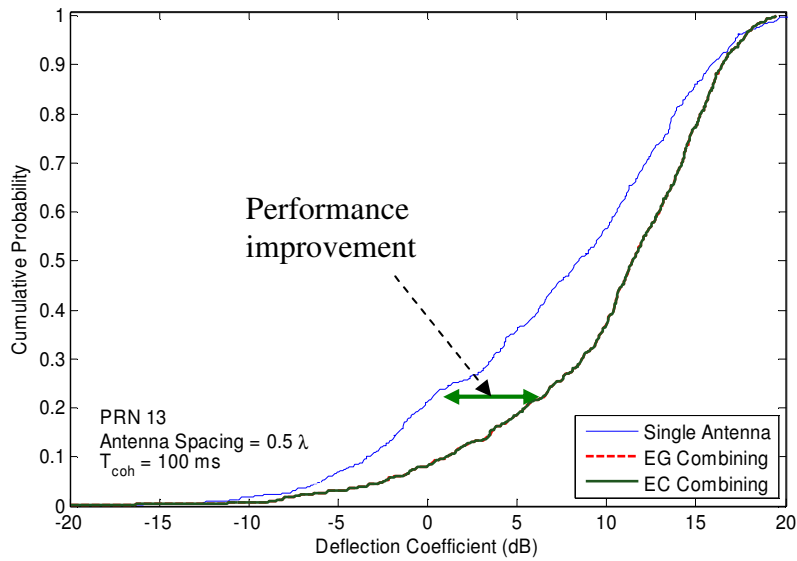
$$d^2 = \frac{\{E(z; H_1) - E(z; H_0)\}^2}{\frac{1}{2}\{\text{var}(z; H_0) + \text{var}(z; H_1)\}} \quad (5.3)$$

where  $z$  denotes the final detection output i.e. the test statistic as described in Chapter 3 and  $\text{var}(\bullet)$  is the variance operation. Since the detection statistics are no longer modeled as Gaussian random variables, the *deflection coefficient* provides only an approximate measure of diversity gain. For the dual-antenna GNSS signal reception, the final detection output  $z = T(x)$  is a sum of two Chi-square random variables, and that is why the expression of the deflection coefficient  $d^2$  has taken a generalized form as shown in eq. (5.3) and its denominator has taken into consideration the effects of the variance of  $z$  in both  $H_0$  and  $H_1$  conditions. Figure 5.7 shows the deflection coefficient measures for the single and dual antenna combining schemes corresponding to the indoor data set of  $0.5 \lambda$  antenna spacing for PRN-13. The cumulative distribution function is also plotted for the same dataset. As shown in Figure 5.7 (a), the deflection coefficient for the spatial combining techniques has experienced a lower number of fades as compared to the single antenna processing. Correspondingly, for a given smaller value of the cumulative probability, the deflection coefficient values increases drastically. The gap in performance between single antenna and diversity antennas has been marked in Figure 5.7(b) and this performance improvement is due to the diversity gain with spatial signal combining. However, both the EG and EC combining are characterized by similar distributions. Figure 5.8 shows the average gain in deflection coefficient at a cumulative probability of 0.1, i.e. 10% of the time, for various diversity combining schemes as a function of antenna spacing. The deflection coefficients for equal-gain (EG) and estimator-correlator (EC) combining were first calculated and then the deflection coefficient gain was calculated with respect to a single antenna. The deflection coefficient gains thus obtained are then averaged over all available PRNs and the results

are shown in Figure 5.8(a). The maximum diversity gain of 6.3 dB was obtained for an antenna spacing of  $0.5\lambda$ , i.e. 9.5 cm. However, as mentioned earlier, it is noted that the deflection coefficient here is not an accurate measure of the diversity gain. The error bars for EG and EC combining are also shown in green-shaded areas. As shown in Figure 5.8(a) there is an averaged diversity gain of 6.3 dB at  $0.5 \lambda$  antenna spacing, which agrees with the theoretical diversity gain of approximately 6.5 dB for the case of dual-antenna EC combining as shown in Appendix B.

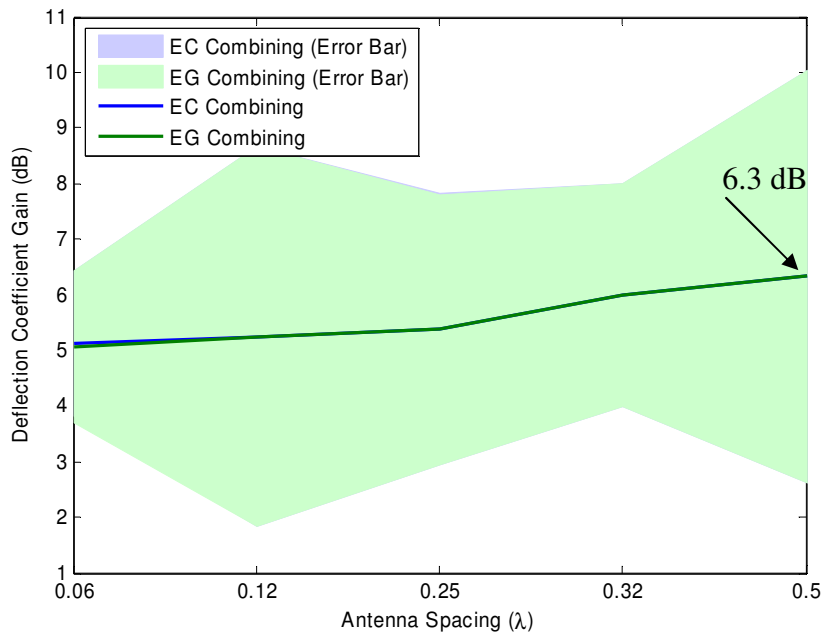


(a)

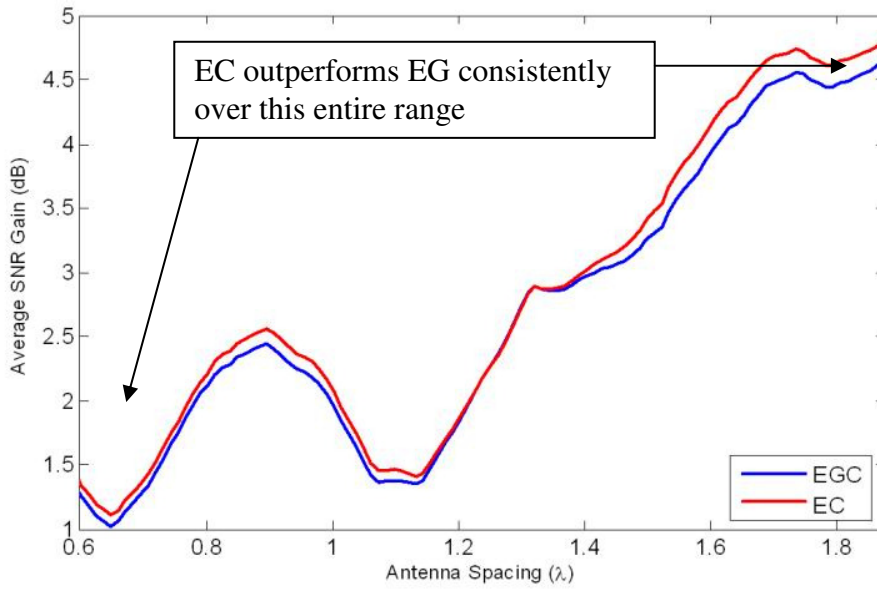


(b)

**Figure 5.7 Deflection coefficient characteristics (a) as a function of time (b) CDF of deflection coefficient, PRN-13,  $d=0.5\lambda$ ,  $T_{coh}=100$  ms**



(a) Average deflection coefficient gain (assumed cumulative probability is 90%)



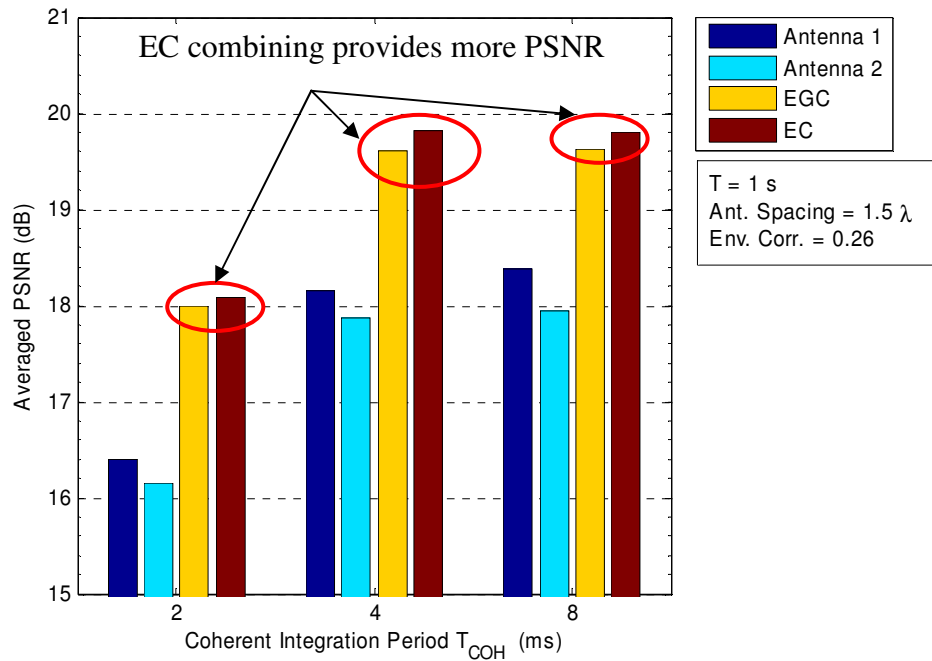
(b) Average PSNR gain over single antenna PSNR

**Figure 5.8 Performance evaluation as a function of antenna spacing**

### 5.2.4 Post-correlation Signal to Noise Ratio (PSNR)

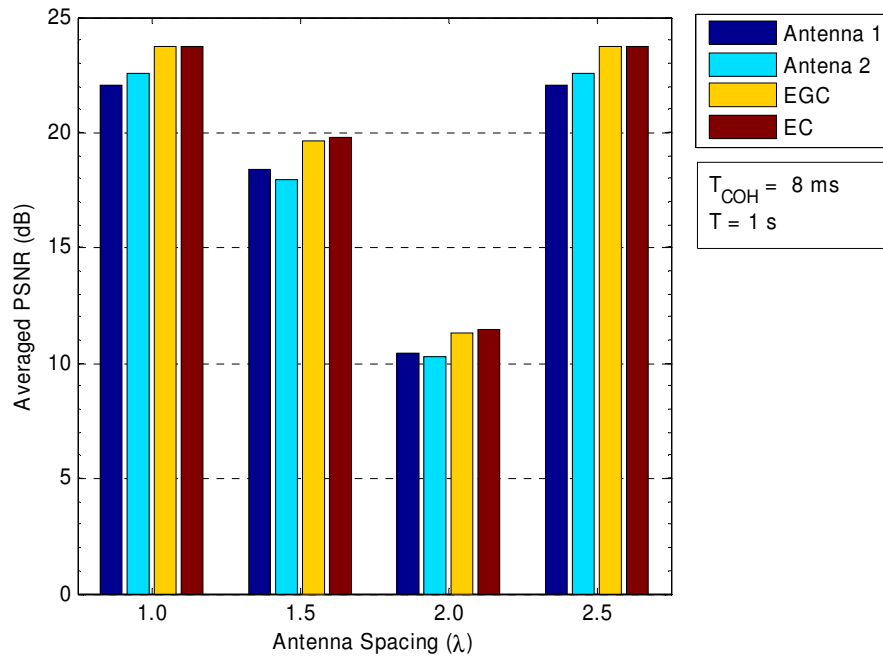
In this section, the spatial combining of GPS signals has been addressed in terms of post-correlation SNR (PSNR) gain between equal-gain (EG) and estimator-correlator (EC) techniques. The latter considers the estimate of the phase difference, i.e. the correlation between two antennas. Using the difference in calculated PSNRs between single antenna and spatial combining with a synthetic array configuration, Figure 5.8(b) compares the performances between EG and EC combining techniques. The PSNR gain has been averaged over all PRNs to show a realistic comparison between EG and EC methods. EC combining shows a consistent performance improvement over EG combining. The comparison in Figure 5.8(b) is a useful result to evaluate the performance of EC in comparison to EG combining, although the exact amount of gain depends on the antenna correlation at that particular antenna spacing.

Figure 5.9 shows the average PSNR for different combining schemes as a function of coherent integration times for the data set corresponding to  $1.5\lambda$  antenna spacing. As shown in Figure 5.9, using diversity antennas provides more PSNR compared to single antenna, however, EC combining provides slightly improved performance compared to EG combining in terms of PSNR gain. For this particular condition, the envelope correlation coefficient is calculated as 0.26. It is clear from Figure 5.9 that the PSNR achieved from individual antennas increases as coherent integration time increases, but when spatial combining is considered, EC combining provides improved performance compared to EG combining, regardless of the coherent integration time. For example, with  $T_{\text{coh}}=4$  ms, the PSNR achieved from the first and second antennas are 18.2 dB and 17.8 dB, respectively; however, when spatial combining is considered, EC combining provides approximately 0.3 dB more PSNR compared to EG combining.



**Figure 5.9 Averaged PSNR for different combining schemes as a function of coherent integration times, indoor location**

An investigation into the achievable PSNR has also been made for different antenna spacings averaged over all PRNs and the results are shown in Figure 5.10. A coherent integration period of 8 ms and a total observation period of 1 s for non-coherent summation are considered. As shown in Figure 5.10, both EG and EC spatial combining techniques show superior performance to single antenna performance, which is desired. However, EC combining shows a slightly better performance compared to EG combining. This is because the performance of EC combining is influenced by the correlation coefficient  $\rho$  between the antennas. Increasing the antenna spacing reduces the correlation coefficient  $\rho$  and both EG and EC combining techniques show similar performance.



**Figure 5.10 Averaged PSNR for different combining schemes as a function of antenna spacing, indoor location,  $T_{coh}= 8$  ms,  $T=1$  s**

Figure 5.11 shows the CDF of PSNR for both the antennas for different coherent integration times of 1 ms, 2 ms and 4 ms. As shown in Figure 5.11, for any given cumulative probability if the  $T_{coh}$  is increased there is improvement in PSNR for both the antennas, which is desired. It is also shown in Figure 5.11 that for any given  $T_{coh}$ , the antenna PSNRs do not vary much (less than 0.5 dB).

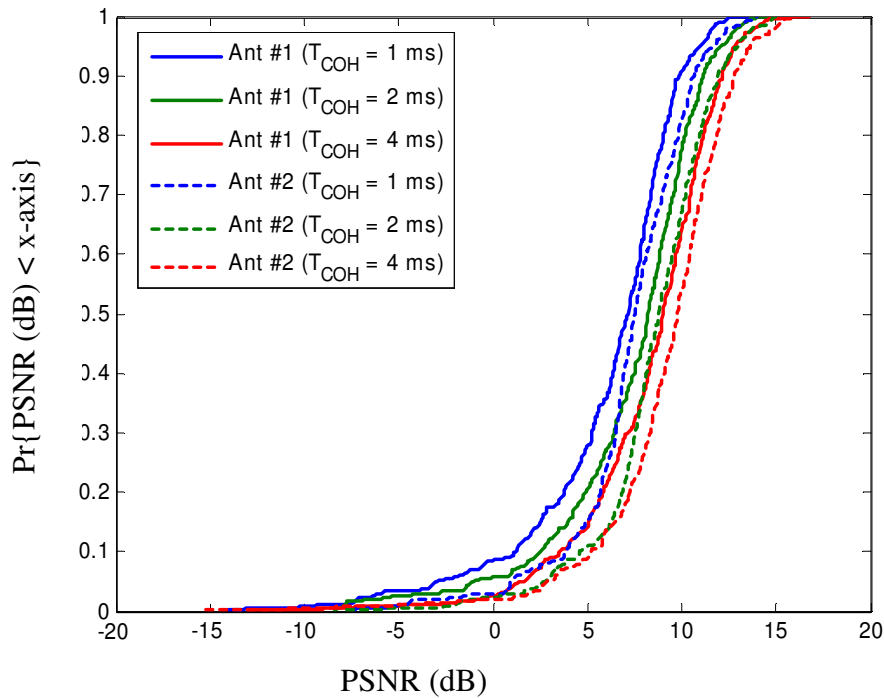


**Figure 5.11 Cumulative distribution function of PSNR at different coherent integration times, location: inside office room**

### 5.2.5 Improvement in Detection Performance

As mentioned earlier, performance evaluation in terms of deflection coefficient is only an approximation of the improvements but not an accurate measure, so in this case detection performance has been measured directly using the indoor test data, in the form of receiver operating characteristics (ROC). The coherent integration period of 100 ms was used such that a good probability of detection is achieved. In order to obtain test statistics for  $H_1$ , i.e. in the presence of a signal, the correct code-phase estimate was used and the corresponding detection output was computed. Incorrect code-phase/Doppler was used to

obtain the test statistics at  $H_0$  condition. The average  $C/N_0$  values for the PRN's processed in the dataset were between 12 to 18 dB-Hz.

The CDF of the detection output for single antenna and diversity antennas at  $0.5\lambda$  antenna spacing is shown in Figure 5.12. The detection output was based on 100 ms coherent integration time. For both  $H_0$  and  $H_1$  hypotheses, single antenna performance, spatial combining with equal-gain (EG) and estimator-correlator (EC) combining are illustrated. Figure 5.12 readily indicates the benefits of using multiple antennas for signal detection purposes. For any given percentage of time, estimator-correlator (EC) combining provides slightly better detection performance than that of equal-gain (EG) combining.

The receiver operating characteristic (ROC) curves for the single antenna and spatial combining schemes are plotted in Figure 5.13. For a 2% false alarm probability, GNSS spatial combining schemes provide a detection probability improvement of around 0.23 over single antenna detection probability. Besides that, the ROC curves for both equal gain and estimator-correlator based combining schemes are similar.

The detection probability improvement with diversity combining over single antenna processing is plotted in Figure 5.14 as a function of antenna spacing. The estimator-correlator (EC) based spatial combining shows a slightly improved detection probability compared to equal-gain (EG) combining when the antenna spacing ranges from 0 to  $0.5\lambda$ . The detection probability improvement for EC in this case comes from the correlated multipath condition with a small antenna separation. However, for higher antenna

spacing values (over  $0.5\lambda$ ), both equal-gain (EG) combining and estimator-correlator (EC) combining perform almost the same, providing a detection probability improvement of approximately 0.21 over the single antenna average detection probability of 0.66. When the antenna spacing is over  $0.5\lambda$ , the similar detection performance for EC and EG can be explained in the following way: when antenna spacing is greater than  $0.5\lambda$ , the correlation coefficient  $\rho$  between the antennas is low due to independent fading statistics experienced by the two antennas and thus the estimator-correlator (EC) combining can be approximated as equal-gain (EG) combining. As a result, both EC and EG techniques behave the same for antenna spacing greater than  $0.5\lambda$

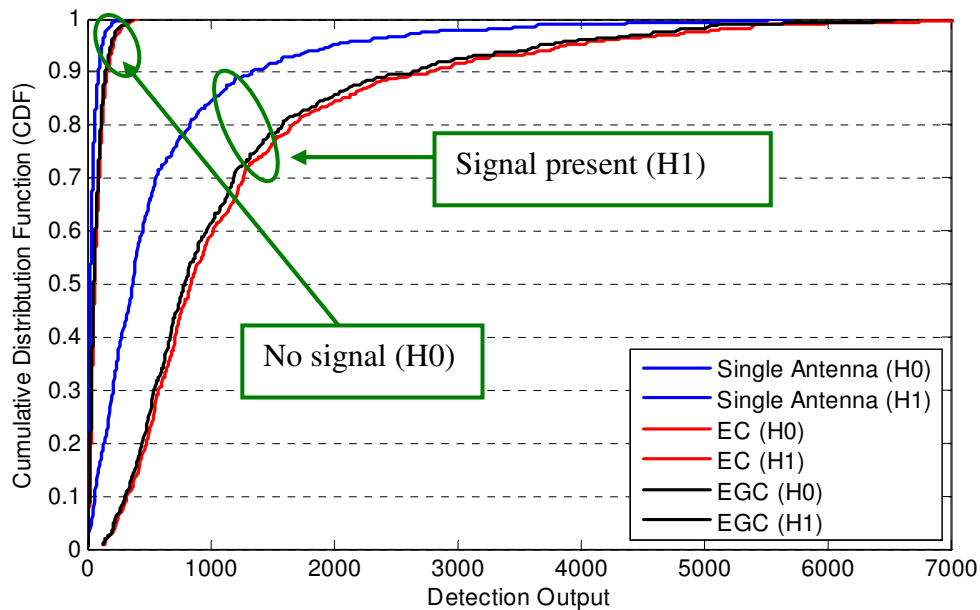


**Figure 5.12 CDF of detection output using synthetic array case,  $T_{\text{coh}}=100$  ms and  $T=5$  s, indoor location**

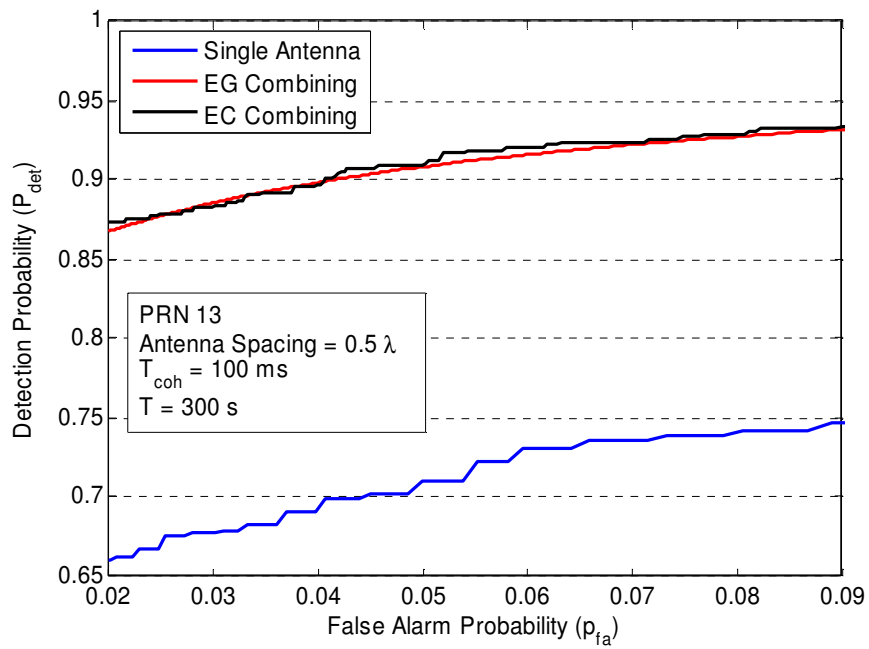


**Figure 5.13 Receiver operating characteristic (ROC) curves for single antenna and spatial diversity combining schemes (PRN 13,  $d = 0.5\lambda$ ,  $T_{\text{coh}} = 100 \text{ ms}$ ,  $T = 300 \text{ s}$ )**

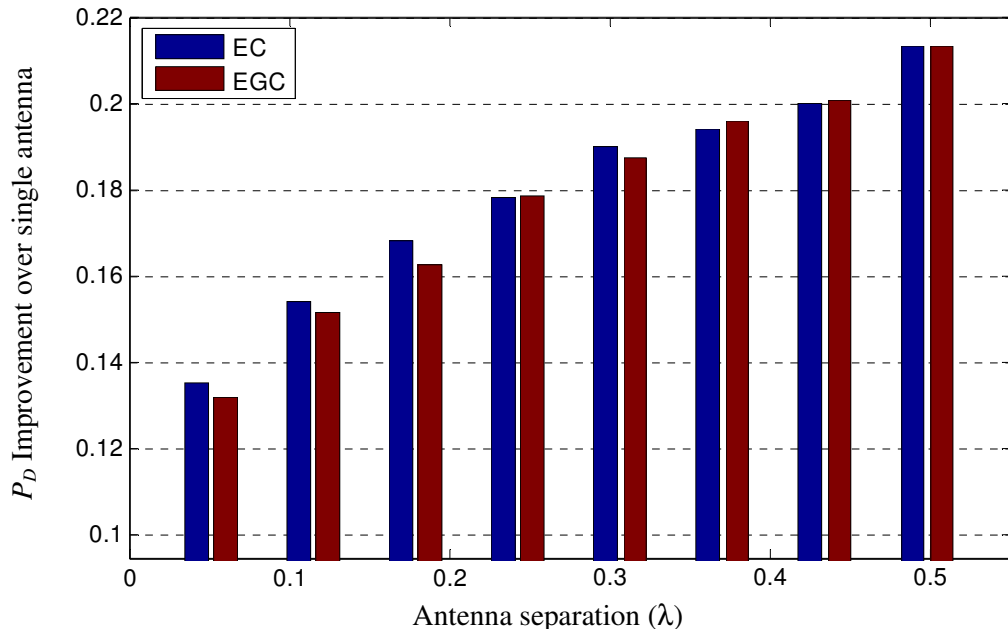


**Figure 5.14 Detection probability improvement over single antenna ( $P_D=0.66$ ) performance. Results are averaged over 6 available PRNs for indoor location with  $P_{FA}=0.05$**

### 5.3 Conclusions

While some of the intermediate results have been provided in the previous chapter, this chapter principally contains several important results in regard to spatial signal combining with equal-gain (EG) and estimator-correlator (EC) combining techniques. Since this research mainly focuses on GNSS signal detection and GNSS signals suffer a significant amount of attenuation indoors, fading statistics in the form of  $C/N_0$  and its CDF have been illustrated at the beginning of the chapter. According to the GNSS signal combining theory developed in Chapter 3, the correlation coefficient between antenna elements is a significant factor in combining the signals spatially. Spatial correlation between receiver antennas has been described first with the help of synthetic array and

then the results have been validated using two spatially apart patch antennas indoors. The results obtained from the synthetic array antenna and the two patch antennas indoors are matched with each other and with the theoretical antenna correlation. The PSNR gain improvement using two antennas with EG and EC combining applied has been shown and compared with the single antenna performance. Different cases of coherent integration times and antenna spacing have been considered and their probability analyses have been performed. Finally, detection performance in the form of improvements in the detection probability has been explained.

## **CHAPTER 6: Conclusions and Recommendations**

The benefits of spatial combining schemes for the detection of weak GNSS signals was successfully demonstrated herein. The detection performance improvement achievable with diversity combining was established in terms of theory and later validated using experimental results. The following sections summarize the major findings of this work and make recommendation for potential improvements.

### **6.1 Synopsis**

Chapter 1 describes the indoor detection and positioning problem in general. The GNSS challenges with signal attenuation and fading indoors have been discussed. The concept of spatial diversity and its potential prospects are briefly addressed as an approach to the solution of indoor GNSS challenges. An overview in the form of motivation and limitations of previous research has been presented, the major objectives of the thesis were summarized and an outline of the thesis was presented.

In Chapter 2, the concept of spatial diversity for weak GNSS signals was discussed. Beginning with a brief description of signal reception by uniform linear antenna array, the chapter discussed the fundamentals of spatial diversity applied to GNSS signal reception. The concepts of switched-, selective-, equal-gain- and maximum-ratio combining methods were briefly described. Diversity gain was briefly explained. Finally, antenna correlation and post-correlation SNR (PSNR) was explained as well as the criteria for performance evaluation of diversity combining of GNSS signals.

Chapter 3 introduced the proposed experimental system model in detail. The corresponding detection statistics for diversity combining schemes were introduced with respect to a single antenna processing. As a combining scheme for GNSS signals, Chapter 3 introduced the estimator-correlator (EC)-based spatial combining technique applicable to weak GNSS signals, with two scheme variations, namely for uncorrelated antenna and for correlated antenna signals. With a detailed description of the spatial covariance and its signal processing treatment based on eigen-analysis, performance evaluation has been done between equal-gain (EG) combining and estimator-correlator (EC) combining.

In Chapter 4, the test methodology and the corresponding GNSS signal processing techniques were discussed in detail. Preliminary results in terms of basic signal processing of multiple antenna system were presented. These intermediate results support the accuracy of the dual-antenna GPS receiver system developed at the hardware level and the feasibility of the test methodology dealing with real GPS raw data at indoor locations.

Chapter 5 focused on the experimental results of the spatial diversity combining schemes for weak GNSS signal detection. The various assumptions made during the preceding chapters were verified in terms of empirical results. The indoor fading statistics was initially validated as a Rayleigh distribution. The antenna correlation was determined using a synthetic array setup as well as using a dual antenna system. The theoretical

antenna correlation was readily supported in terms of experimental measurements for a number of PRN's in the collected data set. The diversity gain analysis was carried out by measuring the corresponding PSNR measures for single antenna and dual antenna spatial combining schemes. The achievable detection probability gains through spatial combining schemes were also determined experimentally from the indoor data sets. The diversity combining schemes showed substantial improvements in terms of PSNR gain as well as detection probability. The estimator-correlator based combining showed small improvements over equal gain combining for small antenna separations due to increased antenna correlation. For nominal antenna correlations, the estimator-correlator (EC) combining was readily approximated to equal-gain (EG) combining scheme.

## **6.2 Research Contributions**

The main contributions of this thesis in the area of multiple-antenna GNSS signal detection are as follows:

1. Fundamental theoretical formulations for diversity combining of GNSS signals have been developed.
2. A hardware system consisting of two front-ends for real-time GPS data collection and storage system has been assembled to verify the theory.
3. Using the dual-antenna data collection setup, field data has been collected for selected indoor locations representative of a modern office building. A software receiver processing algorithm has been developed in Matlab™ and the datasets have been successfully processed with the developed algorithm.

4. After successful testing of the algorithms with real data, it has been found that a multiple-antenna GPS receiver provides a significant improvement in terms of PSNR and detection probability over a single antenna receiver.

### **6.3 Future Research**

Based on the aforementioned conclusions, it is important to identify the limitations of the research presented herein and, accordingly, to formulate the following recommendations for further improvement of the presented research.

- Measurement of further channel characteristics: In the present thesis, a dual-antenna GNSS receiver system has been developed in hardware and the corresponding performance is examined. However, future research should include the measurement of further channel characteristics. It should investigate the use of more than two, possibly three antennas in the array to evaluate the system performance indoors. The software algorithms should be modified accordingly.
- Experimental limitations: An effective data collection system should be developed. The data collection system would have to be straightforward and effective in terms of hardware connections, compactness and functioning. Such a system would definitely mitigate experimental limitations and allow for provisions to collect large spatial data samples at numerous locations laboring an effective manner. Although a typical indoor environment of a modern office building has been considered in this thesis and a good amount of data have been

used, similar tests for a mixed LOS-NLOS environment, e.g. for urban canyons, should be considered.

- Finally, a coherent beamforming approach should be considered. In beamforming the signal from each antenna may be amplified by a different weight. Different weighting patterns for the antennas can be used to achieve desired radiation patterns, e.g. the main lobe width, the side lobe levels, the position of a null can be controlled. Such an approach in multi-antenna GNSS signal reception would be useful to deal with noise or jammers from particular directions, while enhancing signals in other directions. With the availability of an appropriate experimental setup and real GNSS data, such a technique would be interesting to investigate.

## References

Adachi, F., M. T. Feeney, A. G. Williamson, and J. Parsons (1986) "Cross correlation between the envelopes of 900 MHz signals received at a mobile radio base station site," in *IEE Proceedings on Radar and Signal Processing*, vol. 133, no. 6, pp. 506-512, October

Aguirre, S., L. H. Loew and Yeh Lo (1994) "Radio Propagation into Buildings at 912, 1920, and 5990 MHz Using Microcells," in *Proceedings of 3<sup>rd</sup> IEEE ICUPC*, October 1994, pp. 129-134

Backén, S. (2007) *Towards Dynamic Array Processing for GNSS Software Receivers*, Licentiate Thesis, Department of Computer Science and Electrical Engineering, Luleå University of Technology, Sweden,  
2007:65, ISSN: 1402-1757, ISRN: LTU-LIC – 07/65 – SE

Bolcskei, H., D. Gesbert, C.B.Papadias, and A-J van der Veen (2006) *Space-Time Wireless Systems – From Array Processing to MIMO Communications*, Cambridge University Press, UK, July 2006

Bryant, R., S. Dougan and E. Glennon (2001) "GPS Receiver Algorithms and System for Weak Signal Operation," in *Proceedings of ION GPS 2001*, 11-14 September, Salt Lake City, UT, USA.

Cannon, M. E., G. Lachapelle, G. MacGougan, P. Boulton, and A. Read (2003)  
“Mobile Telephony: Testing a High Sensitivity GPS Receiver in Weak Signal  
Environments,” *GPS World*, March, 2003

Clarke, R. (1968) “A statistical theory of mobile radio reception,” *Bell System Technical  
Journal*, no. 2, pp. 957-1000

Colburn, J., Y. Rahmat-Samii, M. Jensen, and G. Pottie (1998) “Evaluation of personal  
communications dual-antenna handset diversity performance,” in *IEEE Trans. On  
Vehicular Technology*, vol. 47, no. 3, pp. 737-746, August

Dedes, G. and A. G. Dempster (2005) “Indoor GPS Positioning Challenges and  
Opportunities,” in Proceedings of IEEE Vehicular Technology Conference, 2005. VTC-  
2005-Fall, Dallas, 28-25 September, pp. 412-415

Durgin, G. D. and T. S. Rappaport (1999) “Effect of multipath angular spread on the  
spatial cross-correlation of received voltage envelopes”, in *Proceedings of VTC 1999*,  
Houston, TX, pp. 996 –1000.

Gao, Y. (2007) *Characterization of Multiple Antennas and Channel for Small Mobile Terminals*, Ph.D. thesis, Department of Electronic Engineering, Queen Mary, University of London, UK, June

Gesbert, D., M. Shafi, D. Shiu, P. J. Smith, and A. Naguib (2003) "From Theory to Practice: An Overview of MIMO Space-Time Coded Wireless Systems," in *IEEE Journal on Selected Areas in Communications*, Vol. 21, No. 3, April 2003

Haykin, S. (2001) *Communication Systems*, 4<sup>th</sup> Edition, 2000, John Wiley & Sons, Inc.

Hu, T. (2006) *Controlled Indoor GPS Signal Simulation*, MSc Thesis, Department of Geomatics Engineering, University of Calgary, Canada, (Available at <http://plan.geomatics.ucalgary.ca>)

ICD200C (2000) "NAVSTAR GPS Space Segment / Navigation User Interfaces," *GPS Interface Control Document*

Intarapanich, A., P. L. Kafle, R. J. Davies, A. B. Sesay, and John McRory (2004) "Spatial Correlation Measurements for Broadband MIMO Wireless Channels," in *Proceedings of IEEE 60<sup>th</sup> Vehicular Technology Conference, VTC2004-Fall*, Los Angeles, 26-29 Sept. 2004, Vol. 1, pp. 52-56

Jakes, W. C. Ed. (1994) *Microwave Mobile Communications*, IEEE Press, NJ

Jensen, M. and Y. Rahmat-Samii (1994) "Performance analysis of antennas for hand-held transceivers using FDTD," *IEEE Trans. on Antennas and Propagation*, Vol. 42, No. 8, pp. 1106-1113, August

Kaplan, E.D., ed. (1996) *Understanding GPS Principles and Applications*, Artech House Publishers, London, February

Kaplan, E. D. and C. Hegarty, *Understanding GPS Principles and Applications*. Artech House, UK, 2006.

Kay, S. M. (1998) *Fundamentals of Statistical Signal Processing, Part-2, Detection Theory*, Prentice Hall PTR, NJ

Kim, S-J and R. A. Iltis (2004) "STAP for GPS Receiver Synchronization," *IEEE Trans. on Aerospace and Electronic Systems*, Vol. 40, No. 1, pp. 132-144, January

Klukas, R., O. Julien, L. Dong, M. E. Cannon, and G. Lachapelle (2004) "Effects of Building Materials of UHF Ranging Signals," *GPS Solutions*, Vol. 8, No. 1, pp. 1-8, Springer Verlag, April 2004

Lachapelle, G. (2006) "NAVSTAR GPS: Theory and Applications," *ENGO 625 Course*

*Notes*, Department of Geomatics Engineering, University of Calgary, Canada

Lachapelle, G., H. Kuusniemi, D. T. H. Dao, G. MacGougan, and M. E. Cannon (2003) "HSGPS Signal Analysis and Performance under Various Indoor Conditions," in *Proceedings of ION GPS/GNSS*, 9-12 September, Portland, OR, pp. 1171-1184, U.S. Institute of Navigation, Fairfax VA

MacGougan, G. D., G. Lachapelle, R. Klukas, K. Siu, L. Garin, J. Shewfelt, and G. Cox (2002) "Degraded GPS Signal Measurements with A Stand-alone High Sensitivity Receiver," in *Proceedings of ION NTM*, 28-30 January, San Diego, pp. 191-204, U.S. Institute of Navigation, Fairfax VA

MacGougan, G. D. (2003) *High Sensitivity GPS Performance Analysis in Degraded Signal Environments*, MSc Thesis, Department of Geomatics Engineering, University of Calgary, Canada, (Available at <http://plan.geomatics.ucalgary.ca>)

Melvin (2004) "A STAP Overview." in *IEEE Transactions on Aerospace and Electronic Systems*, Vol. 19, No. 1, January, pp. 19-35

Misra, P. and P. Enge (2006) *Global Positioning System*, 2<sup>nd</sup> Edition, Ganga-Jamuna Press, MA

Nielsen, J., S. K. Shanmugam, M. U. Mahfuz, and G. Lachapelle (2008) “Enhanced Detection of Weak GNSS Signals Using Spatial Combining”, submitted to *International Journal of Navigation and Observation (IJNO)*, August

Nielsen, J. (2008a) Personal Communication

NovAtel (2004) *Euro-3M and Enclosures - USER MANUAL*, NovAtel Inc. Canada, Website: <http://www.novatel.com>, last accessed on 03 September 2008

O’Driscoll, C. (2007), Performance Analysis of the Parallel Acquisition of Weak GPS Signals, Ph.D. thesis, National University of Ireland, Ireland, January, 2007.

O’Driscoll, C., and G. Lachapelle (2007) “Can multiple antennas provide improvement in indoor positioning?” *GPS World Discussion Forums*, <http://forums.gpsworld.com/showthread.php?p=83> accessed on 24 October 07

Park, C-K and K-S Min (2005) “A study on spatial correlation characteristic of array antenna for multi antenna system” in *Proceedings of IEEE Asia-Pacific Microwave Conference (APMC 2005)*, 4-7 December

Parkinson, B. W. & J. J. Spilker, eds. (1996) *Global Positioning System: Theory and Applications*, American Institute of Aeronautics and Astronautics, Inc., Washington DC

Peterson, B., D. Bruckner, and S. Heye, (2001) “Measuring GPS Signals Indoors,” in *Proceedings of the ION GPS*, Kansas City, Missouri, 16-19 September, pp. 615–624, U.S. Institute of Navigation, Fairfax VA

Pratt, A. R. (2000) “Multiple Antenna GPS: A Technology Ripe for Development,” in *Proceedings of the 13th International Technical Meeting of the Satellite Division*, Salt Lake City, UT, pp. 368-375, U.S. Institute of Navigation, Fairfax VA

Pritchard, W. (1997) “The Calculation of System Temperature for a Microwave Receiver,” [Chapter-71] in *The Communications Handbook*, J. D. Gibson, ed., CRC Press / IEEE Press, Boca Raton FL, pp. 966–975

Rappaport, T. S. (2002) *Wireless Communications Principles and Practice 2<sup>nd</sup> Ed.*, Pearson Education International, NJ.

Ray, J. K. (2000) *Mitigation of GPS Code and Carrier Phase Multipath Effects Using a Multi-Antenna System*, Ph.D. Thesis, Department of Geomatics Engineering, University of Calgary, Canada (Available at <http://plan.geomatics.ucalgary.ca>)

Ray, J. K. (2007) *Advanced GPS Receiver Technology*, ENGO 699.38 Course Notes, Department of Geomatics Engineering, University of Calgary, Canada

Schwartz, M., W. R. Bennett, and S. Stein (1966), Eds., *Communication Systems and Techniques*. McGraw-Hill

Schwengler, T. and M. Gilbert (2000) “Propagation Models at 5.8 GHz – Path Loss & Building Penetration,” in *Proceedings of IEEE RAWCON Conference*, Denver, CO, September, 2000

Shanmugam, S. K. (2008) *Personal Communication*

Shanmugam, S. K. (2008a) *New Enhanced Sensitivity Detection Techniques for GPS L1 C/A and Modernized Signal Acquisition*, PhD Thesis, Department of Geomatics Engineering, University of Calgary, Canada (Available at <http://plan.geomatics.ucalgary.ca>)

Shanmugam, S. K., R. Watson, J. Nielsen and G. Lachapelle (2005) “Differential Signal Processing Schemes for Enhanced GPS Acquisition,” in *Proceedings of GNSS*, Long Beach, CA, 13-16 September, U.S. Institute of Navigation, Fairfax VA

Stavrou, S. and S.R. Saunders (2003) “Factors Influencing Outdoor to Indoor Radio Wave Propagation”, in *Proceedings of 12th International Conference on Antennas and Propagation (ICAP 2003)*, Vol. 2, 31 March - 3 April 2003 pp. 581 - 585.

Stüber, G.L. (2000) *Principles of Mobile Communications 2<sup>nd</sup> Ed.*, Sringer, December

Taga, T. (1990) "Analysis of mean effective gain of mobile antennas in land mobile radio environments," in *IEEE Trans. on Vehicular Technology*, Vol. 39, No. 2, pp. 117-131, May 1990

Tsui, J. B-Y (2005) *Fundamentals of Global Positioning System Receivers: A Software Approach, 2<sup>nd</sup> Ed.*, Wiley Series in Microwave and Optical Engineering, Wiley Interscience, NJ

Van Digglen and Abraham (2001) "Indoor GPS Technology," in *Proceedings of CTIA Wireless-Agenda*, Dallas, 14-18 May

Van Trees, H.L. (2001) *Detection, Estimation and Modulation Theory, Part 1*, John Wiley & Sons, Inc.

Watson, R. (2005) *High-Sensitivity GPS L1 Signal Analysis for Indoor Channel Modelling*, MSc Thesis, Department of Geomatics Engineering, University of Calgary, Canada (Available at <http://plan.geomatics.ucalgary.ca>)

Website: <http://www.u-blox.com> accessed in July 18, 2008

Wikipedia (2008) *Polarization*, <http://en.wikipedia.org/wiki/Polarization>, last accessed July 30, 2008

## APPENDIX-A

### Probability Distribution Function of Sum of Two Chi-squared Random Variables

Since it has been found that the test statistic is a sum of two scaled  $\chi_2^2$  random variables, it is necessary to determine the pdf of such a test statistic. The pdf of the test statistic is used in order to determine probability of false alarm  $P_{FA}$  and the probability of detection  $P_D$ . Let us assume  $x$  and  $y$  are two scaled  $\chi_2^2$  distributed random variables, the pdf's of which are given as

$$p(x) = \frac{1}{a} e^{-\frac{x}{a}} u(x) \tag{A.1}$$
$$p(y) = \frac{1}{b} e^{-\frac{y}{b}} u(y)$$

where  $a$  and  $b$  are the total variances of  $x$  and  $y$  respectively. Now let us consider another random variable  $z = x + y$ , which is the sum of two scaled  $\chi_2^2$  distributed random variables  $x$  and  $y$ . The pdf of  $z$  is the convolution of the pdf's of  $x$  and  $y$  and is expressed as (Nielsen 2008a)

$$\begin{aligned}
p_z(z) &= p_x(z) * p_y(z) & (A.2) \\
&= \frac{1}{a} e^{-\frac{z}{a}} * \frac{1}{b} e^{-\frac{z}{b}} \\
&= \frac{1}{ab} \int_0^z e^{-\frac{\tau}{a}} e^{-\frac{z-\tau}{b}} d\tau \\
&= \frac{1}{ab} e^{-\frac{z}{b}} \int_0^z e^{-\frac{\tau}{a}} e^{\frac{\tau}{b}} d\tau \\
&= \frac{1}{ab} e^{-\frac{z}{b}} \int_0^z e^{\left(\frac{1}{b} - \frac{1}{a}\right)\tau} d\tau \\
&= \frac{1}{ab} e^{-\frac{z}{b}} \left[ \frac{e^{\left(\frac{1}{b} - \frac{1}{a}\right)\tau}}{\left(\frac{1}{b} - \frac{1}{a}\right)} \right]_0^z \\
&= \frac{1}{b-a} \left[ e^{-\frac{z}{b}} - e^{-\frac{z}{a}} \right] u(z)
\end{aligned}$$

The probability that  $z > \lambda$ , i.e.  $\Pr\{z > \lambda\}$  can be written as

$$\begin{aligned}
\Pr\{z > \lambda\} &= \int_{\lambda}^{\infty} p_z(z) dz & (A.3) \\
&= \int_{\lambda}^{\infty} \frac{1}{b-a} \left[ e^{-\frac{z}{b}} - e^{-\frac{z}{a}} \right] u(z) dz \\
&= \frac{1}{b-a} \left[ -be^{-\frac{z}{b}} + ae^{-\frac{z}{a}} \right]_{\lambda}^{\infty} \\
&= \frac{1}{b-a} \left[ be^{-\frac{\lambda}{b}} - ae^{-\frac{\lambda}{a}} \right]
\end{aligned}$$

If we assume that  $x = |y_0|^2$  and  $y = |y_1|^2$  according to our system model, then the output of the combiner becomes

$$z = \mathbf{x}^H \mathbf{x} = |y_0|^2 + |y_1|^2. \quad (A.4)$$

The symbols  $a$  and  $b$  would then correspond to total variances and so to eigen values in the appropriate way as discussed in Chapter-3. Replacing  $a$  by  $\lambda_0$ , i.e. the eigen value corresponding to first antenna and  $b$  by  $\lambda_1$ , i.e. the eigen value corresponding to the second antenna in the equation of  $\Pr\{z > \lambda\}$  above, we get the  $P_{FA}$  at H0 condition and  $P_D$  at H1 condition respectively.

## APPENDIX B

### Validation of Diversity Gain

In this research, empirical diversity gain has been investigated and it has been found that for an antenna spacing of  $0.5 \lambda$ , where  $\lambda$  is the GPS L1 carrier frequency, on average there is approximately a 6.3 dB diversity gain possible from two antennas. The 6.3 dB diversity gain was achieved for 10% cumulative probability.

However, Nielsen et al (2008) conducted a similar analytical investigation for diversity gain for correlated GPS channels. The correlation coefficient in Nielsen et al (2008) was varied from 0 (i.e. uncorrelated channels) to 1 (i.e. fully correlated channels) and the corresponding diversity gain for two-antenna system was reported analytically. The diversity gain has been plotted as shown in Figure B.1 (Nielsen et al 2008). Both equal-gain (EG) and estimator-correlator (EC) diversity combining techniques have been considered in Nielsen et al (2008).

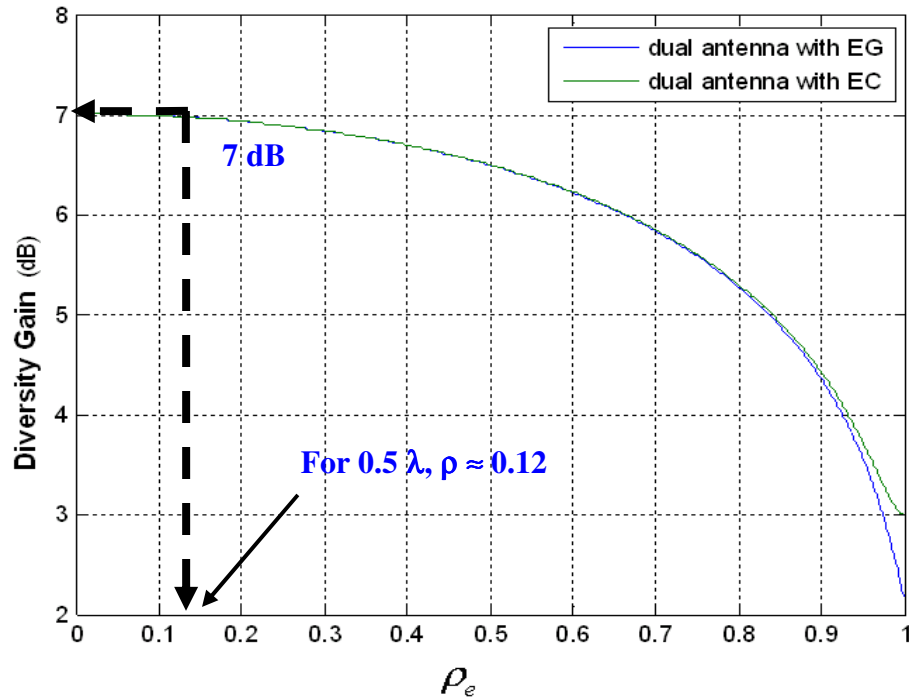


**Figure B.1 Diversity gain from dual antenna combining schemes with  $P_{FA} = 0.1$  and  $P_D = 0.9$  (Nielsen et al 2008)**

The probability of false alarm was fixed at 0.1 and the target detection probability was set to 0.9. It was shown theoretically that a diversity gain of approximately 6.5 dB using two antennas at  $\rho = 0.5$  is achievable.

However, in this research, with the dual-antenna, averaged diversity gain has been found approximately equal to 6.3 dB with experiments dealing with real GPS data. Thus it can be claimed that the experimental results support theory and so the experimental results are justified.